Exploring alternative cetane rating methods using a CRDI Diesel engine serving sustainable fuel development

Victor Sileghem, Simon Vanhaverbeke
Student numbers: 01809957, 01802317

Supervisor: Prof. dr. ir. Sebastian Verhelst
Counsellors: Dr. Tara Larsson, Ir. Tom Robeyn

Ghent, June 2023
Victor Sileghem - Simon Vanhaverbeke

Preface

We are honored to present to the reader our master's dissertation concerning the development of a new alternative cetane rating method, serving the development of sustainable fuels. Writing this work required a lot of dedicated hours in the lab, reading papers, writing, scrapping, and rewriting sections to eventually end up with a coherent and structured thesis. The past year has been an intense, but rewarding period in which we gave the best of ourselves. Not only our technical knowledge, but also our patience and perseverance were challenged as the engine was not always as kind to us, as we were to the engine. The research in this book would not have been possible without the help and guidance of others. For this reason, we would like to thank the people who helped us through the process of writing this thesis.

We thank the Department of Electromechanical, Systems, and Metal Engineering's Sustainable Thermo-Fluid Energy Systems (STFES) research group for allowing us to study the Toyota setup. The engine had not been running for a while, making us think that screeching engine noise would be the soundtrack of the year. This gave us the opportunity to learn a great deal about the real-world application of engines: knowledge that cannot be imparted behind the desk of an auditorium.

We would like to express our gratitude to our counselors Dr. Tara Larsson and Ir. Tom Robeyn as they helped us through the process of writing this thesis. Their guidance and feedback provided during our regular meetings made a significant difference in the course of this thesis. They ensured that we stayed on track with our end goal and helped us in both getting to know the engine, and structuring the thesis. This work would not have been the same without them.

We would like to thank Prof. dr. ir. Sebastian Verhelst for providing us with this intriguing thesis topic as well as with academic advice throughout the year.

A special thanks goes to the technical staff for assisting us in addressing practical issues during our research. Koen Chielens, who showed us around the Toyota engine and was happy to answer any curious *"What happens if we do this?"*-questions. We could rely on him for any mechanical issues, from locating air leaks to refilling engine coolant. We would also like to thank Frederick Martens for his expertise in electronics.

We cannot forget each and every friend or family member who sat through hours of rambling about Diesel, ignition delays and whatnot. This has made not only ourselves, but also you, a little bit more of a Diesel-expert. Thank you for your patience, and injections of motivation time and time again.

Finally, we would like to thank each other for the smooth and pleasant collaboration. We had many joyful moments: from measurement days filled with a low Diesel rumble, to days at home with newly-discovered music playing in the background, to ending the day in the bar or concert hall to see a new music group. These moments made this thesis not only interesting, but great fun at the same time. It was pleasant to share this experience with one another and it delivered us friendship in the end.

Exploring alternative cetane rating methods using a CRDI Diesel engine serving sustainable fuel development

Victor Sileghem, Simon Vanhaverbeke

Supervisor: Prof. dr. ir. Sebastian Verhelst
Counsellors: Dr. Tara Larsson, Ir. Tom Robeyn

Summary

The thesis investigates alternative cetane rating methods using a common rail direct injection Diesel engine, serving the development of future sustainable fuels. **Part I** is a literature review composed of three chapters that frame the topic of this work. **Chapter 1** situates the social and environmental importance of this research, discussing the challenges the automotive industry is facing today and explaining different pathways towards sustainable transportation. **Chapter 2** explains the fundamental principles of a compression ignition engine along with the specifications that a fuel must meet in order to operate in a Diesel engine. **Chapter 3** discusses the importance of the cetane number, followed by a detailed description of the various cetane rating methods in use today, as well as possible criticism towards these methods. **Part II** consists of chapters 4 through 8 and includes the measurements and analysis performed in this experimental work. **Chapter 4** describes the experimental setup, as well as the modifications made to fit this work. **Chapter 5** explains how the two time instances that define the ignition delay are determined. This is important as the igntion delay is heavily related to the cetane number of a fuel. An analysis of multiple metrics to estimate start of combustion metrics, from which the most suitable one is chosen. Since the goal of this work is to develop an alternative cetane method, **Chapter 6** discusses various alternative control strategies (throttle valve, boost pressure and exhaust gas recirculation) that can be used to mimic the current standardized cetane rating method. The chapter ends with a brief description of the operating conditions and fuel blends used in this work. **Chapter 7** evaluates the effect of exhaust gas recirculation on the ignition delay using different fuel blends. After discussion of the measurements, a model is proposed in **Chapter 8** with the purpose of predicting the cetane number of future sustainable fuels. The model is evaluated with several fuel blends. **Chapter 9** forms a conclusion on the performed work along with future perspectives to improve the experimental set up and model.

Keywords: alternative cetane rating method, compression ignition, cetane number, ignition delay, exhaust gas recirculation, diesel, hydrotreated vegetable oil

EXPLORING ALTERNATIVE CETANE RATING METHODS USING A CRDI DIESEL ENGINE SERVING SUSTAINABLE FUEL DEVELOPMENT

Victor Sileghem, Simon Vanhaveberke, Dr. Tara Larsson, Ir. Tom Robeyn, Prof. dr. ir. Sebastian Verhelst
Department of Electromechanical, Systems and Metal Engineering
Ghent University
Sint-Pietersnieuwstraat 41, B9000 Gent, Belgium
E-mail: victor.sileghem@ugent.be, sivhaver.vanhaverbeke@ugent.be

ABSTRACT

This article discusses the development of an alternative cetane rating method using a production common rail direct injection (CRDI) Diesel engine. The method is based on the ASTM D613 standard, but uses exhaust gas recirculation (EGR) to control the oxygen concentration of the intake gas, and thereby controlling the ignition delay. A number of metrics to estimate the start of combustion (SOC) are analysed. It is chosen to detect SOC based on the location of the maximum of the second-order pressure derivative. Experiments using blends of Diesel, hydrotreated vegetable oil (HVO), iso-octane and n-dodecane show a cetane number (CN) resolution of 3.4 to 5 CN units around Diesel, and a measurement range between 48 and 90 CN. The correlation by Hardenberg and Hase has been extended to account for reduced intake oxygen concentrations. Based on this model, a CN resolution of 5 CN units is expected. The limited encoder resolution forms the main limitation to the CN resolution. The goal of the development of this method is to finally assess the suitability of newly developed second-generation biofuels in engines representative of current practice, without major modifications.

INTRODUCTION

Setting the scene

"Climate change affects us all", is the conclusion drawn from the sixth assessment report of the Intergovernmental Panel on Climate Change [1]. The effects accelerate and become more extreme every year. Without additional measures, Earth's temperature will increase with 2.8°C above pre-industrial levels by the end of the century. Therefore, broad modifications are necessary to stay as close to the most optimal scenario to date, of 1.8°C, as possible [2, 3]. Transportation is accountable for 15% of the total greenhouse gas (GHG) emissions, with road applications being the main polluter in this industry [1]. With continuously growing transport activities, it is clear that efforts to reduce the CO_2-impact of transportation are of vital importance to limiting the Earth's temperature rise.

NOMENCLATURE

AD-LIBIO		Advanced liquid biofuels
BTDC		Before top dead center
CFR		Cooperative Fuel Research
CN	$[-]$	Cetane number
CRDI		Common rail direct injectrion
DP1, DP2, DP3	$[°ca]$	Crank angle corresponding to the maximum of the first-, second- and third-order derivative of the cylinder pressure
EGR		Exhaust gas recirculation
GHG		Greenhouse gas
HRR		Heat release rate
HVO		Hydrotreated vegetable oil
ID	$[°ca]$	Ignition delay
IMEP	$[bar]$	Indicated mean effective pressure
MFB	$[\%]$	Mass fraction burned
SOC	$[°ca]$	Start of combustion
SOI	$[°ca]$	Start of injection
TDC		Top dead center
VGT		Variable geometry turbocharger

Special characters

M_{ps}	$[m/s]$	Mean piston speed
O_{2in}	$[vol\%]$	Intake oxygen concentration
p_{cyl}	$[bar]$	In-cylinder pressure
p_{in}, p_{out}	$[bar]$	Inlet and outlet manifold pressure
p_{TDC}	$[bar]$	Cylinder pressure at TDC
T_{in}, T_{out}	$[°C]$	Inlet and outlet manifold temperature
T_{TDC}	$[°C]$	Cylinder temperature at TDC
θ	$[°ca]$	Crank angle
R	$[J/mol \cdot K]$	Universal gas constant
R^2	$[\%]$	Coefficient of determination

Pathways toward sustainable transportation

To this purpose, a number of possible solutions to reduce transport emissions are being researched: electrified vehicles, new engine technology, and sustainable fuels. These all aim to achieve increased efficiencies - which reduces our primary energy need-, defossilization of fuels, or both at once. Electric vehicles offer high effiency and low emissions levels, therefore the European Union has decided to aid their establishment in the market [4]. However, some life cycle assessment studies claim that biofuels, especially second generation, show a bigger potential to reduce the impact of transportation on the climate, compared to electric vehicles [5]. Besides this, forecasts indicate that 40% of the global vehicle fleet will still be powered by internal combustion engines by 2040 [6]. This calls for solutions capable of reducing the GHG-intensity of the legacy fleet,

using a minimum of adaptations.

For this reason, the pathway of sustainable fuels will be emphasized in this work. Biofuels are regarded as an established technology with the potential to be a low-carbon fuel, if produced and consumed wisely [7]. In particular, sustainable fuels, such as HVO and AD-LIBIO[1], have the potential to significantly improve the sustainability of the vehicle fleet. Such fuels, which are functionally equivalent to petroleum fuels and are compatible with the existing infrastructure are better known as drop-in fuels [8].

These fuels must meet the European Diesel norm before they may be used in today's Diesel engines [9]. A minimum value of the cetane number (CN) is specified in this norm. The CN is a quantitative indicator of a fuel's quality, for use in a Diesel engine. It indicates the readiness to autoignition during the compression ignition process and is related to the ignition delay (ID). The ID signifies the interval (expressed in crank angles) between the start of injection (SOI) and the start of combustion (SOC). Fuels with a high CN show short IDs, which is required for smooth engine operation, high fuel conversion efficiency, low smoke emissions and ease of starting in Diesel engines [10]. Several standardized methods are currently in use for testing a fuel's CN.

Cetane rating methods

The ASTM D613 is the oldest standardized method for measuring the CN. This method makes use of a Cooperative Fuel Research (CFR) engine, which is a single-cylinder Diesel engine with a variable compression ratio [11]. The compression ratio of the engine is manipulated to achieve an ID of 13 $°ca$, resulting in SOC at top dead center (TDC), for any given fuel. To determine the CN of a fuel, reference fuels are used. N-cetane and heptamethylnonane are considered reference fuels and have a CN of 100 and 15, respectively. A fuel's CN is the same as the blend of reference fuels if both require the same compression ratio to achieve SOC at TDC.

This method is the standard up to this day. However, its high fuel and time consumption, as well as issues with reproducibility and repeatability, have not made its existence without criticism. Above this, the CFR engine does not represent the architecture of current state-of-the-art Diesel engines [12]. These objections led to the development of the ASTM D6890 ignition quality rating, which is based on fundamental fuel properties, studied in constant-volume combustion bombs [13]. It is however not fit for our purpose, as the conditions differ significantly from engine conditions. Simple numerical methods also exist to estimate the CN of a fuel based on its physical properties [14].

This work aims to quantify the CN of sustainable fuels using a production Diesel engine. This allows to assess the drop-in capabilities of these fuels in conditions representative of current engine practice. The developed method in this thesis will use the ASTM D613 as a starting point, as it is the only standardized method operating under engine conditions.

EXPERIMENTAL SETUP

Experiments are conducted in a Toyota 1AD-FTV D4D: a 4-cylinder Diesel engine with 4 valves per cylinder and a dual overhead camshaft. Its properties are listed in Table 1. The electric common rail direct injection (CRDI) system and the piezoelectric injectors (Denso G3) allow rapid high-pressure fuel injections. A hydraulic dynamometer serves as engine load.

Table 1: Main Toyota 1AD-FTV D4D properties.

Engine property	Value
Bore [mm] x Stroke [mm]	86.0 x 86.0
Displacement volume [cm^3]	1998
Number of cylinders	I4
Firing order	1 - 3 - 4 - 2
Compression ratio	15.8:1
Max torque	310 Nm at 2000 rpm
Fuel system	Electric common-rail direct injection
Camshaft	Dual overhead camshaft

Figure 1 shows a schematic representation of the air flow path with its main components and sensor measurements. Since the new method employs exhaust gas recirculation (EGR) as a mean to control the ID, the air flow path is stated. Fresh intake air passes through the compressor stage of a variable geometry turbocharger (VGT), followed by an intercooler. The high-pressure EGR loop is equipped with an EGR cooler, which can be bypassed using a vacuum switch valve (VSV). The intake line is also fitted with a throttle valve, allowing smooth engine shut-off, but also to feed more EGR gases to the intake manifold.
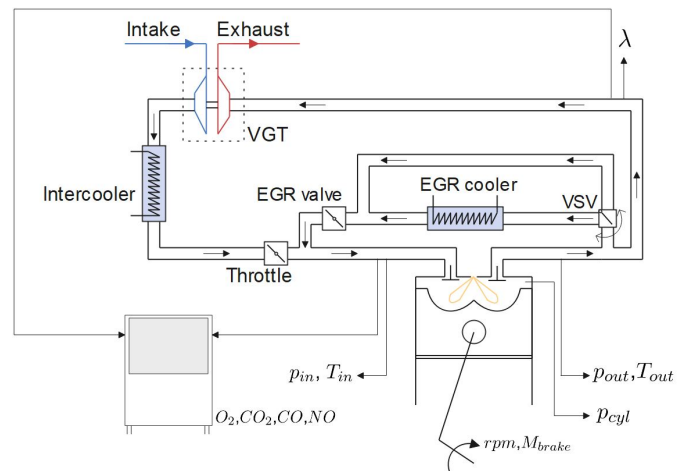
Figure 1: A schematic representation of the air flow path in the engine with the main components and measurements.

Additional sensors provide accurate information to perform detailed combustion analysis. An AVL GH13P piezoelectric pressure sensor, coupled to an AVL Microifem 4G4P amplifier, measures the in-cylinder pressure of the first cylinder (p_{cyl}). Two Keller M5-HB type piezoresistive pressure transducers and K-type thermocouples measure the in- and outlet manifold pressure (p_{in}, p_{out}) and temperature (T_{in}, T_{out}). A Kistler optical encoder is mounted to the engine shaft to couple measurements to the corresponding engine position with a resolution of $0.5°ca$. The exhaust gas line is equipped with an Innovate LM-2 lambda sensor. A Siemens Ultramat 23 gas analyzer is used to obtain measurements of the intake gas composition.

The engine test bench is fitted with a National Instru-

---

[1]This work is framed within the advanced-liquid biofuel (AD-LIBIO) project: a project funded by the Belgian Energy Transition fund, which aims at the development of a second-generation biofuel.

ments Powertrain Control System for engine control and data acquisition.

IGNITION DELAY

An accurate and reliable method of determining the ID is indispensable in this work, as it forms the basis for all standardized experimental CN-rating methods. This requires accurate detection of SOI and SOC.

It is common practice to equip fuel injectors with a needle lift sensor. For this work, the injector actuation signal is used to mark the SOI, as no needle lift sensor is installed at current time.

Determining SOC is one of the most important, but contentious, subjects in combustion analysis. The complexity of the auto-ignition process of a Diesel fuel jet makes it nearly impossible to allocate a unique time instance to the SOC. As a result, numerous metrics for estimating SOC have been proposed in literature, based on pressure analysis, temperature rise, heat release rate (HRR), or light emissions.

Metrics based on the HRR correspond to the moment at which there is a net positive release of heat, i.e. when the heat generation due to exothermic reactions offsets the cooling effect of the evaporating fuel. The fraction of the fuel that has been burned for each time interval during the combustion, called MFB, can be estimated from a normalization of the cumulative heat release. The points where MFB reaches 2%, 5%, or 10% are often used to estimate SOC. The single zone model, used to model the HRR, is based on strong simplifications, leading to higher uncertainties. It was experienced that the MFB metrics gave less consistency for SOC estimation between measurements. A good metric should be able to determine SOC accurately for each cycle.

The rapid increase in cylinder pressure associated with ignition can also be detected with the use of pressure derivatives. SOC is often estimated by the location of the maximum of the first-, second-, or third-order derivative of the pressure signal, denoted as DP1, DP2 and DP3 respectively. The location of the DP metrics showed to be consistent over a large number of measurements under varying conditions. The DP2 metric was chosen as it shows a lower inter-cycle variability than DP1, and has also been recommended in literature for signals with noise [15].

ALTERNATIVE TEST METHOD
Alternative control input

To emulate the ASTM D613 standard, an alternative control input, which replaces the variable compression ratio, is required to influence the ID. Furthermore, an appropriate combination of engine load and speed should be chosen. Three options are discussed.

The intake throttle valve can be used to decrease the intake manifold pressure, resulting in decreased pressures at SOI, and a longer ID. This was investigated in literature, but showed only a limited measurement range of 9 CN units [16].

An external compressor or controllable turbocharger can be used to increase the intake manifold pressure and temperature. This emulates an increased compression ratio and results in a decreased ID. As expected, a sufficiently high speed and load are required to significantly reduce the ID when using the VGT. Another alternative is considered for practical reasons.

Lastly, the use of EGR is examined. This reduces the intake oxygen concentration, as well as the pressure and temperature at SOI. The latter is the result of an increased ratio of specific heats in the intake gas as a result of EGR. Figure 2 shows that the ID increases nonlinearly with reduced intake oxygen concentration O_{2in} [17].
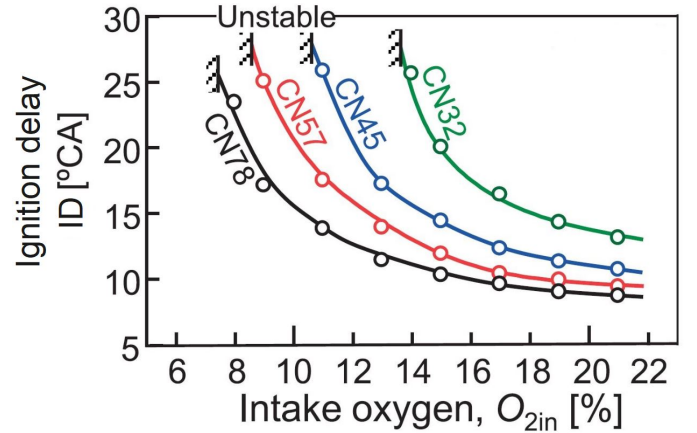
Figure 2: The effect of a reduced intake oxygen concentration (O_{2in}), through the use of cooled EGR, on the ignition delay (ID) for different CN fuels. Adapted from [17].

Furthermore, a higher sensitivity of the ID to the CN is achieved at reduced O_{2in}. This makes it easier to distinguish between fuels with different CNs, and results in a higher CN measurement resolution, given the limited measurement resolution on the ID. For these reasons, measurements will be performed using EGR as control input to the alternative cetane rating method.

Operating conditions

In this work, a speed of 1300 rpm and an injection quantity of 3.68 mg/cycle is used for all tests. This results in a relatively low engine load of around ≈ 4.5 bar IMEP. The moderate engine load increases the sensitivity of the ID to the CN [10], which increases the CN resolution of the test. SOI is set at 10°ca BTDC, with a moderate rail pressure of 900 bar. Control of the EGR and intake throttle valve influences the amount of EGR, and thus the intake oxygen concentration. The EGR cooler is used to allow higher EGR rates.

Fuels

Evaluation of the test method requires fuel blends with a different CN. Several mixtures of Diesel, HVO, iso-octane, and n-dodecane are used to create various CN number fuels. Table 2 depicts the CN and a selection of physical properties of these fuel components.

In this work, two batches of Diesel are used, denoted as 'Diesel$_1$' and 'Diesel$_2$'. The CN of HVO and both Diesel batches were measured in an accredited laboratory (indicated in bold). The result confirmed a clear difference in CN between both Diesel batches. The other CN values and physical properties originate from literature [18]. The CN of the fuel blends is estimated using a weighted average based on the molar fractions of each component. Table 3 shows the various blends, their CN, and the abbreviation that will be used from here on.

Table 2: The CN and physical properties of reference fuels.

Property	Diesel$_1$	Diesel$_2$	HVO	iso-octane	n-dodecane
Cetane number	**54.5**	**52.9**	**89.6**	20.1	75.6
Density $[kg/m^3]$	832.5	832.5	780	687.77	750
Viscosity $[\frac{mm^2}{s}, 25°C]$	3.25	3.25	3	0.7041	/
Lower heating value $[\frac{MJ}{kg}]$	42.9	42.9	44.1	44.2	43.84
Flashpoint $[K]$	347	347	367	261	347.15

Table 3: The abbreviation and CN of the various fuel blends.

Blend	Abbreviation	CN
100 vol.% HVO	HVO100	89.6
100 vol.%Diesel$_1$	Diesel$_1$	54.5
100 vol.% Diesel$_2$	Diesel$_2$	52.9
50 vol.% Diesel$_1$ + 50 vol.% HVO	HVO50	72.1
76 vol.% Diesel$_2$ + 24 vol.% n-dodecane	Diesel$_{2,CN+5}$	57.9
87 vol.% Diesel$_2$ + 13 vol.% iso-octane	Diesel$_{2,CN-5}$	47.9

EXPERIMENTAL RESULTS
Concept evaluation

Figure 3 shows the ID of the different fuel blends under varying intake oxygen concentrations. It is clear that the ID follows the tendency from Fig. 2. The CN of the different blends ranges from 89.6 (blue curve) to 42.9 (purple curve).
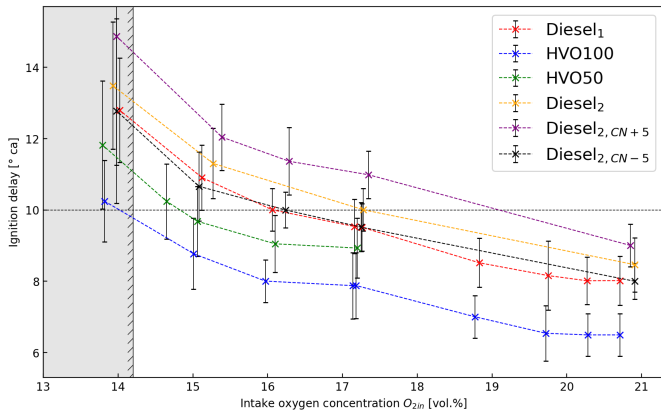
Figure 3: The measured ignition delay for fuels with a CN ranging from 89 - 43 under intake oxygen concentrations varying between 21% and 14% through the use of EGR.

The black dotted line on Figure 3 indicates a constant ID of 10°ca, corresponding to ignition at TDC. Clearly, EGR allows to control fuels with a wide CN range to manifest the same ignition delay. This proves that EGR may serve as a valuable alternative control input to the cetane rating test developed in this work.

The error margin on the ID is composed of two parts. Firstly, the encoder resolution limits the ID accuracy to maximum 1°ca. Secondly, a 95% confidence interval based on the inter-cycle variability is added. Overall, the limited encoder resolution is responsible for about 60% of the error margin of the ID measurements, making this a strong limitation to the accuracy of the resulting cetane test. A significant increase in inter-cycle variability is achieved at the lowest values of O_{2in}. During tests, the engine runs

noticeably less stable in these conditions. This instability may be caused by a slight variation in the intake throttle valve position, which may affect the EGR flow rate, and thus ID. The unstable zone is indicated by a shaded area.

CN resolution and accuracy

The ID of Diesel$_1$ appears to be indistinguishable from Diesel$_{2,CN-5}$, despite their difference of about 3.4 CN units. However, Diesel$_2$ and Diesel$_{2,CN\pm5}$ are clearly distinguishable from each other, with a difference in ID of about 0.5°ca, i.e. one encoder pulse. These four measurements would thus suggest a resolution between 3.4 and 5 CN units.

The ID difference between Diesel$_{2,CN-5}$ and Diesel$_{2,CN+5}$ is somewhat bigger than 1°ca. This corresponds to the ID accuracy, without taking inter-cycle variability into account. Based on this, the CN accuracy would be maximum 10 CN units.

Other factors influencing the ignition delay

It was noticed that the intake temperature increases linearly with decreasing O_{2in}, due to the introduction of hot exhaust gases. This is the result of the limited size of the stock EGR cooler. An increased intake temperature results in an increased temperature at SOI, lengthening the ID. This decreases the sensitivity of the ID to the intake oxygen concentration, resulting in a lower CN measurement range of the test. A closer control on the intake temperature would benefit both the CN measurement range and accuracy, and provide added flexibility.

The actuation of the EGR and throttle valves also influences the intake manifold pressure. The pressure changes are minimal however, and its effect on the ID is assumed to be negligible.

Furthermore, it is important to acknowledge that the EGR composition depends on the chemical composition of the fuel. The EGR composition, mainly its NOx content, can influence the ID [19], resulting in a misleading result of the test.

Model development

The experimental results are used to develop a model that relates the intake oxygen concentration (O_{2in}), CN, and ID: $ID = f(CN, O_{2in})$. This model can be used to inter- and extrapolate between results, and decide on the optimal operation strategy of the test. The Hardenberg and Hase correlation, which correlates the ID to the CN, under atmospheric O_{2in}, is used as a starting point [20]. An additional term is included to model the effect of a reduced O_{2in} on the ID, and the interplay between CN and O_{2in}:

$$ID = (p_1 + 0.22 M_{ps}) \cdot$$
$$exp\left[\frac{p_2}{O_{2in}+p_3}\frac{618840}{CN+25}\left(\frac{1}{RT_{TDC}}-\frac{1}{17190}\right)+\left(\frac{21.2}{p_{TDC}-12.4}\right)^{0.63}\right]$$

The ID also depends on the mean piston speed M_{ps} (m/s), and the temperature and pressure at top dead center: T_{TDC} (°C) and pressure p_{TDC} (bar) respectively. R denotes the universal gas constant, $8.3143 J/mol \cdot K$. The values of the fitting parameters, p_1, p_2 and p_3, are determined using a non-linear least square fit.

Figure 4 shows all measurements together with the fitted curves. The fuels used to fit this model are plotted with a solid line, others are indicated by a dashed line. The model provides a reasonable prediction of the measurements using HVO50.
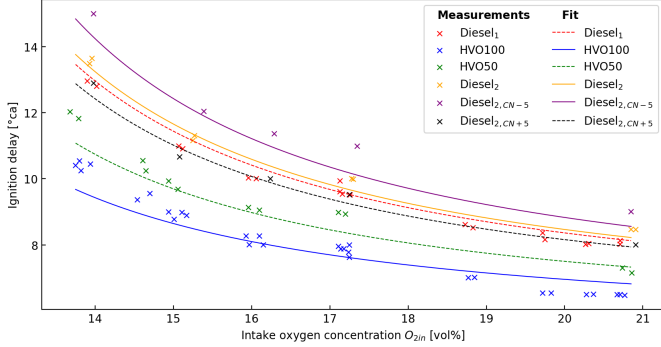
Figure 4: The measured and fitted ignition delay under varying intake oxygen concentrations for Diesel$_1$, HVO100, HVO50, Diesel$_2$, Diesel$_{2,CN-5}$ and Diesel$_{2,CN+5}$.

As the aim of this thesis is to develop a cetane rating method, the inverse relation $CN = f(ID, O_{2in})$ is more interesting. Finally, it is desired to generate calibration curves relating the CN of the tested fuel to a single measured variable. Two approaches are possible.

By means of EGR, the engine can be controlled to a constant O_{2in}, which relates the measured ID to the CN of a sample: $CN = f(ID)$. On the other hand, EGR can be used to control the engine to operate at a constant ID. The required O_{2in} is then related to the CN of the fuel sample: $CN = f(O_{2in})$. These two approaches correspond to an intersection of the lines in Fig. 4 with a vertical and horizontal respectively.

Constant intake oxygen concentration

Figure 5 shows the relation $CN = f(ID)$ under constant intake oxygen concentrations of 20.8%, 17.2%, 15% and 13.7%. The yellow dashed calibration curve indicates that these measurements fall within the zone of unstable engine operation. The black dotted lines show the minimum and maximum CNs that are tested.

This representation shows the benefit of operating at reduced O_{2in}: the sensitivity of the ID to changes in CN is increased. This increases the measurement resolution and accuracy of the CN, given the limited ID resolution and accuracy. Operating at $O_{2in} = 17.2\%$ results in measurements where SOC occurs after TDC (i.e. $ID > 10°ca$) to span the current CN range. Temperature and pressure decreases after TDC, resulting in a further increase of the ID, making the comparison with other measurements difficult. Thus, achieving SOC before TDC forms a limit to the CN measurement range. This may be extended by an advanced injection timing.

The calibration curves shown in Figure 5 can also be used to estimate the CN resolution and accuracy of the test. This yields 5 CN units and about 10 CN units re-
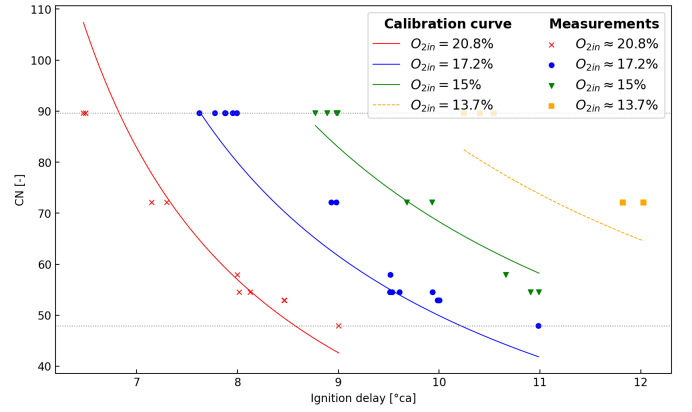
Figure 5: Calibration curves showing the relation between CN and ID under a constant intake oxygen concentration of 20.8%, 17.2%, 15% and 13.7%.

spectively. The same conclusions followed from the experimental data.

At a given value of O_{2in}, the CN of a fuel sample can be estimated by substituting the measured ID in the calibration curve: $CN_{calc} = f(ID_{measured})$. Figure 6 shows the relation of CN_{calc} to CN for the current measurements and the corresponding coefficients of determination, R^2. Clearly, no unity relation $CN = CN_{calc}$ is achieved. This is caused by inconsistent results for repeated measurements of the same fuel, and discrepancies between the measurements and the fitted model.
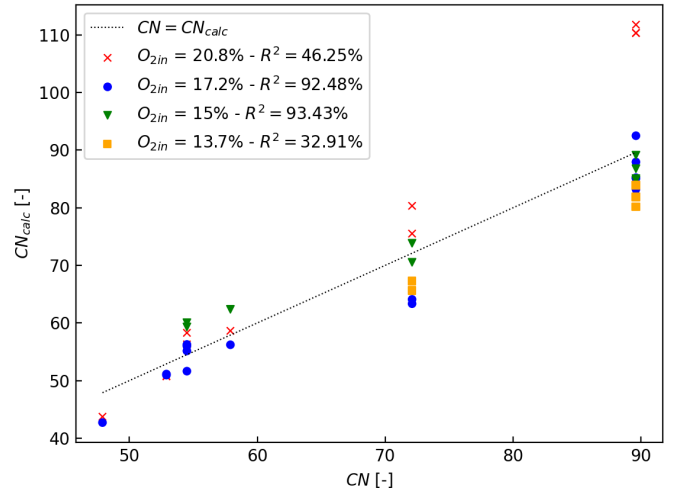
Figure 6: The actual CN of different tested fuels vs CN_{calc} using calibration curves at constant O_{2in}.

Constant ignition delay

Figure 7 shows the relation $CN = f(O_{2in})$ at constant values for the ID of 8°ca, 9°ca, and 10°ca, together with the measurements which achieve these IDs. The black dotted lines show the minimum and maximum CNs that are tested.

It is clear that, with an ID of 9°ca, the values of O_{2in} required to span this CN range stay within the stable zone, while at an ID of 10°ca this would require measurements in the unstable zone. An appropriate ID can be chosen based on the CN range to be tested.

At a given value of the ID, the CN of a fuel sample can be estimated by substituting the measured O_{2in} in the calibration curve: $CN_{calc} = f(O_{2in,measured})$. Figure 8 shows
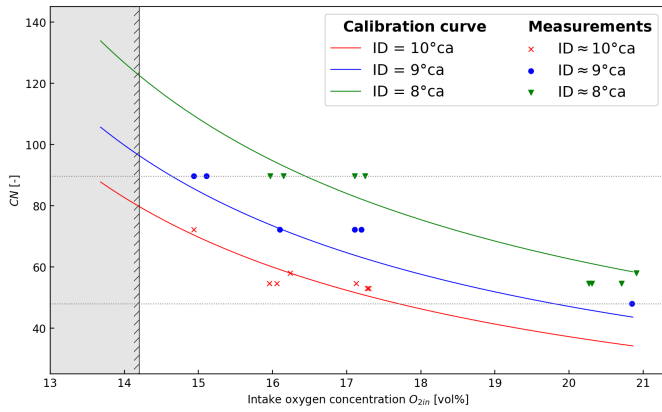
Figure 7: Calibration curves showing the relation between CN and the intake oxygen concentration to achieve a set ignition delay of 8°ca, 9°ca and 10°ca.

the relation of CN_{calc} to CN for the current measurements and the corresponding values of R^2.

Again, no unity relation is achieved. The values of R^2 would suggest an ID of 8°ca to provide the best CN estimations. Overall, the values of R^2 are lower than for operation at constant values of O_{2in}. However, the authors hypothesize that operation under a constant ID results in a better comparison of the fuels. In this case, different fuels undergo almost the same history of pressure and temperature during the ignition delay. This provides the closest approximation of the ASTM D613 method. A better prediction may be achieved with the use of more measurements, controlled to a set ID and recorded with an improved encoder resolution.
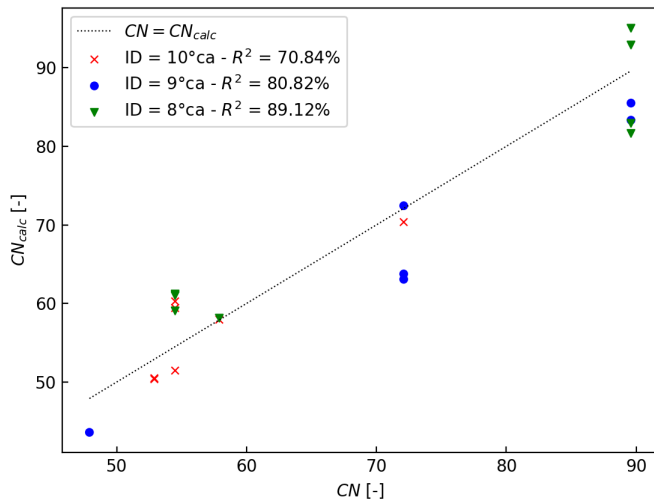
Figure 8: The actual CN of different tested fuels vs CN_{calc} using calibration curves at constant ID.

CONCLUSIONS

In this work, alternative cetane rating methods using a production CRDI Diesel engine are explored, in the prospect of evaluating sustainable fuels. Different alternative control inputs were explored to emulate the CFR's variable compression ratio. It was chosen to use EGR for a number of reasons:

- The ID can be influenced significantly, resulting in a high CN measurement range

- The achievable CN measurement range is not bound by engine speed and load

- Reduced intake oxygen concentrations amplify the difference in ID between fuels with a different CN, resulting in an increased measurement resolution and accuracy.

Experiments using blends of Diesel, HVO, iso-octane and n-dodecane show that EGR indeed allows to control fuels with a wide CN range to manifest the same ignition delay. This proves that EGR may serve as a valuable alternative control input to the cetane rating test developed in this work.

The Hardenberg and Hase correlation is extended with an additional term to include the effect of O_{2in} on the ID for different CNs. This model provides an reasonable prediction of the measurements recorded using HVO50. Based on the current fit, it would be expected to achieve a better CN estimation when operating under constant values of O_{2in}. However, the authors hypothesize that operation under a constant ID results in a better comparison of the fuels, as this provides a closer approximation of the ASTM D613 method. Further investigation with a more controlled set of fuel samples can give conclusion to this question.

Based on the measurements and model, the CN resolution and accuracy are estimated to be 5 CN units and 10 CN units respectively. The encoder resolution forms the strongest limitation to the accuracy of the test. Upgrading the current encoder would largely improve the CN accuracy. Also an improved intake temperature control may be a worthwhile adaptation to the setup.

REFERENCES

[1] IPCC, *Climate Change 2022: Mitigation of Climate Change. Contribution of Working Group III to the Sixth Assessment Report of the Intergovernmental Panel on Climate Change.* Cambridge, UK and New York, NY, USA: Cambridge University Press, 2022.

[2] UNEP, "Emissions gap report 2022." `https://www.unep.org/resources/emissions-gap-report-2022`, October 2022.

[3] UNEP, "Climate change: No 'credible pathway' to 1.5c limit, unep warns." `https://news.un.org/en/story/2022/10/1129912`, October 2022.

[4] E. Comission, "Reducing co2 emissions from passenger cars." `https://climate.ec.europa.eu/eu-action/transport-emissions/road-transport-reducing-co2-emissions-vehicles/co2-emission-performance-standards-cars-and-vans_en`, October 2019.

[5] Öivind Andersson and P. Börjesson, "The greenhouse gas emissions of an electrified vehicle combined with renewable fuels: Life cycle assessment and policy implications," *Applied Energy*, vol. 289, p. 116621, 2021.

[6] N. Bloomberg, "Electric vehicle outlook 2020," *Executive Sum*, 2020.

[7] P. Baker, O. Chartier, R. Haffner, L. Heidecke, K. van Hussen, L. Meindert, B. P. Oberč, K. Ryszka, P. Capros, A. De Vita, *et al.*, *Research and Innovation perspective of the mid-and long-term Potential*

for Advanced Biofuels in Europe. European Commission, Directorate-General for Research and Innovation, 2017.

[8] S. van Dyk Et al., "Drop-in biofuels: The key role that co-processing will play in its production," *IEA Bioenergy*, 2019.

[9] "NBN EN 590:2013+A1:2017." `https://www.nbn.be/data/r/platform/frontend/detail`, October 2017.

[10] J. B. Heywood, *Internal combustion engine fundamentals.* McGraw-Hill Education, 2018.

[11] A. C. D.-. on Petroleum Products and Lubricants, *Standard test method for cetane number of diesel fuel oil.* ASTM International, 2005.

[12] N. Bezaire, K. Wadumesthrige, K. S. Ng, and S. O. Salley, "Limitations of the use of cetane index for alternative compression ignition engine fuels," *Fuel*, vol. 89, no. 12, pp. 3807–3813, 2010.

[13] D. ASTM, "6890 standard test method for determination of ignition delay and derived cetane number (dcn) of diesel fuel oils by combustion in a constant vol," *American Society for Testing and Materials (ASTM)*, 2011.

[14] N. Ladommatos and J. Goacher, "Equations for predicting the cetane number of diesel fuels from their physical properties," *Fuel*, vol. 74, no. 7, pp. 1083–1093, 1995.

[15] D. Assanis, Z. Filipi, S. Fiveland, and M. Syrimis, "A predictive ignition delay correlation under steady-state and transient operation of a direct injection diesel engine," *Journal of Engineering for Gas Turbines and Power-transactions of The Asme - J ENG GAS TURB POWER-T ASME*, vol. 125, 04 2003.

[16] R. B. Pešić, A. L. Davinić, and S. P. Veinović, "New engine method for biodiesel cetane number testing," *Thermal Science*, vol. 12, no. 1, pp. 125–138, 2008.

[17] H. Ogawa, A. Morita, K. Futagami, and G. Shibata, "Ignition delays in diesel combustion and intake gas conditions," *International Journal of Engine Research*, vol. 19, no. 8, pp. 805–812, 2018.

[18] F. vom Lehn, L. Cai, R. Tripathi, R. Broda, and H. Pitsch, "A property database of fuel compounds with emphasis on spark-ignition engine applications," *Applications in Energy and Combustion Science*, vol. 5, p. 100018, 2021.

[19] Y. Kobashi, M. Todokoro, G. Shibata, H. Ogawa, T. Mori, and D. Imai, "Egr gas composition effects on ignition delays in diesel combustion," *Fuel*, vol. 281, p. 118730, 2020.

[20] H. Hardenberg and F. Hase, "An empirical formula for computing the pressure rise delay of a fuel from its cetane number and from the relevant parameters of direct-injection diesel engines," *SAE Transactions*, pp. 1823–1834, 1979.

Contents

List of Figures

List of Tables

Nomenclature

Abbreviations

CO_2	Carbon dioxide
2G	Second generation
NOx	Nitrogen oxide
AD-LIBIO	Advanced liquid biofuels
AFR	Air-to-fuel ratio
ASI	After start of injection
ASTM	American Society for Testing and Materials
ATDC	After top dead center
BEV	Battery electric vehicle
BMEP	Break mean effective pressure
BTDC	Before top dead center
CA	Crank angles
CA10	Crank angle corresponding to 10% of the fuel fraction burned
CA2	Crank angle corresponding to 2% of the fuel fraction burned
CA5	Crank angle corresponding to 5% of the fuel fraction burned
CAS	Combustion Analysis System
CFR	Cooperative Fuel Research
CI	Compression ignition
CN	Cetane number
CR	Compression ratio
CRDI	Common rail direct injection
DAQ	Data acquisition
DCN	Derived cetane number
DI	Direct injection
DOHC	Dual overhead camshaft

DP1	Crank angle corresponding to the maximum of the first derivative of the cylinder pressure
DP2	Crank angle corresponding to the maximum of the second derivative of the cylinder pressure
DP3	Crank angle corresponding to the maximum of the third derivative of the cylinder pressure
ECS	Engine Control System
ECU	Engine control unit
EGR	Exhaust gas recirculation
EN	European norm
EOC	End of combustion
EVC	Exhaust valve closed
EVO	Exhaust valve open
GHG	Greenhouse gas
HC	Hydrocarbon
HEV	Hybrid electric vehicle
HMN	Heptamethylnonane
HVO	Hydrotreated vegetable oil
ICE	Internal combustion engine
IMEP	Indicated mean effective pressure
IPCC	Intergovernmental Panel on Climate Change
IQ	Injection quantity
IQT	Ignition quality tester
IVC	Intake valve closed
IVO	Intake valve open
LCA	Life-cycle assessment
NI	National Instruments
PHEV	Plug-in hybrid electric vehicle
PRF	Primary reference fuel
SI	Spark ignition
SOC	Start of combustion
SOI	Start of injection
SRC	Short rotation coppice
TDC	Top dead center
TtW	Tank-to-Wheel

VGT	Variable geometry turbocharger	
VRV	Vacuum regulating valve	
VSV	Vacuum switch valve	
WtW	Well-to-Wheel	

Greek Symbols

γ	Ratio of specific heats	[-]
θ	Engine position	[°ca]

Roman Letters

ID	Ignition delay	[°ca]
MFB	Mass fraction burned	[%]
O_{2in}	Intake oxygen concentration	[vol%]
HRR	Heat release rate	[J/°ca]

Part I

Literature study

Chapter 1

Introduction

"Climate change affects us all", is the conclusion drawn from the sixth assessment report of the Intergovernmental Panel on Climate Change (IPCC) [1]. The effects accelerate and become more extreme every year: the amount and duration of heat waves have tripled since the 1960s, the rising sea levels are threatening coastal areas, and the changing ecosystem influences the behavior and amount of wild species left on our planet [2, 3, 4]. Human activity has been confirmed to be the main cause of global warming [5]. Large-scale research efforts are aimed at reducing our carbon intensity. This thesis dissertation considers the role of transportation in the energy transition, with a strong emphasis on short-term solutions for Diesel engines. The focus is sustainable fuels for current state-of-the-art engines and methods to estimate their suitability. This is important since these fuels have the potential to significantly reduce carbon dioxide (CO_2) and hydrocarbon (HC) emissions [6].

1.1   The rise of CO_2

The planet is constantly interacting with its atmosphere through animal respiration, human activity, agriculture, etc. These activities generate energy from biomass by consuming or burning it. Carbon compounds are released as CO_2 and become widely available in the atmosphere, where they can again be absorbed by plants via photosynthesis or by ocean surfaces. The global use of fuels, chemicals, plastics, and other materials with fossil origins has brought this circularity of the biosphere in imbalance. To reduce the risk of biodiversity loss, more extreme weather, and food crises, policymakers and industry must focus on measures that stabilize the Earth's temperature. Recent studies demonstrate that the Paris agreement's aim of limiting global temperature rise to 1.5 ℃ above pre-industrial levels has become infeasible due to inadequate action taken by all agreeing parties [7]. Without additional measures, Earth's temperature will increase with 2.8 ℃ by the end of the century. Therefore, the majority of human activities need a fossil-free wake-up call, and broad modifications are necessary to reach as close to the most optimal scenario to date of 1.8 ℃ [7, 8].

Figure 1.1 shows the amount of anthropogenic greenhouse gas (GHG) emissions over the last few decades. Each GHG is represented in its CO_2-equivalent and the global fraction is shown at the end of every decade. It can be seen that the amount of GHG emissions continues to rise, with the largest fraction being CO_2 [5]. CO_2 is not the sole culprit; other greenhouse gases such as methane, which originate mostly from agriculture, but also from the production, processing, and distribution of natural gas for industry and electricity production, play a considerable part [9]. The biggest contributors to the GHG emissions are industry, electricity production, agriculture, and transport. Efforts by each and every sector are essential to prohibiting a steady rise in global temperature.
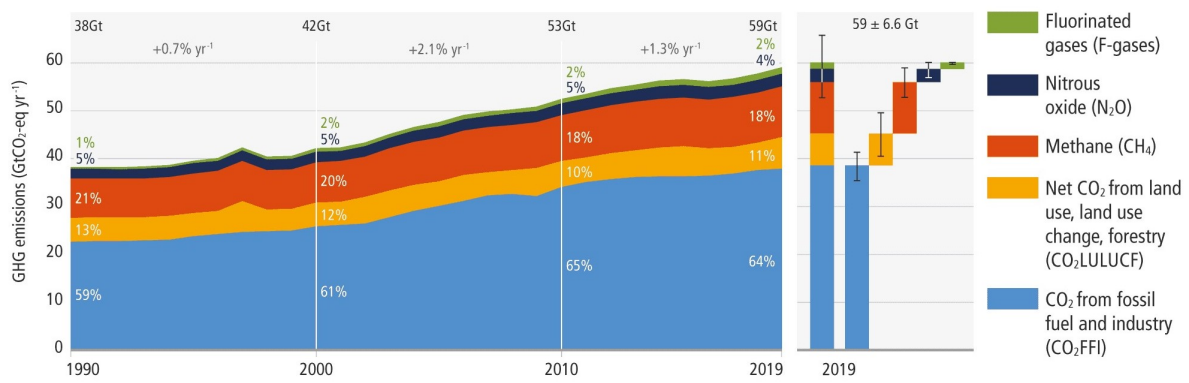
Figure 1.1: The level of global GHG emissions emitted from 1990 to 2019 in Gt CO_2-equivalent each year [5].

1.2 Focussing on transportation

Transportation is accountable for 15 % of the total GHG emissions each year and maintains a steady growth, with an annual increase of 1.8% [9]. The impact of this sector cannot be ignored. Figure 1.2 depicts the amount of GHG emissions emitted by the various transportation modes each year in gigatonnes CO_2-equivalents (GtCO$_2$eq). This clearly demonstrates that road applications are the primary pollutants in this industry.
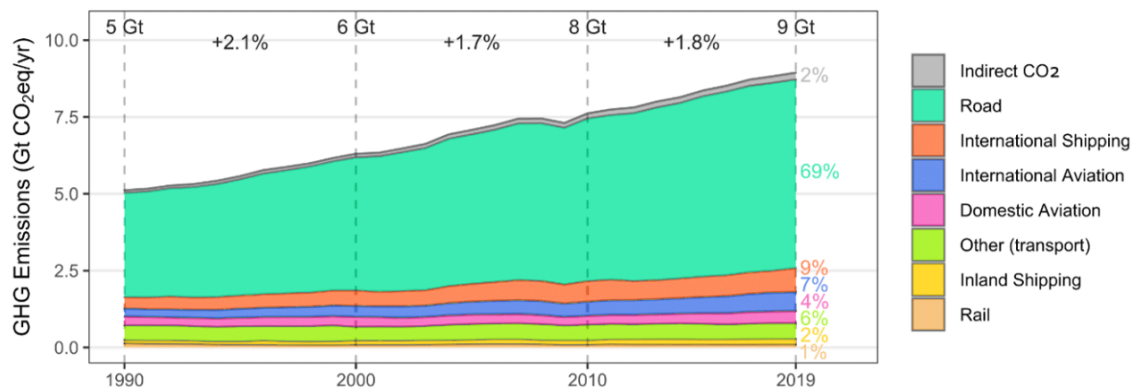
Figure 1.2: The level of global GHG emissions originating from different modes of transportation 1990-2019 in GtCO$_2$eq [5].

Currently, the world-total car fleet amounts to approximately 1.45 billion vehicles [10]. With continuously growing transport activity, it is clear that efforts to reduce the CO_2-impact of transportation are of vital importance to limiting the Earth's temperature rise.

In order to achieve this, a lot of research effort is aimed at reducing our transportation emissions by looking at different alternatives such as: electrified vehicles, new engine technology, and sustainable fuels. These aim to achieve increased efficiencies - which reduces our primary energy need-, defossilization of fuels, or both at once.

1.3 Towards renewable transportation

Clearly, significant reductions in the GHG-intensity of transportation, and other sectors, are necessary. Three general pathways for reducing transportation's impact on climate change have been identified. These are the continuous increase of energy efficiency, electrification and the development of sustainable energy-dense molecules. Figure 1.3 depicts these pathways and the order in which they should be considered.
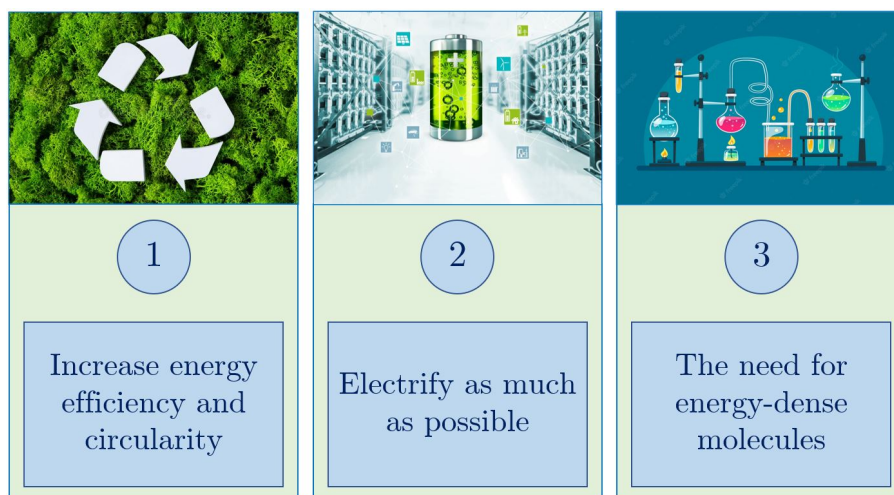
Figure 1.3: Three pathways towards a sustainable energy system.

Firstly, one should aim at increasing the efficiency of current technology and increase the circularity where possible. This reduces our primary energy needs and material consumption using well-known technology. While this is a logical step to take, in many cases, this is not enough.

Secondly, if feasible, technologies should be electrified to the greatest extent. In many cases, electrical counterparts have increased efficiency, again reducing primary energy consumption. Car manufacturers have not only gained enormous interest in battery electric vehicles (BEV) because of efficiencies of up to 85 %, but also because of new legislation, approved by the European Commission, to promote the production of nearly zero tailpipe emission vehicles [11, 12]. As current regulation is based on Tank-to-Wheel (TtW) emissions, upstream GHG emissions resulting from power generation and raw material mining are not taken into account. This makes the current certification method beneficial for BEVs, as they do not possess any tailpipe emissions. It is critical to understand that the consequences of global warming do not scale with TtW emissions, but rather with well-to-wheel (WtW) emissions, which include the impact of a product from material extraction until disposal.

Thirdly, it is important to recognize that people generally buy vehicles to last 8 to 11 years [13]. Figure 1.4 represents a forecast of the global amount of internal combustion engine (ICE), BEV, fuel cell electric, and plug-in hybrid electric vehicles (PHEV) by the year 2040.
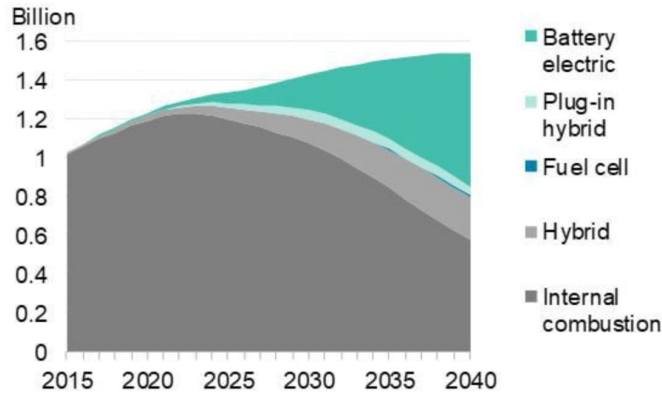
Figure 1.4: A forecast of the global long-term passenger vehicle fleet by drivetrain up to 2040 [14].

Clearly, the legacy ICE vehicle fleet remains to have a large share in the years to come, and BEVs alone will not reach climate neutrality by 2050. Besides passenger cars, it should be considered that not all transportation applications can be electrified. Long-distance shipping and aviation require energy densities which are not achievable with electrification [15]. This illustrates the need for a pathway of sustainable fuels with high energy density, storability, and transportability for years to come. These sustainable fuels are not defined unilaterally, and therefore, several production pathways exist, using green electricity, biomass, or a combination of both. Electrofuels and biofuels are both examples of sustainable fuels. While electrofuels, also known as e-fuels, are made from green hydrogen and CO_2, biofuels, particularly second-generation biofuels, are made from non-food crops or waste products [16, 17, 18].

To gain a sense of the impact of the various engine technologies available today, Figure 1.5 provides a WtW comparison between a hybrid electric vehicle (HEV), plug-in hybrid vehicle (PHEV), and BEV considering the CO_2-intensity of the electricity mix of 2020. The ICE is considered to run on gasoline, Diesel[1], E85 (85 % ethanol and 15 % gasoline) or hydrotreated vegetable oil (HVO), which is a second-generation biofuel (discussed in Section 2.2.2). The horizontal line indicates the target goal: the limit of 95 gCO_2/km emissions set by the European Commission [20].
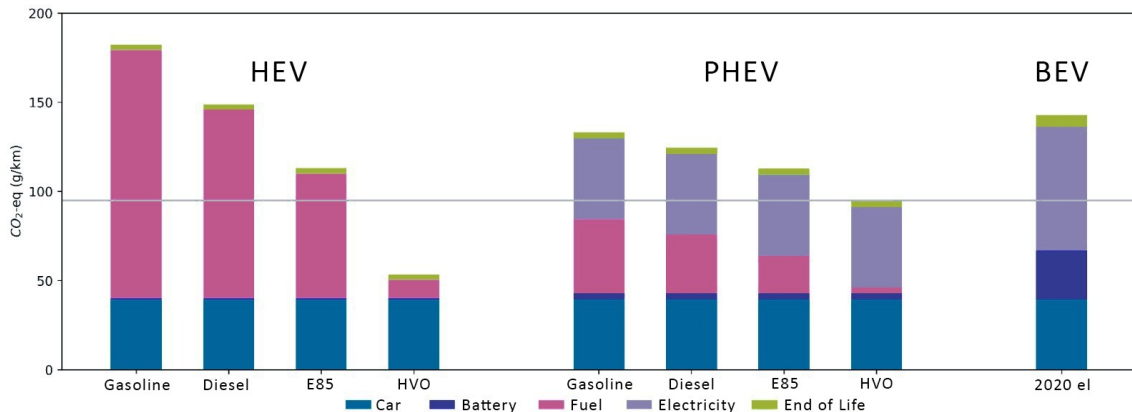
Figure 1.5: A comparison of the WtW life cycle emissions of a passenger car using different drivetrains and fuels expressed in $g\text{CO}_2$eq/km, considering the 2020 electricity mix [12, 19].

---

[1]The original study by Andersson [12] does not include Diesel fuel. As this work focuses on CI engines, a data figure for Diesel fuel is added. The WtW CO_2-emissions for Diesel in a comparable vehicle are used by Thiel et al. [19]. The CO_2-emissions of Diesel are scaled with the HVO case, based on WtW emissions.

It is apparent that HEVs running on gasoline or Diesel are the worst emitters of CO_2 due to the high emissions during the use phase of their life cycle. However, a BEV is the worst emitter of the renewable solutions due to the energy-intensive process of producing lithium-ion batteries [21]. Furthermore, fossil fuels still account for roughly 60 % of global electricity generation [22]. The best results are obtained for a HEV running on HVO, which is able to meet the 95 gCO_2eq/km with a factor two. Andersson et al. claim that until now, the global warming reduction potential of biofuels is estimated to be bigger than electrification, since current electricity production still has a relatively high CO_2-intensity[2][12].

For this reason, the pathway of sustainable fuels will be emphasized in this work. Significantly lower GHG-emissions can be achieved if these fuels are produced and consumed wisely. Both e-fuels and biofuels have been mentioned as potential paths to sustainable fuels. E-fuels have the potential to store renewable energy but are a novel technology, which will require time and investments to become affordable and widely available [16, 17]. Biofuels, on the other hand, are a more established technology and have the potential to be a low-carbon fuel [23]. The IEA points biofuels out as a crucial pathway to climate change mitigation [24].

In particular, the adoption of sustainable fuels, such as HVO and AD-LIBIO, have the potential to significantly improve the sustainability of the vehicle fleet. Such fuels, which are functionally equivalent to petroleum fuels and are compatible with existing petroleum infrastructure are better known as drop-in fuels [25, 26]. These allow to increase the sustainable fraction of fuels utilized in existing engine technology and thus allow for a rapid reduction in transportation GHG-intensity. The latter can be seen as a combination of pathways one and three, as the introduction of new fuels in present-day engines may also result in increased efficiencies.

1.4   Aim of this thesis

This thesis work is framed within the advanced-liquid biofuel (AD-LIBIO) project. This is a research project, funded by the Belgian Energy Transition fund, which aims at the development of a second-generation biofuel. The goal of the project is to investigate the potential of the AD-LIBIO fuel blend as a drop-in fuel in compression ignition (CI) engines.

The preceding highlights the importance of continued research on ICE technology in combination with sustainable fuels, which will be the topic of this master thesis. The aim of this thesis is to estimate the cetane number (CN) using a state-of-the-art production Diesel engine, instead of a dedicated research engine. The CN is often seen as the quality of a Diesel fuel. This allows to evaluate the drop-in capability of newly developed sustainable fuels in conditions representative of current engine practice. An alternative cetane rating method is explored and evaluated using a number of fuel blends with a known (CN). The goal of the testing method is to eventually estimate the CN of sustainable fuels during the development phase, like the AD-LIBIO fuel, using this production engine.

The next chapter describes the development of classic and modern CI engine technology, in order to understand the behavior of different fuels and their properties inside a CI engine. This is followed by an in-depth review of the current cetane rating methods in use today.

---

[2]The analysis states no negative indirect land-use changes using 2G biofuels. This assumption may have large consequences on the outcome of the analysis and thus further investigation is still required.

Chapter 2

Compression ignition engines

2.1 The basic operating principles

It is vital to have a basic understanding of the operating principle of compression ignition (CI) engines and the mechanisms behind the ignition process of the fuel. This section goes over the working principles of a CI engine.
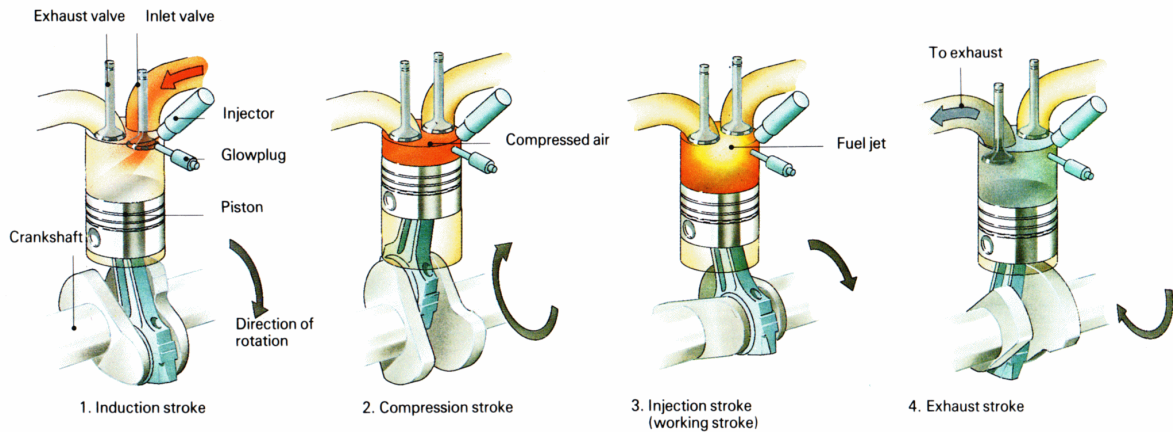
Figure 2.1: A schematic representation of the four-stroke compression ignition cycle [27].

Figure 2.1 illustrates the typical four-stroke direct injection (DI) compression ignition cycle. The first engine stroke comprises the intake of air (1). During the compression stroke (2), the air is compressed. Towards the end of the compression, fuel is injected directly into the cylinder via a single injector [28]. The fuel jet breaks up into small droplets which evaporate and form a flammable fuel-air mixture. This mixture ignites if the temperature in the cylinder remains above the autoignition temperature of the mixture (3). The cylinder pressure rises as a result of the combustion, generating a downward force on the piston, which rotates the crankshaft. This conversion of fuel-bound chemical energy to mechanical energy occurs during the power or working stroke. Finally, the upwards movement of the piston drives out the reaction products through the exhaust valves during the exhaust stroke (4), after which the process repeats.

The complete process of injection, atomization, and evaporation of the fuel has to occur around top dead center (TDC) and thus a limited amount of time is available. This requires fast injection and proper atomization to achieve a sufficiently rapid mixture formation [28, 29]. The cylinder pressure rise due to combustion does not occur immediately after the start of

injection (SOI). There is a distinct ignition delay period between the SOI and the manifestation of significant pressure rise and heat release, as indicated in Figure 2.2. This ignition delay is often conceptually separated into a physical ignition delay and a chemical ignition delay. The former comprises the time required for fuel atomization, evaporation, mixing and heating, while the latter consists of the time required for preflame combustion reactions. In comparison to the combustion reaction, these preflame combustion reactions are relatively slow. In reality, no clear separation can be made between these processes, as they occur partly simultaneously. After the ignition delay period, autoignition occurs simultaneously at multiple points across the Diesel jet. This results in a fuel-rich premixed or uncontrolled combustion phase due to the sudden combustion of accumulated vaporized and mixed fuel. Subsequently, the combustion transitions into a mixing-controlled phase, where the fuel burning rate is limited by the rate at which fuel is properly vaporized and mixed with air. The combustion event is concluded with a late combustion phase after the end of injection [30, 31, 32, 33].
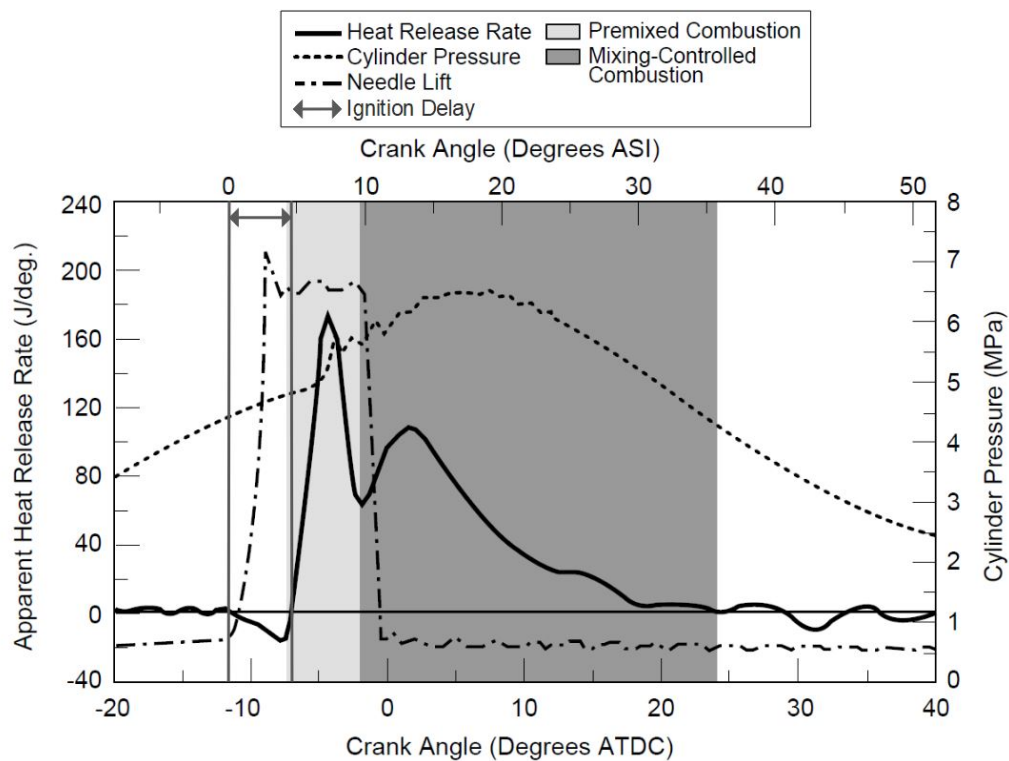
Figure 2.2: A typical pressure trace and heat release rate for a DI Diesel engine plotted against the engine position in degrees after TDC (ATDC) and after start of injection (ASI). Adapted from [34].

A CI engine differs from a spark ignition (SI) engine in several ways. Because Diesel engines are not knock-limited, higher compression and improved efficiency are possible. Furthermore, qualitative load control is accomplished through the amount of fuel injected into the cylinder, whereas SI engines employ a throttle valve. This results in a higher part-load efficiency of CI engines compared to SI engines [27]. Given their high power density and efficiency, CI engines are currently used in heavy-duty applications and will continue to be an important drive in applications that cannot be electrified [35].

The main drawback of a CI engine is their trade-off between emissions of soot and nitrogen oxides (NO_x). Road transportation was responsible for more than 36 % of NOx and 10 % of soot emissions in 2018. It is estimated that road transport is the cause of 70 000 premature deaths in Europe in 2018 [29, 36, 37]. The characteristic NOx-soot trade-off of CI engines increases the difficulty of emission optimization, as measures to decrease NOx-production (often through

exhaust gas recirculation) typically increase soot production [29, 38]. However, modern after-treatment systems have lowered the tailpipe emissions of both NOx and soot significantly, but remain to be more complex and expensive compared to SI.

2.2 Fuel requirements

2.2.1 Diesel norm

Fuels for CI engines need to comply with the EN590 fuel norm to be allowed on the market. Some key properties of this norm are listed in Table 2.1. The cetane number is essential for the engine to run properly and will be discussed more in-depth in Ch. 3. Furthermore, limits are posed on the amount of contaminants, oxidation stability, distillation curve etc. These properties will not be discussed in greater detail, as this falls outside the scope of this thesis.

Table 2.1: A listing of some key properties specified in the EN590 fuel norm [39].

Property	Units	Limits	
		Min	Max
Cetane number	[-]	51	-
Cetane index	[-]	46	-
Density at 15°C	$[kg/m^3]$	820	845
Flash point	$[°C]$	55	-
FAME content	[vol%]	-	7
Lubricity	$[\mu m]$	-	7
Viscosity at 40°C	$[mm^2/s]$	2	4.5

Flow properties of a fuel, such as density and viscosity, largely impact the spray formation in a Diesel engine, and hence affect the ignition delay of the fuel. Knowledge of the operating principle of CI engines indicates that this spray formation is paramount for proper engine operation and emission control.

A lower viscosity improves the mixing of the fuel and air, which reduces the physical ignition delay period [40]. However, the effects of viscosity on the ignition delay were found to be minimal at warm engine operating temperatures, and only the spray formation was impacted. [27]. Both density and surface tension are seen as key factors which determine the droplet size of the fuel after injection, and may influence the atomization of the fuel. Lower density and surface tension result in a decrease in ignition delay [41]. It should be noted that other factors (such as molecular structure, heat of evaporation, etc.) that affect the ignition delay are included in the cetane number, but are not specified in the Diesel norm [39].

The flash point of a liquid fuel is the lowest temperature at which the presence of a flame close to the liquid surface results in a frame propagating over this surface. This corresponds to the temperature at which the mixture of air and fuel vapour above the fuel surface exceeds the lower flammability limit of the fuel [42]. In terms of engine operation, a low flash point is desired as ignition will occur more rapidly. However, the fuel norm poses a lower limit on the flash point out of safety considerations.

The high-pressure Diesel fuel pumps in CI engines are lubricated mostly by the fuel itself. In the past, only viscosity limits were imposed, without specification of the lubricity. As premature engine failure occurred due to changes in the production process of Diesel, lubricity has been included in the Diesel norm and lubricity-improving additives are being added [43].

2.2.2 Drop-in fuels

Substituting current, fossil, fuels with fuels that have a higher sustainable fraction can rapidly increase the sustainability of the legacy fleet, as explained in Section 1.3. Such fuels are called drop-in fuels, as they do not require modifications to the engine hardware or software before their adoption [44]. These fuels must meet the Diesel standard before they may be used in today's CI engines. The following paragraphs provide a brief overview of the sustainable fuels relevant to this work.

Hydrotreated vegetable oil

Hydrotreated vegetable oil (HVO) is a second-generation (2G) biofuel produced from waste, residue oils and fats [45]. HVO is a drop-in fuel for CI engines: pure HVO (HVO100) or any blend with Diesel complies with the Diesel standard and can be used in current CI engines without any modifications to hardware or software [46]. This property along with the high CN, reduced emissions, and outstanding cold-weather performance makes HVO an appealing solution for Diesel vehicles [47].

The significant reduction in emissions using this 2G biofuel has already been pointed out in Figure 1.5. Researchers state that a BEV will not be able to emit fewer pollutants than an HVO-fueled Diesel car until 2050 [12]. The main obstacle to the HVO production process is the hydrotreating process, i.e. adding hydrogen, which is expensive and may result in additional emissions if the hydrogen is produced in an unsustainable manner [48].

AD-LIBIO

The AD-LIBIO fuel blend is a cellulosic 2G biofuel derived from short rotation coppice (SRC). SRC is a collection of fast-growing tree species, usually grown with the aim to deliver large biomass yields within a short time period [49, 50].

Cellulose is extracted from the feedstock, which is subsequently catalytically converted into a mix of naphta-like molecules and oxygenates. Green hydrogen can be used in the process to reduce the amount of oxygenates and increase the volumetric energy density. This results in a hybrid process combining green carbon from biomass and green hydrogen [51]. Lignin-based fuels may also be developed

At this time, the AD-LIBIO blend's composition is not suitable for use in a CI engine. The goal of this thesis, on the other hand, is to investigate a novel cetane rating method that will eventually estimate the CN of this newly developed sustainable fuel in the future.

Chapter 3

Cetane number

This chapter gives a more in-depth discussion of the cetane number since it will play a predominant role in this thesis dissertation. The importance of the cetane number will be elaborated, followed by a discussion of the different measurement methods.

3.1 Importance of the cetane number

As explained in Section 2.1, the time required for a Diesel jet to atomize, evaporate, mix and autoignite accumulates in an ignition delay (ID). The cetane number (CN) is a quantitative measure for the readiness to autoignition of a fuel under the process of compression ignition, and is related to the ID [52]. It is often thought of as the quality of a Diesel fuel. Short IDs are desirable in a Diesel engine.
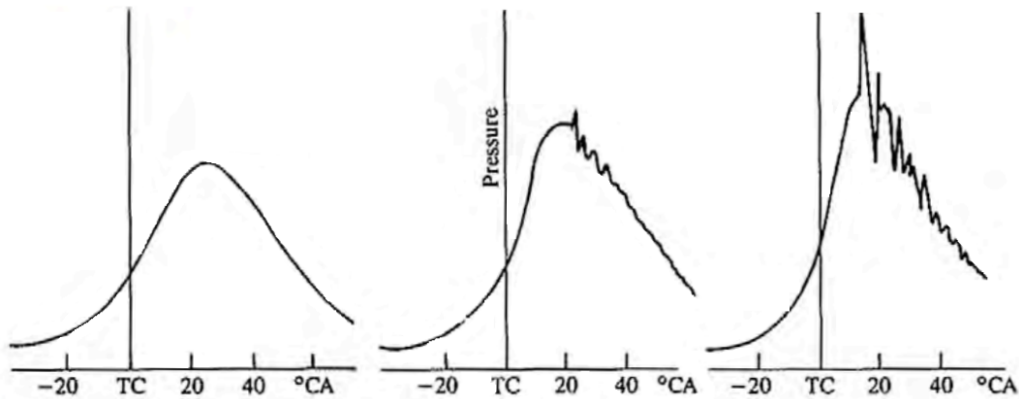
Figure 3.1: A Diesel engine pressure trace under normal conditions (left) and severe knocking (right) [53].

Fuels with a low CN exhibit a higher auto-ignition resistance and thus a longer ID. This leads to an accumulation of fuel before the combustion process starts, resulting in a violent premixed combustion phase. This is characterized by a large pressure rise followed by pressure pulses, as shown in Figure 3.1. This leads to a distinct knocking sound, often called Diesel knock [29, 54]. Diesel knock gives rise to excessive noise, reduced engine lifetime, and low thermal efficiency [54]. For exceptionally low CN fuels, autoignition only occurs well in the expansion stroke, resulting in combustion quenching. This leads to incomplete combustion, with a reduced power output as a consequence [29].

Fuels with a higher CN ignite soon after the start of fuel injection into the cylinder. The rate

of heat release and pressure rise are controlled mainly by the fuel injection rate and the mixing with combustion air. This results in smooth engine operation, reduced tailpipe emissions, low noise levels, and an increased fuel economy [29, 54]. Lastly, the importance of the ID, and thus the CN, increases with engine speed.

Since it has become clear that the long-term supply of conventional petroleum-based fuels will be challenging and that emission regulations are tightening over time, the use of sustainable fuels in CI engines (such as HVO) has increased considerably [55]. The composition of these fuels can differ from that of conventional fuels, which may have an impact on the CN. Some CN measurement techniques, which will be discussed in the following section, fail to capture the effect of these different fuel compounds on the CN, resulting in an incorrect estimation of the CN [54]. As the percentage of sustainable fuels grows, it is critical to be able to accurately measure the CN of these fuels.

3.2 Cetane number measurements

During the search for sustainable Diesel fuels, adequate measurement methods of the cetane number are critical. Since this thesis aims to develop an alternative cetane rating method, the existing conventional tests will be discussed, together with some novel methods. The conventional tests are standardized by the American Society for Testing and Materials (ASTM).

3.2.1 ASTM D613

The ASTM D613 is the oldest standardized method for measuring the CN. This method makes use of a Cooperative Fuel Research (CFR) engine, shown in Figure 3.2a, which is a single-cylinder Diesel engine with a variable compression ratio. Each fuel with a different CN shows a different ID in the engine. The compression ratio of the engine is manipulated to achieve a fixed ignition delay of 13 °ca for any given fuel. The other engine conditions (speed, valve timing, intake air temperature, injection pressure, etc.) are kept constant during the test [56].

(a) The CFR Engines Inc. Cetane Rating Unit [57].

(b) Totally Automated Laboratory Model of a Ignition Quality Tester apparatus [58].

Figure 3.2: Test equipment for the a) ASTM D613 and b) ASTM D6890 standards.

In order to derive the CN of the test sample, the notion of primary reference fuels (PRFs) and their blends should be introduced. The primary reference fuels n-cetane and heptamethylnonane (HMN) have a CN of 100 and 15 respectively, by definition. Any blend of these two components results in a CN which scales with the volumetric proportions of the mixture:

$$CN = \%n\text{--}cetane + 0.15(\%HMN) \tag{3.1}$$

The CN of the tested fuel sample is determined by comparing the compression ratio obtained during the test, to the compression ratio for the corresponding blend of n-cetane and HMN. Figure 3.3[1] shows the influence of the cetane number and compression ratio on the ignition delay in a Diesel engine.[2] Lower CN fuels require a higher compression ratio to achieve a given ID.

---

[1]The measurements represented by Figure 3.3 do not originate from the CFR engine, but the trend is universal to Diesel engines.

[2]The compression ratio is expressed as a reduction ϵ with respect to a value of 21.3.
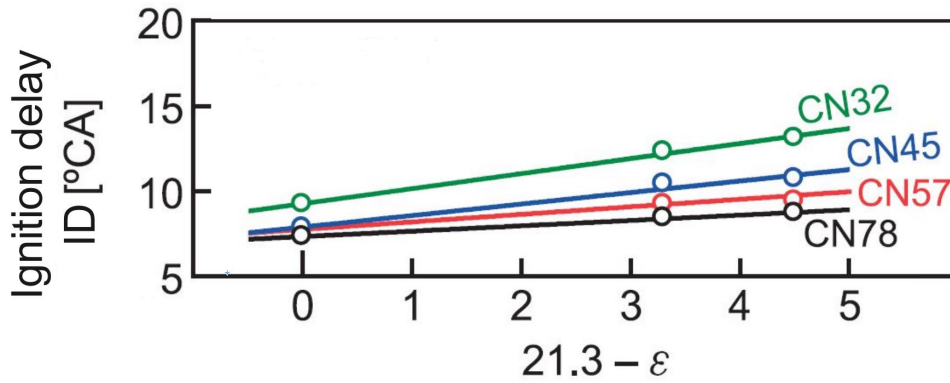
Figure 3.3: The relationship between the ignition delay (ID) and compression ratio (denoted as ϵ) in a given engine for fuels with different cetane number (CN). Adapted from [59].

This method has been the standard since its invention in the 1930's, and it is to this day. However, its existence through the years has not been without criticism. Researchers have identified several issues in this cetane rating practice [32, 54, 60, 61, 62]

- The CN does not represent a fundamental fuel property: it depends on many properties such as viscosity, density, volatility, and chemical composition of the fuel. Some of these properties influence the physical ID, whereas others influence the chemical component. Since all of these properties are intricately linked by the CN, it is impossible to distinguish between a physical and chemical ID.

- The CN is only directly related to one single, specific engine. This means that the test method does not allow to determine the influence of different injection systems and combustion chambers: i.e. different engines. The CFR engine does not represent the architecture of current state-of-the-art Diesel engines[3]. Different engine designs are sensitive to different fuel properties. The ID in the CFR may be heavily influenced by a specific fuel property, whereas it is not in another engine.

- The CN does not show a linear relation with other fuel properties, nor with other engine performance metrics.

- The CFR method requires relatively large fuel samples (almost 1 liter), high time consumption, and operator skills, and has problems with reproducibility and repeatability.

- The CFR test engine is an expensive piece of lab equipment which only little laboratories possess.

Lewis and von Elbe stated that the knowledge obtained for CI engine practice has been built on collecting numbers on various fuels that don't really improve the understanding of the combustion process in real engines [63].

3.2.2 ASTM D6890

The disadvantages of the CFR created interest in a more reliable (i.e. high reproducibility and repeatability), automated, and cost-efficient cetane rating method. This was manifested by research towards the development of an ignition quality rating which is based on fundamental fuel properties, studied in constant-volume combustion bombs. This resulted in a new standardized method, presented in the late '90s.

---

[3]As an example, the CFR engine is equipped with an indirect injection system, whereas direct injection is standard these days.
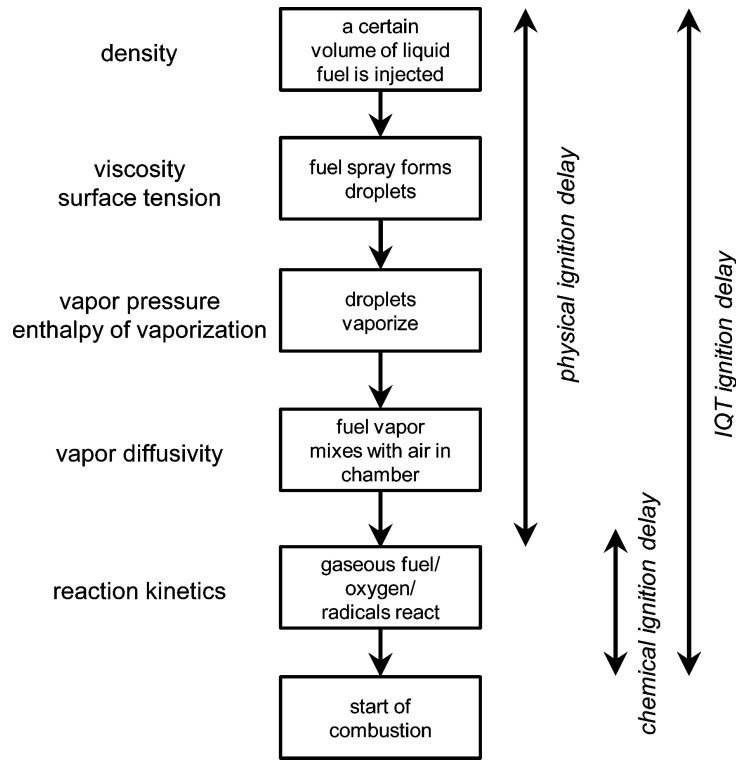
Figure 3.4: A schematic showing processes occurring in the IQT after injection until combustion [64].

The ASTM D6890 uses an alternative way of determining the CN of a fuel using an Ignition Quality Tester (IQT), shown in Figure 3.2b [65]. This apparatus consists of a constant volume chamber, which is filled with compressed hot air at specified conditions[4] [65]. A controlled amount of fuel is injected and the ID is measured. Figure 3.4 shows the processes occurring from injection to start of combustion, together with the factors influencing each process. A sequence of 32 cycles is performed, from which the ID is measured and averaged. The average ID is then used to calculate the derived cetane number (DCN) using Eq. 3.2, depending on the value of the ID [65]. The equation is stated to be less accurate if the ID falls outside the range of $3.4 - 6.24\ ms$.

$$\begin{cases} DCN = 4.460\ +\ \frac{186.6}{ID}\quad,\ ID \in\ (3.4, 6.24)\ ms \\ DCN = 88.39 \cdot (ID\ -\ 1.512)^{-0.658} + 3.547\quad,\ ID \notin\ (3.4, 6.24)\ ms \end{cases} \tag{3.2}$$

As shown in Figure 3.5, the relationship between DCN and CN is, as expected, linear. It is not, however, a unity (DCN = CN) relationship.

---

[4]As with the previous cetane measurement method, the intake air temperature and pressure, and coolant temperature are all specified in the norm
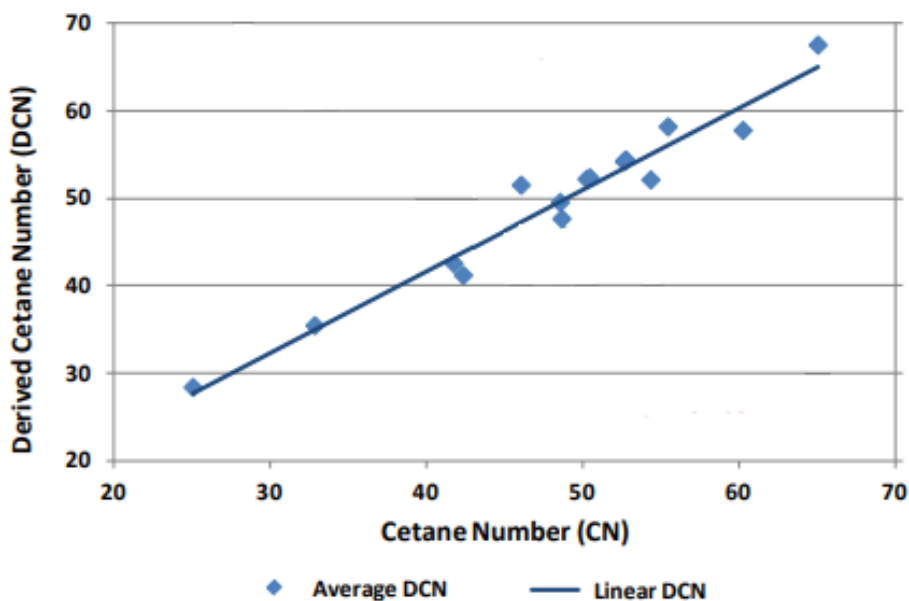
Figure 3.5: A comparison of the cetane number (CN) and derived cetane number (DCN), acting as a validation of the IQT method compared to the CFR engine. Adapted from [66].

The main advantages of using an IQT are the reduced test complexity, higher repeatability, lower fuel requirements (50 mL), and the potential of determining the CN number of a fuel with high sensitivity (0.1 ms/CN) [33, 67]. The IDs are similar to those observed in real CI engines as this method is able to mimic the conditions and process of combustion. It is also possible to evaluate the ID of cetane-improved fuels. From the above, one can conclude that the IQT gives a reliable and fast determination of the CN number, and can be seen as a worthy complimentary to the CFR engine.

Nonetheless, the CN is not a fundamental fuel property, but is dependent on fuel properties and engine design in a non-linear way. The volume of the IQT remains constant during combustion, which differs from the varying volume in an engine. As stated before, the CN of a fuel is highly related to the ID, which can conceptually be split into a physical and chemical part. The chemical reaction kinetics that occurs may be sped up during further compression, resulting in faster combustion. Therefore, some fuel properties which are incorporated in the CN, that are sensitive to engine design, are not taken into account in the IQT method and may result in a reduced accuracy of the CN estimation [32].

3.2.3   Numerical CN estimation methods

Next to experimental CN rating methods, numerical alternatives may provide efficient estimations. Firstly, a cetane index uses a correlation based on physical properties of the fuel and is used only when a test engine or IQT for evaluating the CN rating is not available [54]. These correlations however are only valid under limited circumstances and for certain types of molecules. This is to be expected since there is no direct and universal correlation between physical properties and autoignition behavior. A wide variety of correlations is required for different fuel types. The most generally used cetane indices are ASTM D4737 and ASTM D976, but there are other equations available in the literature [68].

As these correlations are based solely on physical properties (density, boiling point, etc.), they do not account for the chemical composition of the fuel. As a result, fuels with approximately the same physical properties will have a similar CN according to the cetane index. In practice however, fuels encompass a wide range of components that alter the CN chemically (e.g. trace

amounts of cetane improvers have a negligible effect on the physical properties, but will increase the CN significantly) [69].

Despite the numerous cetane indices available in the literature, these are all derived for a specific group of fuels. Their predictive capability is fairly poor when these equations are applied to alternative Diesel fuels, which are not utilized in the model's development. Attempts were made to develop more generally applicable cetane index calculators. These show a better predicatbility than that ASTM standardized cetane indices, but have the tendency to underpredict the CN [70, 71]. Unfortunately, current attempts are only applicable to fossil fuels, and in the absence of cetane improvers.

Besides correlations based on physical properties, methods are proposed which incorporate the molecular structure of a fuel [72]. In contrast to the development of more elaborate CN models, others explore the possibilities of neural networks [73, 74]. Early attempts allow a higher accuracy than multiple linear regression models [75]. Such networks may prove to be more effective in estimating the complex behavior of the cetane rating.

Part II

Measurements & Analysis

Chapter 4

Experimental Setup

This work aims to conduct cetane rating tests using a state-of-the-art production common rail direct injection (CRDI) Diesel engine. Figure 4.1 gives a front view on the test bench, showing the engine (1), the torque meter (2), the emission cabinet (3) and the engine control and data acquisition (DAQ) equipment (4). This chapter discusses the engine and its main components, the hardware backbone of the DAQ system and finally the software and engine control.
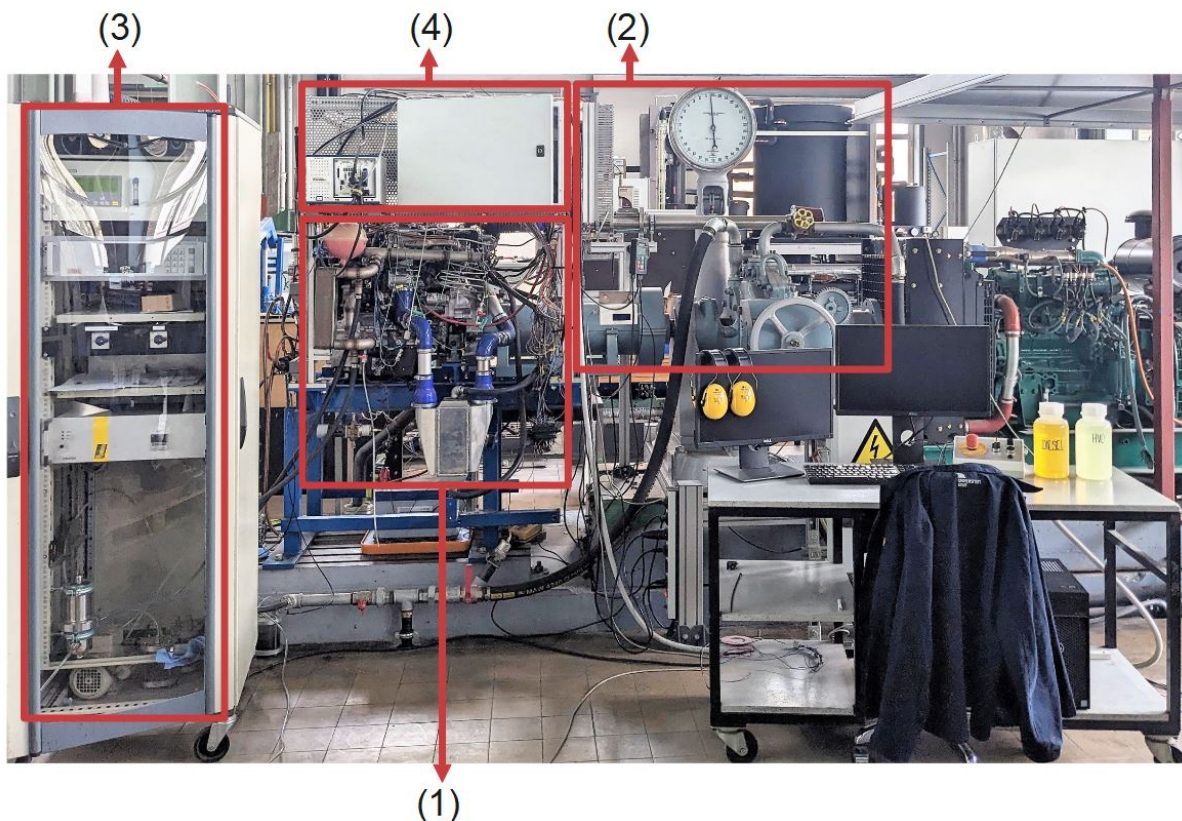
Figure 4.1: An overview of the Toyota 4D4 test bench showing the engine (1), the torque meter (2), the DAQ system (3) and emission cabinet (4).

4.1   Toyota 4D4 engine

The Toyota 1AD-FTV D4D is a EURO IV Diesel engine produced for the Toyota Avensis and Corolla models from 2005 until 2019. It is equipped with typical features of modern Diesel

engines: 4 in-line cylinders, 4 valves per cylinder with a dual overhead camshaft (DOHC), an electric common-rail direct injection system (CRDI), an intercooled variable geometry turbocharger (VGT) and an exhaust gas recirculation (EGR) system with EGR an cooler. The exhaust aftertreatment system of the engine is not focused on in this thesis, and will not be further discussed. The main properties of the engine are listed in Table 4.1.

Table 4.1: Main Toyota 1AD-FTV D4D properties.

Engine property	Value
Bore [mm] x Stroke [mm]	86.0 x 86.0
Displacement volume [cm^3]	1998
Number of cylinders	I4
Firing order	1 - 3 - 4 - 2
IVO (°ca) - IVC (°ca)	2 BTDC - 31 ABDC
EVO (°ca) - EVC (°ca)	51 BBDC - 2 BTDC
Compression ratio	15.8:1
Max torque	310 Nm at 2000 rpm
Fuel system	Electric common-rail direct injection
Camshaft	Dual overhead camshaft

4.1.1 Fuel system

The engine is equipped with an electronic CRDI fuel system. The system allows for fuel pressures between 250 bar and 2000 bar. A pressure sensor allows to control the rail pressure using a PID controller through the NI control system. This controller may still be tuned to achieve a more stable rail pressure, as currently pressure oscillations occur occasionally. Denso G3 type piezo injectors allow rapid high-pressure fuel injections into the combustion chamber. The high response time of these piezoelectric injectors allow for up to seven separate injections per cylinder stroke, again electronically controlled through the ECU.

The fuel lines leading to the engine have been rerouted this year in order to reduce the volume of the system to a minimum. This reduces the amount of fuel that needs to be flushed when switching between different fuels.

4.1.2 Air flow path

Figure 4.2 shows a schematic of the air flow path with its main components and sensor measurements. It is important to state the air flow path of the engine since the alternative cetane rating method developed in this work relies on the use of EGR.
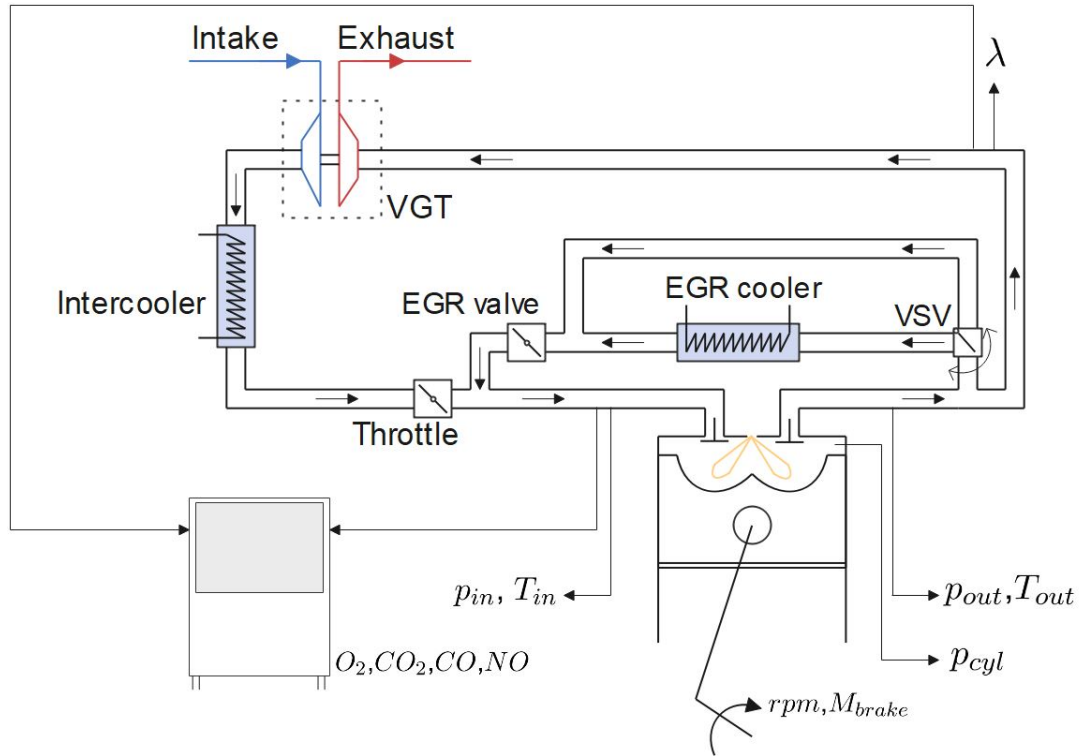
Figure 4.2: A schematic representation of the air flow path in the engine with the main components and measurements.

Fresh intake air passes through the compressor stage of a variable geometry turbocharger (VGT). A vacuum regulating valve (VRV) changes the inlet nozzle angles of the turbine, allowing to control the amount of compression of fresh intake air. The charged air subsequently flows through a water-cooled intercooler to compensate for the increased temperature during compression. The exhaust gases flow over the turbine stage of the turbocharger before passing to the aftertreatment system. The VGT allows for boost pressures up to $150 - 170kPa$.

The engine is also equipped with a high-pressure EGR loop with EGR cooler. The cooler can be bypassed using a vacuum switch valve (VSV), controlled by a switch on the start box of the engine. This can be done to prevent excessive EGR cooling at low loads. The intake line is also fitted with a throttle valve, serving two functions. Firstly, the throttle valve allows smooth engine shut-off, but secondly also serves a role in the EGR loop. Restricting the flow of fresh air through the intake line allows to feed more EGR gases to the intake manifold. Figure 4.3 indicates to position of the main components in the air flow path and fuel system of the engine.
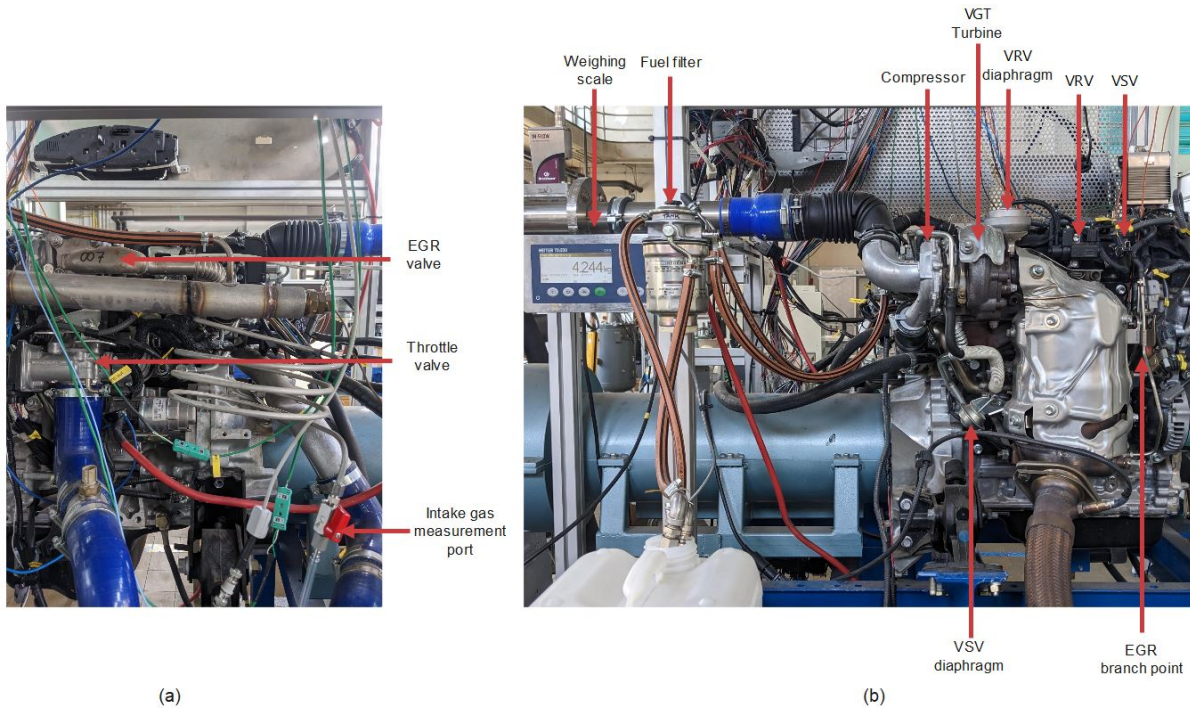
Figure 4.3: An overview of the main components in the air flow path and fuel system on the intake side (a) and exhaust side (b) of the engine.

4.1.3 Gas analyzer

A Siemens Ultramat 23 gas analyzer is used to obtain measurements of the CO_2, CO, NO_2, NO and O_2 content of the intake or exhaust stream of the engine. The measurement cabinet is also equipped with a NO_2-NO converter. This allows the gas analyzer, which only measures the NO-concentration, to determine the total NOx emissions. The gas analyzer is located left of the engine bench on Figure 4.1, and is shown schematically in Figure 4.2. The analyzer has maximum measurement ranges of 0-100vol% CO_2, 0-5vol% CO, 0-5000 ppm NO and 0-25vol% O_2, with a resolution of 0.01 and an error of 1% of the set measurement range. Setting the measurement range to the lowest value possible for ongoing experiments maximizes the accuracy. The cabinet also shows a measurement of the flow rate of gas through the system, using a floating ball flow meter. Before every measurement, it should be checked whether the flow rate drops to zero when closing off the intake line. If not, the system is not airtight and incorrect measurements are obtained.

4.2 Data acquisition and engine control

The engine test bench is fitted with a National Instruments Powertrain Control System for engine control and data acquisition. This section briefly discusses the software programs, combustion analysis equipment and current engine maps. The hardware and software used for the engine control and DAQ is described more elaborately in the user manual of this test setup.

4.2.1 PC and RT software

The engine control and DAQ software consists of a modified version of the Engine Control System (ECS) Example Software. The project is constructed for RT target and FPGA based engine control for the majority of modern engine features, such as variable valve actuation, variable geometry turbochargers, multi-pulse injection strategies, throttle and EGR valve actuation, etc.

The user can control and monitor the engine by aid of graphs, engine maps, sensor calibrations, etc. based on a continuous exchange of data between the PC and the National Instruments (NI) hardware. The software was customized to the specifications of this engine by De Geyter [76]. These adaptations will be discussed shortly in Sect. 4.2.3.

The PC also runs the NI Combustion Analysis System (CAS). In-cylinder pressure data is coupled to the measurements of the optical encoder, creating a trend of the pressure in function of the angle of the crankshaft, enabling cycle-to-cycle analysis of important combustion parameters such as the mass fraction burned, heat release rate, peak pressure, PV-diagrams.

4.2.2 Combustion analysis equipment

Additional sensors were fitted to the engine, to provide accurate information on the combustion process to be used in the CAS software. An AVL GH13P piezoelectric pressure sensor, coupled to an AVL Microifem 4G4P amplifier, measures the in-cylinder pressure of the first cylinder. The AVL amplifier can be configured using the AVL IndiSignal software installed on the test bench PC. Two Keller M5-HB type piezoresistive pressure transducers and K-type thermocouples measure the in- and outlet manifold pressure and temperature near the valve of cylinder one. A Kistler optical encoder is mounted to the engine shaft to couple measurements to the corresponding engine position with a resolution of $0.5\,°ca$. The exhaust gas line is equipped with an Innovate LM-2 lambda sensor.

4.2.3 Engine maps and control

The inclusion of additional sensors enables real-time combustion analysis using the Powertrain Control System, while each control parameter of the engine can be set to desire. De Geyter used this to provide updated engine maps enabling efficient and smooth engine operation. This work mainly focused on maps for the injection quantity (IQ) and injection timing. The latter was tuned to achieve a 50% mass fraction burned[1] at about $8-10\,°ca\,ATDC$ [76]. Besides this, the peak cylinder pressure position is kept between $10-20\,°ca\,ATDC$. The current engine maps feature a main injection only, except during start-up where a pilot injection is used [76].

Engine maps of other engine parameters were kept a simple as possible. Currently, the engine operates at 900 bar rail pressure throughout. The VGT nozzle position is not controlled by engine maps. A turn knob on the engine start box controls the VRV valve through a pulse width modulated signal. The current engine maps do not change under boost, i.e. the injection quantity remains the same under boosted conditions. De Geyter did also produce engine maps with increased injection quantities under full boost conditions. These can be replaced manually in the software.

4.2.4 Adaptations of the engine control and DAQ system

Some adaptations have been made to the engine control system throughout this thesis. These involve making adequate connections to enable measurement logging, starting up the engine and enabling control of the throttle valve. These are discussed in further detail in Appendix G, serving as documentation for future work.

As it has become possible to log sensor measurements on this engine bench, a new post-processing framework was built using Python. The modular structure of the code allows to flexibly compute pressure traces, HRR curves, ignition timings etc. However, recording measurements often times results in the engine stalling. This has been a recurring issue on this test bench, of which the origin has not yet been found. Attempts to increase the CPU capacity of the

---

[1]Calculated by the SCM software.

PC, or the bandwidth of the connection between the PC and NI chassis have not resolved the problem. It was hypothesized this semester that higher engine speeds resulted in more frequent engine stalls, but this was not confirmed and requires further testing. This software-related limitation has played a role in the decisions made during this work.

Chapter 5

Determination of the ignition delay

The ASTM D613 method, using the CFR engine, is used as a starting point for the development of an alternative cetane rating method in this work, as it is the only normalized engine test. Its working principle, discussed in Section 3.2, illustrates the importance of an accurate and reliable method to determine the ignition delay (ID). This chapter discusses how to determine the two bounding time instants of the ID, namely the start of injection (SOI) and the start of combustion (SOC).

5.1   Start of injection

The SOI indicates the starting point of the ID. This event is controlled by the engine control system by actuating the injectors. It is common practice to equip fuel injectors with a needle lift sensor, as there often is a delay between the timing of the control signal and the actual start of injection. This delay time depends both on the characteristics of the injection system and the physical properties of the fuel. Firstly, the reaction time of injectors results in a delay between injector actuation and SOI. Secondly, a common-rail injection system generates pressure waves in the fuel feed lines, influencing the fuel delivery rate by the injector. This results in a constant offset between the sensor actuation signal and actual SOI when considering a constant rail pressure, injection strategy, engine speed, and fuel. This would not influence the conclusions of our work if tests were conducted with one fuel only. However, physical fuel properties such as density, viscosity, and bulk modulus affect these pressure waves and thus influence the actual SOI, injection process, and the resulting total injected fuel mass [77, 78]. Previous studies have concluded that the effect of these physical fuel properties is minimal under single injection strategies, as the time between injection events allows for the waves to be damped out before the next injection [79]. This study considers an engine speed of 2000 rpm. The alternative cetane rating method developed in this work will be conducted at engine speeds below 2000 rpm, which further reduces the effect.

For this work, the injector actuation signal is used to mark the SOI as no needle lift sensor is installed. The previous arguments make this a viable option.

5.2   Start of combustion

Determining the start of combustion (SOC) is one of the most important, but contentious, subjects in combustion analysis. The SOC will mark the end point of the ID. As discussed in Ch. 2, the time between SOI and SOC can separated into the physical and chemical ID, both depending on different fuel properties. However, the separation of both phases is found to be

extremely difficult [80]. As a consequence, it is nearly impossible to allocate a unique time instance to the SOC. Figure 5.1 shows a typical Diesel operation pressure trace, where each blue dotted line denotes a different metric for determining SOC. This illustrates the difficulty of uniquely locating the SOC event. Also, the ID varies from cycle to cycle. As SOI is assumed to be constant, the cyclic variation in the calculated ID is caused solely by the allocation of SOC. To avoid the effect of sample size on the statistical analysis, data must be collected from a sufficient number of consecutive cycles [81].
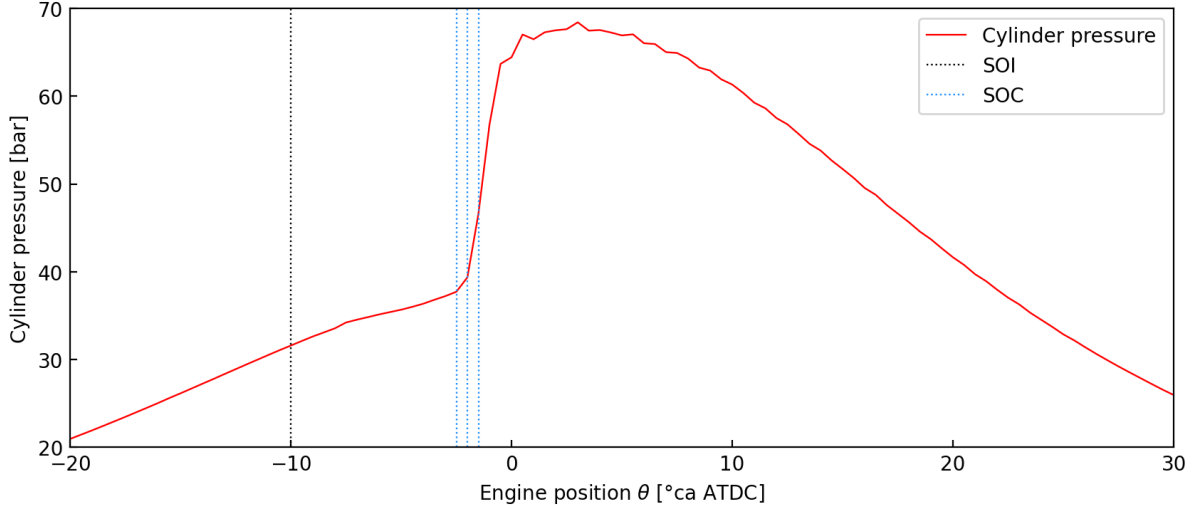
Figure 5.1: A typical Diesel operation pressure trace and several SOC metrics at an engine speed of $1300\,rpm$ and an IMEP of $4.3\,bar$.

In literature, methods for estimating SOC are mainly based on pressure analysis, combustion temperature rise, heat release rate, or light emissions [82, 83]. The following sections investigate a number of SOC metrics based on pressure analysis and heat release rate, from which a final selection will be made to fit the purpose of this work.

5.2.1 Derivatives of the cylinder pressure

One way to detect the sudden pressure rise due to ignition is to study the derivatives of the pressure signal. Ideally, a SOC metric is independent of engine load and speed. This constitutes a problem for all pressure diagnostics as they do not satisfy this criterion [82]. The goal of this thesis, however, is to investigate an alternative cetane rating method in which the load and speed of the engine are constant. As a consequence, transient engine conditions are ruled out and pressure-derivatives are a worthy metric to estimate SOC.

Compression ignition is characterised by its premixed combustion phase, which results in a large initial pressure-rise. The pressure trace's first derivative $\frac{dp_{cyl}}{d\theta}$ reflects the instantaneous change in pressure. Because this large initial pressure rise is always present, estimating SOC using the location of maximum slope of the pressure signal (DP1) can be considered a reliable method [84]. Equation 5.1 clarifies the calculation used to obtain DP1.

$$DP1 = \theta\left(\frac{dp_{cyl}}{d\theta} = \frac{dp_{cyl}}{d\theta}\bigg|_{max}\right) \tag{5.1}$$

The acceleration of the pressure signal is represented by the second derivative of the in-cylinder pressure $\frac{d^2p_{cyl}}{d\theta^2}$. The slope of the pressure signal changes drastically during the ignition event. As

a result, the location of maximum change in slope (DP2), shown in Eq. 5.2, can be interpreted as SOC. DP2 is located before DP1 because the maximum change in slope always appears before the maximum slope of the pressure signal. Syrimis et al. found this method to be the most reliable as it is insensitive to signal noise. Therefore it can also be applied to unfiltered pressure traces [83, 85].

$$DP2 = \theta \left(\frac{d^2 p_{cyl}}{d\theta^2} = \left. \frac{d^2 p_{cyl}}{d\theta^2} \right|_{max} \right) \tag{5.2}$$

The third-order pressure derivative $\frac{d^3 p_{cyl}}{d\theta^3}$ is also studied in literature. According to T. Katranik et al. [82], the maximum of the first (DP1) and second pressure derivatives (DP2) seem to overestimate the ID. SOC may be estimated by the location at which the third-order pressure derivative goes through its maximum:

$$DP3 = \theta \left(\frac{d^3 P_{cyl}}{d\theta^3} = \left. \frac{d^3 P_{cyl}}{d\theta^3} \right|_{max} \right) \tag{5.3}$$

There are still several other methods discussed in the literature. For example, the pressure recovery point[1]. For this thesis, the methodology suggests the derivative methods to be the best options to test.

To give a more graphical understanding of the methods outlined above, Figure 5.2 shows the pressure trace around TDC along with the first -, second -, and third derivatives of the average cycle. The same is done for some arbitrarily chosen cycles to illustrate cycle-to-cycle variability and noise.

---

[1]defined as the point at which the in-cylinder pressure is recovered to the compression value without fuel evaporation
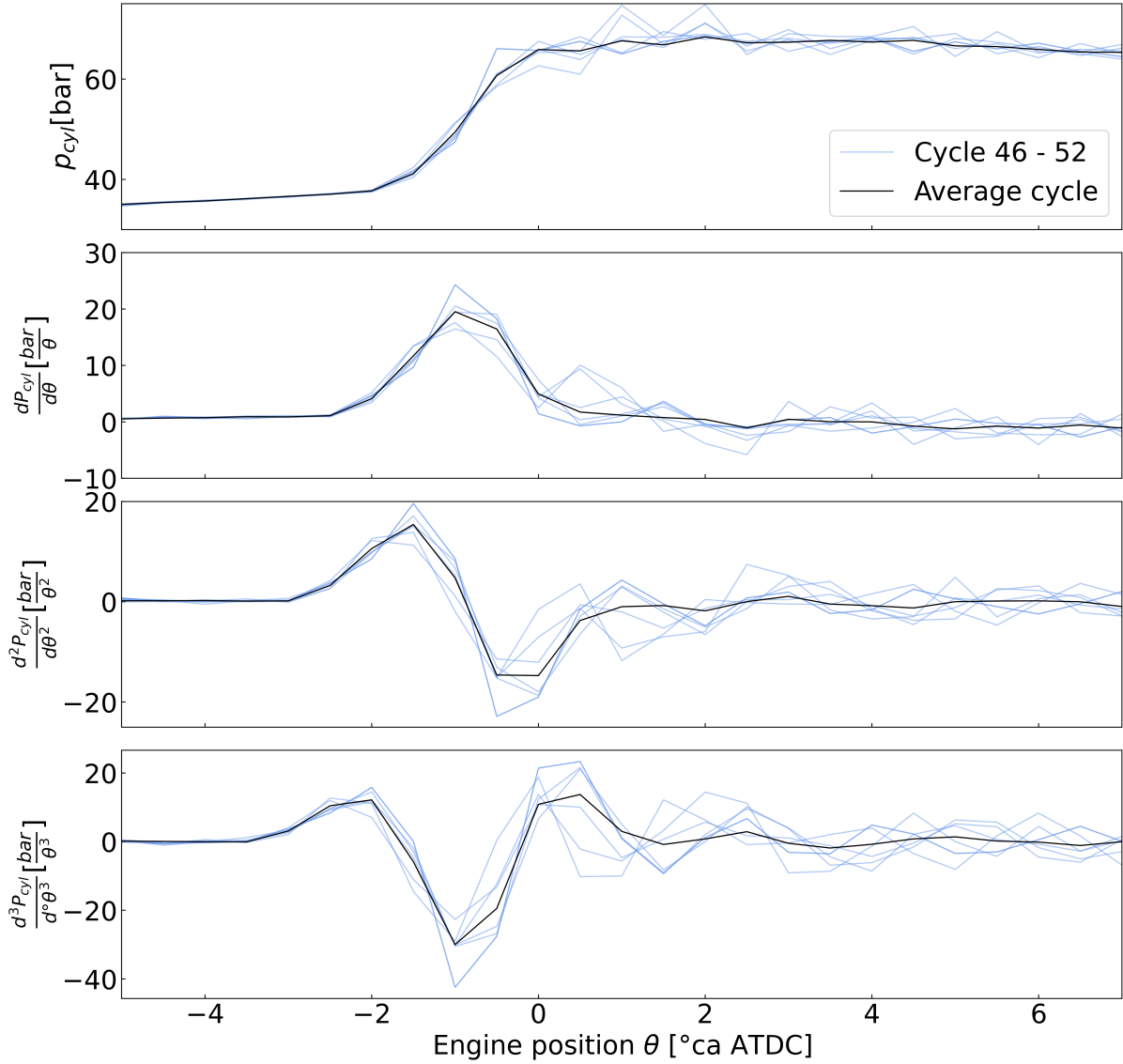
Figure 5.2: The pressure trace, first -, second -, and third derivative for the average and and some arbitrarily chosen cycles around TDC.

Because signal noise is not filtered, it is amplified through consecutive derivation. As a result, the certainty that the maximum of the pressure derivative is located at the beginning of the signal decreases with each derivative. Figure 5.2 shows that triggering SOC solely based on the maximum of the derivative can result in an incorrect SOC position. This is especially visible for the third derivative, where noise peaks exceed the peak originating from the ignition. Filters can help to reduce the influence of noise on the signal. The correct point, i.e. the first significant peak in the signal, is selected during post processing without the use of filters, as described in Appendix B.

5.2.2 Rate of heat release

The SOC intuitively corresponds to the moment at which there is a net positive release of heat, i.e. when the heat generation due to exothermic reactions offsets the cooling effect of the evaporating fuel. The heat release inside the combustion chamber of an engine can be estimated using calculations based on measurements of volume and pressure. Heywood [29] describes a simple model to calculate the net heat-release rate (HRR) starting from the first

law of thermodynamics, shown in Eq. 5.4.

$$\frac{dQ_n}{d\theta} = \frac{dQ_g}{d\theta} - \frac{dQ_w}{d\theta} = \frac{dW}{d\theta} + \frac{dU_s}{d\theta} \tag{5.4}$$

The net heat release Q_n is the difference of the gross heat release Q_g and the heat transfer from the charge to the wall Q_w. The work done by the piston can be written as $dW = p_{cyl}dV$, with p_{cyl} the in-cylinder pressure and V the instantaneous combustion chamber volume. The change in sensible energy $dU_s = mc_v dT_{cyl}$, with trapped mass m, cylinder temperature T_{cyl} and heat capacity at constant volume c_v, can be further simplified using the ideal gas law in Eq. 5.5. The ratio of specific heats is denoted as γ, and R signifies the specific gas constant.

$$dU_s = mc_v dT = \frac{c_v d(p_{cyl}V)}{R} = \frac{1}{\gamma - 1}d(p_{cyl}V) \tag{5.5}$$

Combining Eqs. 5.4 and 5.5 finally results in the HRR, expressed in $\frac{J}{^\circ ca}$, given in Eq. 5.6. A typical HRR curve has already been shown in Fig. 2.2 .

$$\frac{dQ_n}{d\theta} = \frac{\gamma}{\gamma - 1}p_{cyl}\frac{dV}{d\theta} + \frac{1}{\gamma - 1}V\frac{dp_{cyl}}{d\theta} \tag{5.6}$$

The cumulative heat release Q_{cumul} can be calculated by integrating the HRR starting from intake valve closure (IVC). The fraction of the fuel that has been burned for each time interval during the combustion, called MFB, is estimated from a normalization of the cumulative heat release with its value at the end of combustion (EOC), as shown in Eq. 5.7.

$$MFB(\theta) = \frac{Q_{cumul}(\theta)}{Q_{EVO}} = \frac{1}{Q_{EOC}} \int_{\theta=\theta_{IVC}}^{\theta} \frac{dQ_n}{d\theta} \, d\theta \tag{5.7}$$

Several metrics to estimate SOC are based on such HRR models. The crank angle position at which the HRR exceeds zero may be seen as the point of ignition [81, 86, 87]. However, the pressure signal may contain noise, which may result in an incorrect estimation of SOC at the zero-crossing point. Therefore, flame development is often considered to begin between MFB 0-10% [88]. The points where MFB reaches 2%, 5% or 10% are often used to estimate SOC. These metrics are denoted as CA2, CA5 and CA10 respectively, and will be evaluated further.

This single-zone HRR model treats the cylinder contents as an ideal gas with uniform composition, pressure and temperature. Also, the ratio of specific heats γ is assumed constant. However, γ varies with charge temperature, pressure, air-to-fuel ratio (AFR) and EGR rate and is known to have a significant effect on the calculated HRR[2] [89]. This model can be further expanded on by implementing a temperature dependence of γ, using heat transfer correlations to estimate heat losses, crevice regions etc. Both these expanded and simple models only provide approximate results due to the difficulties involved in assessing these phenomena [29, 81]. The high number of assumptions in this model lead to higher uncertainties.

Furthermore, signal noise forms a practical drawback to these HRR and MFB calculations. The pressure derivatives in Eq. 5.6 amplify any noise present in the pressure trace. Filters are often applied to cylinder pressure signals to reduce their noise content. Filtering such signals, on the other hand, can be considered a field of expertise on its own, with techniques ranging from basic and robust to advanced and dynamic. It has been experienced that filtering pressure traces without removing their main characteristics is extremely challenging [90, 91]. For example, the abrupt change in pressure at SOC should remain intact, while pressure oscillations during the

---

[2]This is due to the strong non-linear behaviour of $\frac{1}{x-1}$ and $\frac{x}{x-1}$ around $x = 1$.

combustion phase should be filtered out. Figure 5.3 shows how some simple filter and smoothing techniques applied on the pressure trace influence the resulting HRR. Taking an ensemble average of the pressure trace may reduce the noise content of the resulting HRR. Applying a moving average filter to the ensemble averaged pressure trace further reduces noise. Increasing the averaging window, as expected, provides more smoothing but has a significant impact on the signal around SOC, as shown in the zoomed-in section. The use of a smoothing spline on the ensemble averaged pressure signal shows better noise rejection and a lower deviation around SOC.
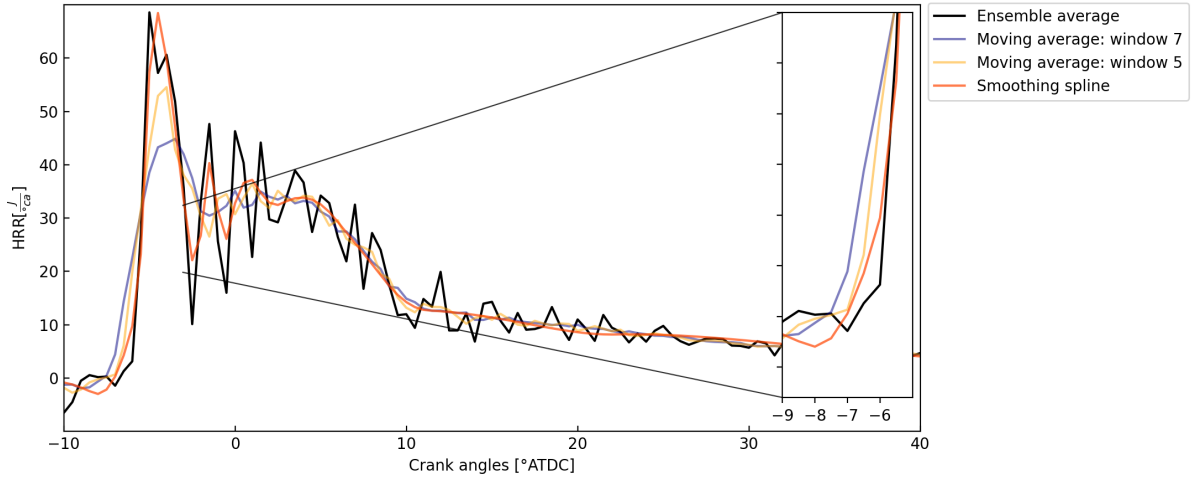
Figure 5.3: A comparison of some simple pressure trace smoothing techniques and their influence on the HRR.

Table 5.1 shows CA5, calculated for the four different smoothing methods, expressed in $°ca$ before top dead center (BTDC). The use of a moving average results in premature SOC detection, again with an increasing offset for larger averaging windows. The smoothing spline gives a closer estimation of SOC, while providing better noise rejection. These quick filter implementations illustrate the difficulties involved. Many filters and smoothing techniques also require precise tuning to achieve a desirable result in a certain load point. This renders these techniques insufficiently robust for our purpose. Advanced filtering techniques are explored in literature [92, 93, 94, 95]. However, these are complex to implement and are not the focus of this master's dissertation. Lastly, this work focuses at the instant of ignition. Fairly low noise levels are observed in this region, making filters inutile in determining SOC. However, the implementation of a more reliable filtering technique may be of use for future work on this test bench.

Table 5.1: CA5 calculated based on different smoothing methods applied to the pressure trace.

Smoothing method	CA5 [°ca BTDC]
Ensemble average	4.6
Moving average: window 5	4.68
Moving average: window 7	4.83
Smoothing spline	4.58

5.3 Determination of a suitable SOC metric

The previous sections have outlined different potential SOC metrics. These are now compared with respect to each other in order to select the most suitable metric for this work. Figure 5.4 displays the position of these SOC metrics applied to a measurement representative for the test conditions.
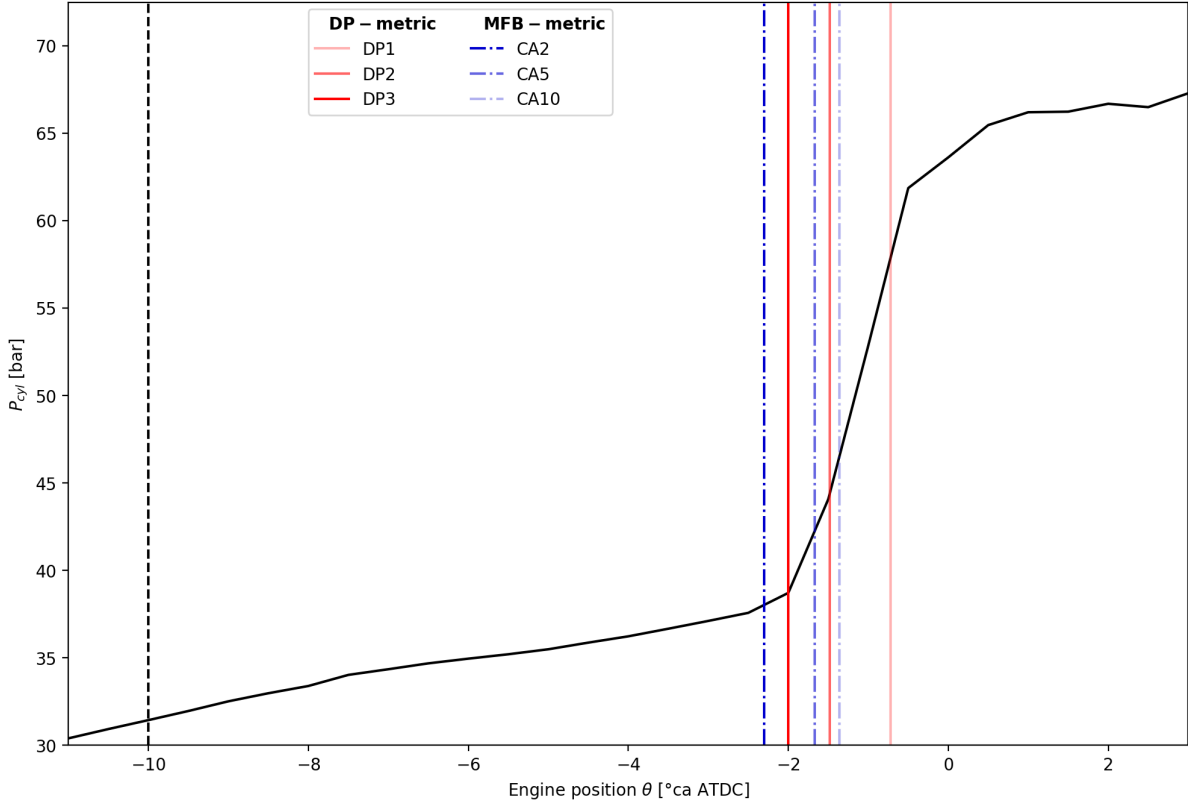
Figure 5.4: Different metrics for determining SOC: the maximum of the first-, second-, and third derivative of the pressure signal (DP1, DP2 and DP3) (Eq. 5.1 - 5.3) and 2, 5 and 10 % fraction of fuel burned (CA2, CA5, CA10) (Eq. 5.7).

Firstly, the DP-metrics are located as expected. Visually, it is clear that the DP1-metric has a delayed response to SOC. The point of maximum pressure rise already occurs during the combustion phase. Logically, further derivation of the signal advances the resulting SOC detection, as is clear from Figure 5.4. The DP-metrics are based on fewer assumptions than the MFB-metrics, therefore leading to less uncertainties. Furthermore, it was experienced that DP-metrics metrics produced consistent results for all measurements, implying the metrics' robustness.

While HRR-calculations can give insight into the combustion process, the strong assumptions and simplifications involved increase the uncertainty of the resulting SOC. One could reason that this still allows us to compare different fuels, as the same assumptions are made during all measurements. During measurements however, it was experienced that the MFB-metrics provide a less consistent location on the pressure signal. Appendix A provides an estimation of the theoretical error on HRR-calculations.

The obtained results and theoretical arguments for each method led to the conclusion that DP-metrics were the better choice for estimating SOC in this case. A good metric should be able to determine SOC accurately for each cycle. The ID can be calculated with the same resolution

as the crankshaft encoder, i.e. 0.5°ca. However, the actual peak of the continuous cylinder pressure signal (and thus the actual ID) can be positioned within a window of $\pm 0.5°ca$ around the calculated ID. Thus the encoder resolution limits the ID accuracy[3] to maximum 1°ca. The inter-cycle variability of the ID forms a second limitation to the accuracy. A stable reading is required to be able to differentiate between fuels with a slightly different CN.

$$CV_{SOC} = \frac{\sigma_{SOC}}{\mu_{SOC}} \qquad (5.8)$$

The inter-cycle coefficient of variation (CV_{SOC}), as shown in Eq. 5.8, represents the variation in SOC between cycles, σ_{SOC}, in relation to the mean SOC value μ_{SOC}. This coefficient reflects the variation in SOC across the number of recorded cycles. The value of CV_{SOC} was found to be lower for the DP2-metric than for the DP1. This metric is also recommended in literature if the pressure signal is not filtered [83]. As a result, DP2 is the selected metric that will be used in this thesis to determine SOC.

---

[3]Note the difference between resolution and accuracy.

Chapter 6

Alternative test method

With an appropriate detection of SOC in place, further development of an alternative cetane rating method is possible. The idea is to base this method on the ASTM D613 standard, as this is the only normalized engine test. This method controls the engine to a set ID by varying the compression ratio (CR) at a given engine speed. An alternative control input is needed in this case, as a production engine has a fixed CR. This control input should influence the ID sufficiently to achieve a sufficiently large CN measurement range.

Besides a control input, an appropriate combination of engine speed and load is required. Ideally, the engine conditions should be chosen to allow for a large range in ID, large control input range, and high sensitivity to fuels with a wide range of CN. These characteristics are desired to achieve a sufficiently large measurement range and accuracy of the ID, and in extension the CN. The following sections briefly explore the different alternative control inputs, and the operating conditions and blends for which measurements are conducted.

6.1 Method development: alternative control input

6.1.1 Throttle valve

A first idea to emulate a variable CR is by throttling the inlet manifold of the engine [61]. Throttling the intake decreases the cylinder pressure at SOI, lengthening the ID.

Diesel can be used for a first trial to find a SOI, with a wide open throttle, that results in SOC at TDC (determined using the DP2 metric). This SOI is remained constant for all further tests. When the engine runs on a fuel with a different CN, the throttle position can be varied to again achieve SOC at TDC. This allows to build a relation between the CN of a fuel, and the required throttle valve position to achieve SOC at TDC (i.e. a calibration curve). After this calibration process, fuels with an unknown CN can be tested. For these fuels, the same SOI as before is used and the throttle position is varied until SOC at TDC. The CN can then be estimated from the throttle valve position, using the calibrated relationship. Conceptually, this method does not differ from the ASTM D613 method (using the CFR engine) as it relies on the correlation between the ID and one engine control parameter. The same approach will be used for other alternative control inputs.

This method appears quite promising at first, as it lowers the CR without the use of highly expensive CFR equipment. However, some objections can be made against the test method. Throttling causes a pressure decrease, whereas a lower CR would result in both lower cylinder pressure and temperature. In order to truly mimic the variable CR, a temperature controller

needs to be installed. Lastly, in literature, it was found that using this method showed only a limited measurement range of 9 CN units [61].

6.1.2 Turbocharger

Alternatively to using a throttle valve (and temperature controller) to emulate a reduced CR, the inlet manifold pressure can be boosted to emulate an increased CR. The increased inlet temperature and pressure result in higher temperatures and pressures at SOI, resulting in a reduced ID. If the pre-compression process is assumed to be comparable to compression in the engine, the effect of a variable CR may be emulated.

This can be achieved using an external compressor, or a controllable turbocharger. The latter option was examined in this work as the VGT of the test engine can be readily controlled. This however makes the amount of available pre-compression dependent on the engine speed and load. A higher speed and load result in a higher exhaust flow rate with a higher energy content, allowing to generate more turbine work, and thus higher intake pressure.

In this work, four load points were tested, each under minimal boost and maximum available boost pressure from the VGT. As the engine maps (fuel injection quantity, SOI, etc.) do not alter under the influence of turbocharger actuation, engine speed and torque did not change drastically under increased boost pressure. If so, the engine was controlled back to the original engine speed by slightly altering the engine load. Figure 6.1 shows the ID of these load points plotted against the intake manifold pressure. The red lines show measurements at 2000 rpm, while the blue lines show measurements at 1300 rpm. The dashed lines represent test points at a lower load compared to the full lines. As expected, a higher intake manifold pressure is possible at high engine speeds (red), resulting in a larger ID reduction over the complete range of the VGT in this load point.
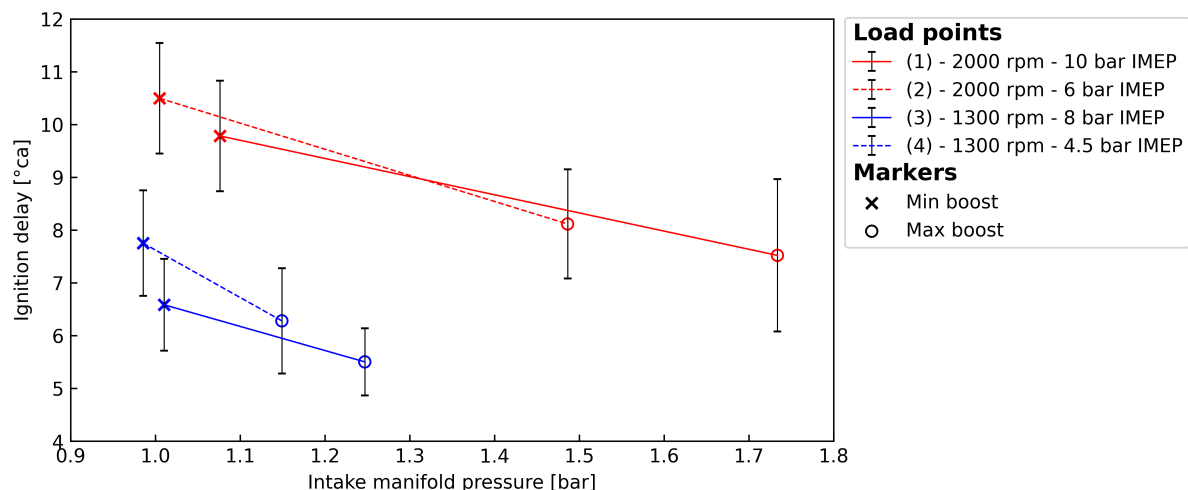
Figure 6.1: Ignition delay (determined using the DP2 metric) as a function of intake manifold pressure for 4 different engine operating conditions.

It is important to recognize that the engine load point itself also influences the ID. The ID (expressed in °ca) increases almost linearly with engine speed [30], which reduces the relative error of the ID. A higher brake mean effective pressure (BMEP) (thus higher engine load) results in decreased IDs. Furthermore, the ID is less sensitive to the CN of the fuel at high BMEP [96]. This reduces the measurement resolution and accuracy of the CN, resulting in a trade-off between CN measurement range and accuracy when selecting a load point. Despite the higher boost pressure in load point 1 (red full line), a larger reduction in ID is achieved in load point 2

(red dashed line). This may be explained by its lower indicated mean effective pressure (IMEP), and thus BMEP. However, the relatively large measurement uncertainty makes the validity of such conclusions questionable.

Overall, it is clear that higher speeds achieve a larger reduction in ID. This would be beneficial for the measurement range of the resulting CN rating test. However, it was hypothesized that higher engine speeds resulted in more frequent software instabilities during measurement logging, as mentioned in Sect. 4.2.4. Moreover, stronger oscillations of the cylinder pressure were observed under the investigated load points. This resulted in a less reliable SOC detection, requiring more manual tweaking of the detection mechanism. The result is a higher inter-cycle variability of the calculated ID. Although the use of a controllable turbocharger or compressor may emulate a variable CR relatively well, a third alternative control input was investigated for the reasons stated.

6.1.3 Exhaust gas recirculation

Exhaust gas recirculation (EGR) allows to increase the ID. The effect of EGR on the ID is twofold, and can be split into a primary and secondary effect. The primary effect is caused by the reduced intake oxygen concentration due to the recirculation of exhaust gas to the intake line. This increases the chemical ID. The secondary effect results from the increased ratio of specific heats of the intake gas. This results in reduced temperature and pressure after compression, again increasing the ID. Figure 6.2 shows that the ID increases non-linearly with a reduced intake oxygen concentration, achieved by cooled EGR [59]. It also shows that this effect is dominant over the secondary effect of EGR on the ID. This strong increase in ID could allow a larger CN measurement range, than possible with the use of the VGT.
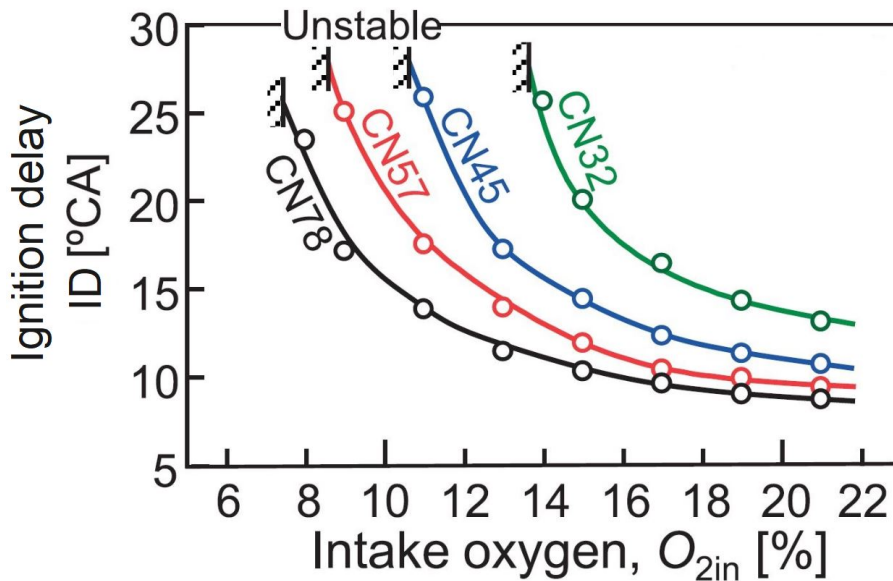
Figure 6.2: The effect of a reduced intake oxygen content O_{2in}, through the use of cooled EGR,on the ignition delay (ID) for fuels with different cetane numbers. Adapted from [59].

Generally, the ID of a fuel, under atmospheric intake oxygen concentrations, increases non-linearly as its CN decreases [29]. Figure 6.2 also shows that this difference in ID between fuels is amplified at reduced intake oxygen concentrations [59].

The use of EGR also holds some practical advantages. EGR can be used to induce large differences in ID, even at limited engine load and speed. This is advantageous over the use of the VGT, where the measurement range is bound by the load point. It was also experienced that the

engine speed and load did not change significantly under reduced intake oxygen concentrations, while more control was required to achieve a fixed engine speed under VGT operation. The use of a low speed also increases the similarity with the ASTM D613 standard [56], for which the CFR engine runs at 900 rpm. It was also hypothesized that software instabilities during measurement logging are less frequent while running at reduced engine speeds, allowing a more reliable measurement recording.

6.2   Final method description

Further measurements will be performed using EGR as control input for the alternative cetane rating method. The used operating conditions, recorded sensor values, and fuels are reported in this section.

6.2.1   Operating conditions

Similarly to the ASTM D613 standard, the engine is controlled to a fixed speed and fuel injection quantity. In this work, a speed of 1300 rpm and an injection quantity of 3.68 mg/cycle is used for all tests. This is achieved by setting the engine control pedal stand to 7% and adapting the engine load to maintain 1300 rpm. This results in a relatively low engine load of around ≈ 4.5 bar IMEP. The moderate engine load increases the sensitivity of the ID to the CN [29], which is beneficial for the purpose of this method. The engine shows stable speed, load, and rail pressure control under these conditions. SOI is set at 10°ca BTDC. This value lies closely to the originally mapped injection timing and is used to ensure stable engine operation. A moderate rail pressure of 900 bar was set in the current engine mapping, and has been maintained throughout this work. Table 6.1 lists the main engine parameters and their respective value.

Table 6.1: The main engine parameters during measurements.

Engine parameter	Value
Speed [rpm]	1300
Injection quantity [mg/cycle]	3.68
Pedal stand [%]	7
IMEP [bar]	≈ 4.5
Start of injection [°ca BTDC]	10
Rail pressure [bar]	900

Control of the EGR and intake throttle valve influences the amount of EGR and thus the intake oxygen concentration. Restricting the flow of fresh air through the intake line allows to feed of more EGR gases to the intake manifold. When the EGR valve is closed and the intake throttle is wide open, the intake oxygen concentration is equal to that of the atmosphere, which is 21%. The intake oxygen concentration is reduced by gradually opening the EGR valve. The EGR cooler is used to maximize the amount of EGR. A wide open EGR valve results in an intake oxygen concentration of ≈ 17%, which can be further reduced by gradually closing the throttle valve. When the throttle valve is nearly completely closed, the intake oxygen concentration reduces to ≈ 14%.

One measurement consists of 100 consecutive engine cycles. The in-cylinder pressure, inlet and outlet manifold pressures and temperatures, intake flow rate, and lambda values are logged to a .tdms file. The engine torque, atmospheric pressure, temperature, and relative humidity are noted down manually. Post processing determines the ID using the DP2 metric for each cycle, resulting in an average ID and inter-cycle variability. The dry intake gas composition is measured using the Ultramat 23 to determine the intake oxygen concentration. An estimate

of the intake oxygen concentration can be calculated using measurements from the engine, as described in Appendix C. These results are not used in the final analysis, but can however be useful to estimate the intake oxygen concentration upfront and allow easier engine control.

6.2.2 Tested fuel blends

Evaluation of the test method requires fuel blends with varying CNs. Several mixtures of Diesel, HVO, iso-octane and n-dodecane are used to create various CN number fuels. The Diesel and HVO fuels that are used in this work come from a commercial gas station. Therefore, their precise CN is unknown in advance. Additionally, the Diesel that was bought at the beginning of this work showed a different ID, compared to a second batch of Diesel fuel. To verify, a sample of each was delivered to an accredited laboratory for a DCN test. The results showed a clear difference in CN between both batches. As both batches of Diesel fuel were bought around the change of seasons, the first batch may have been "winter" Diesel, while the latter batch was "summer" Diesel. In this work, the first batch is denoted as 'Diesel$_1$', whereas the second batch is denoted as 'Diesel$_2$'. The HVO fuel was also submitted for a DCN test. Table 6.2 depicts the CN and a selection of physical properties of the reference fuels used to make blends. The CN numbers which are measured in the accredited lab are indicated in bold. The other CN values and physical properties originate from literature [97].

Table 6.2: Properties of reference fuels used to make blends.

Property	Diesel$_1$	Diesel$_2$	HVO	iso-octane	n-dodecane
Cetane number	**54.5**	**52.9**	**89.6**	20.1	75.6
Density $[kg/m^3]$	832.5	832.5	780	687	750
Viscosity $[\frac{mm^2}{s}, 25°C]$	3.25	3.25	3	0.70	/
Lower heating value $[\frac{MJ}{kg}]$	42.9	42.9	44.1	44.2	43.8
Flashpoint $[K]$	347	347	367	261	347

Pure HVO has a high CN of 89.6, which makes it an appealing upper limit for our measurements. Furthermore, HVO can be blended with Diesel without the need for any additives. A mixture of 50 vol.% HVO and Diesel$_1$ is made, which will be denoted as HVO50. Subsequently, Diesel$_2$ is blended with small amounts of iso-octane, and n-dodecane to achieve a difference of 5 CN units compared to Diesel$_2$. The CN of these blends is estimated using a weighted average based on the molar fractions x_i, as shown in Eq. 6.1. Table 6.3 shows the various blends, their CN and the abbreviation that will be used from here on.

$$CN_{blend} = \sum_i x_i \cdot CN_i \qquad (6.1)$$

Table 6.3: The abbreviation and CN of the various fuel blends.

Blend	Abbreviation	CN
100 vol.% HVO	HVO100	89.6
100 vol.%Diesel$_1$	Diesel$_1$	54.5
100 vol.% Diesel$_2$	Diesel$_2$	52.9
50 vol.% Diesel$_1$ + 50 vol.% HVO	HVO50	72.1
76 vol.% Diesel$_2$ + 24 vol.% n-dodecane	Diesel$_{2,CN+5}$	57.9
87 vol.% Diesel$_2$ + 13 vol.% iso-octane	Diesel$_{2,CN-5}$	47.9

6.2.3 Resolution and accuracy

The discussion in Chapters 7 and 8 uses the notion of resolution and accuracy for the ID and CN. It is important to recognize the difference between these terms. For clarity, an explanation is given upfront. The resolution signifies the smallest change of a quantity that can be measured, while the accuracy is the ability to match the actual, physical value of the quantity that is being measured. Figure 6.3 shows a schematic representation of the factors influencing the resolution and accuracy of the ID and CN.
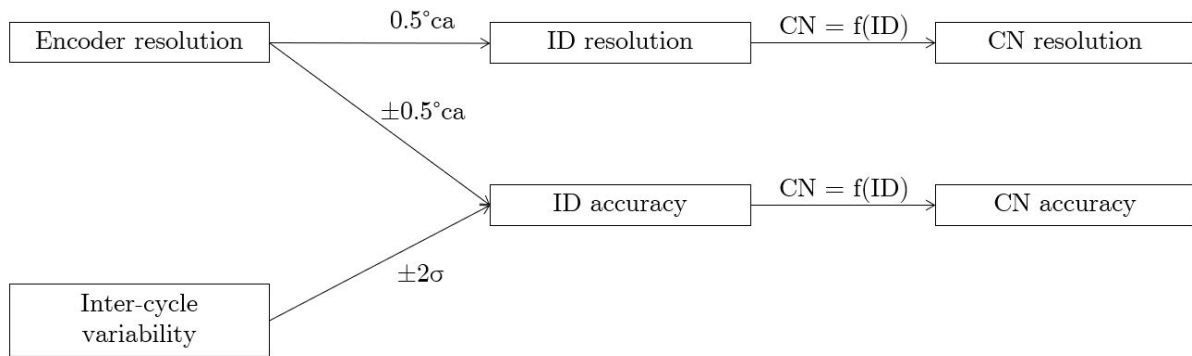
Figure 6.3: A schematic representation of the factors influencing the resolution and accuracy of the ID and CN.

The angular resolution of the encoder is given, and equals $0.5°ca$. Therefore, the ID can be measured with a resolution of $0.5°ca$. The CN resolution follows from the relation between ID and CN. This is visualized in Figure 6.4, showing the second derivative of the pressure signal for three hypothetical fuels. The fuels are represented by their respective CN (CN1 > CN2 > CN3). The CN of fuel CN1 differs sufficiently from CN2 to result in a distinguishable difference in ID, i.e. $0.5°ca$. However, the measured ID of fuels CN2 and CN3 is the same, while their continuous pressure signals differ in reality. Thus, the CN resolution is limited by the encoder resolution. In this case, the CN resolution would lie within the interval $[CN2 - CN3, CN1 - CN2]$.
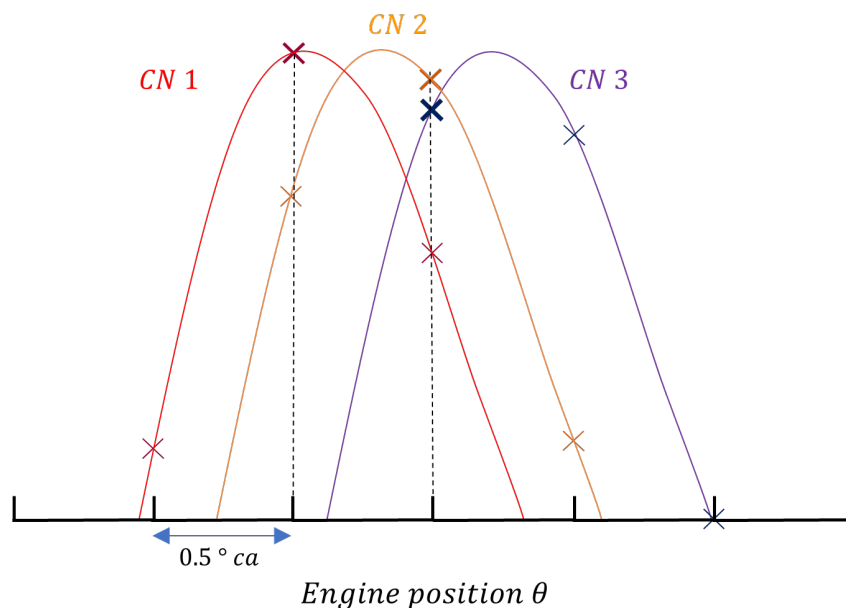
Figure 6.4: Encoder resolution detection of SOC for fuels with CN1, CN 2 , and CN3 respectively.

The ID accuracy, however, differs from the ID resolution and is related to the uncertainty of the measurements. SOC is estimated by the location where the second-order derivative of the pressure reaches a maximum. The continuous pressure signal is sampled at each encoder pulse, resulting in an crankangle-discretization of the signal. As a result, only the maximum of the discretized signal can be detected, which may differ from the maximum of the actual pressure signal. This may result in an error between the actual ID and the measured ID. The peak of the actual signal may lie within an interval of $\pm 0.5°ca$ around the calculated SOC location. Thus the encoder resolution limits the ID accuracy to maximum $1°ca$. Besides this, the inter-cycle variability also limits the accuracy of ID measurements. Two standard deviations σ, forming a 95% confidence interval, are added to the error margin on the ID. These two factors constitute the ID accuracy. Again, the CN accuracy follows from the relation between ID and CN. An error bar is used to indicate the accuracy of a measurement.

Chapter 7

Method evaluation

This thesis aims to develop an alternative cetane rating method using a production Diesel engine. The ASTM D613 method is used as a starting point, where the variable compression ratio as a control input is replaced by exhaust gas recirculation (EGR). Several crucial questions need to be addressed before this test method can be developed further. Firstly, it is essential to verify that the changes in ID, induced by EGR, are large enough to be measured accurately. Additionally, it is important to investigate whether fuels with a different CN show a sufficiently large difference in ID to be distinguished from each other. This is strongly related to the resulting CN measurement accuracy of the test. Furthermore, the influence of EGR on other engine parameters needs to be examined, and whether any of these parameters influence the ID in their turn. Once the above questions are answered, it should be possible to emulate the ASTM D613 method in a production Diesel engine by means of EGR.

7.1 Effect of EGR on ignition delay

It is examined whether the differences in ID due to reduced intake oxygen concentrations and CN are measurable. First, Diesel measurements are discussed to familiarize you with the way in which these results are obtained and presented. Next, the discussion is extended to different fuels.

7.1.1 Diesel operation

Figure 7.1 depicts the pressure trace around TDC for a selection of measurements under Diesel operation; the influence of EGR is clear. The black dotted line represents the start of injection (SOI). A higher EGR rate lengthens the ID, resulting in a lower peak pressure. Obviously, using EGR affects not only the ID but also the pressure during the compression stroke. EGR increases the ratio of specific heats γ of the intake gas, resulting in a lower pressure at SOI.
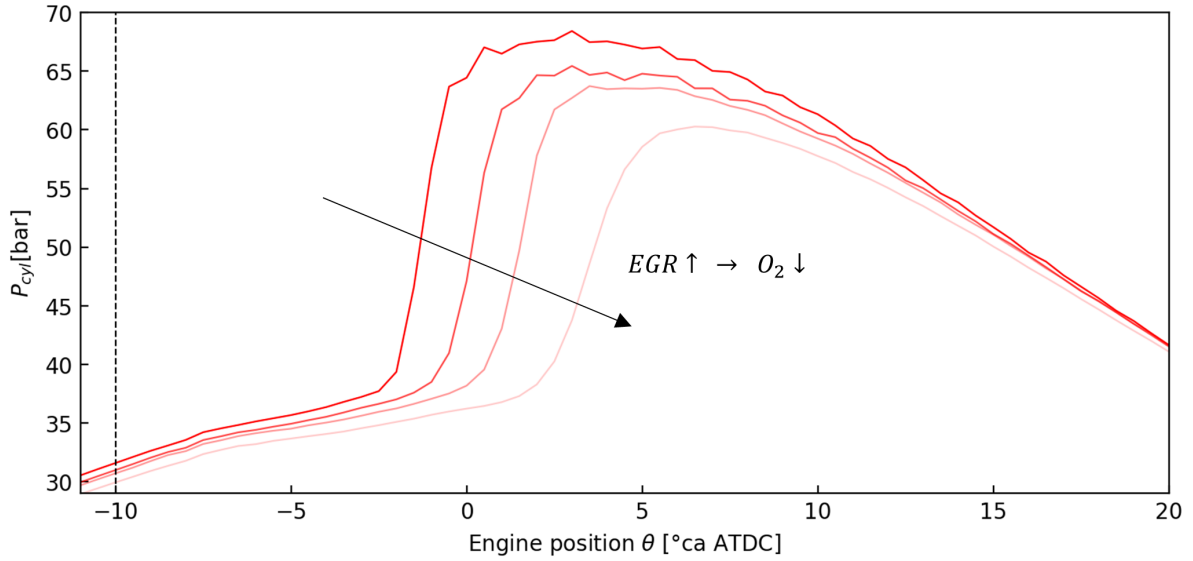
Figure 7.1: The pressure trace around TDC under the specified operating conditions, at varying intake oxygen concentrations.

Plotting the ID as a function of the intake oxygen concentration gives a clearer view. Figure 7.2 shows this, for a larger set of measurements under Diesel operation. As expected, the ID increases nonlinearly with a reduced intake oxygen concentration (see Fig. 6.2). Two series of measurements were performed on different days, showing consistent results. This strategy achieved an increase in ID of about $5°ca$, which is about twice the range obtained with the VGT in Section 6.1.2. This shows that it indeed is advantageous to use EGR as a control input in this case, in order to achieve a larger CN measurement range.
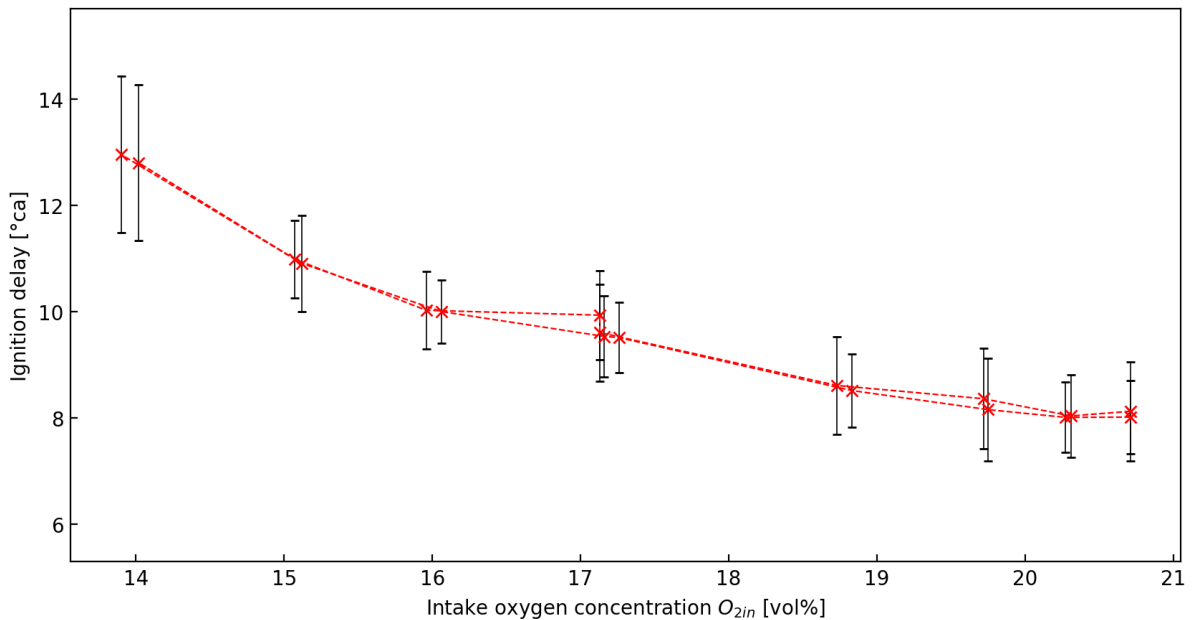
Figure 7.2: The effect of a reduced intake oxygen concentration through EGR on the ignition delay under Diesel operation.

The error margin on the ID in Figure 7.2 is composed of two parts: the ID accuracy due to the encoder resolution and inter-cycle variability (as discussed in Section 6.2.3). Overall, the limited encoder resolution is responsible for about 60% of the error margin of the measurements, making this the main limitation to the accuracy of the resulting cetane test. A significant increase in inter-cycle variability is achieved at the lowest intake oxygen concentration. During tests, the engine runs noticeably less stable in these conditions. For instance, the lambda sensor shows an oscillating reading, and a slow oscillatory behaviour is noticeable by ear. This is illustrated in Appendix F. This instability may be caused by the control of the throttle valve position. The throttle valve is only open for 10% at this point. It was observed that the the PID controller of the valve constantly generates small position corrections. This slight variation in throttle position may affect the EGR flow rate, and thus ID. Alternatively, a cyclic aerodynamic effect over the throttle valve may be the cause for this fluctuating EGR rate. A shaded zone will be added on following graphs, indicating this zone of unstable operation.

It is also important to recognize that the measurements at an intake oxygen concentration of 14% and 15% show an ID greater than 10°ca. This results in ignition after TDC, as SOI is set at 10°ca BTDC. Temperature and pressure decrease after TDC, resulting in a further increase of the ID, making the comparison with other measurements difficult. However, this has not hindered the conclusions based on the measurements presented hereafter. To avoid this situation, it could be opted to perform future measurements with an injection timing of 13°ca BTDC, as is done in the ASTM D613 method.

7.1.2 Concept evaluation

The discussion on the effect of the intake oxygen concentration on the ID can now be extended to different fuels. Figure 7.3 shows the ID under varying intake oxygen concentrations for the fuels discussed in Table 6.3. The shaded zone indicates the zone of unstable engine operation. For clarity, each blend is represented by a single measurement set. All measurements are shown in Appendix D, indicating the repeatability of these measurements.
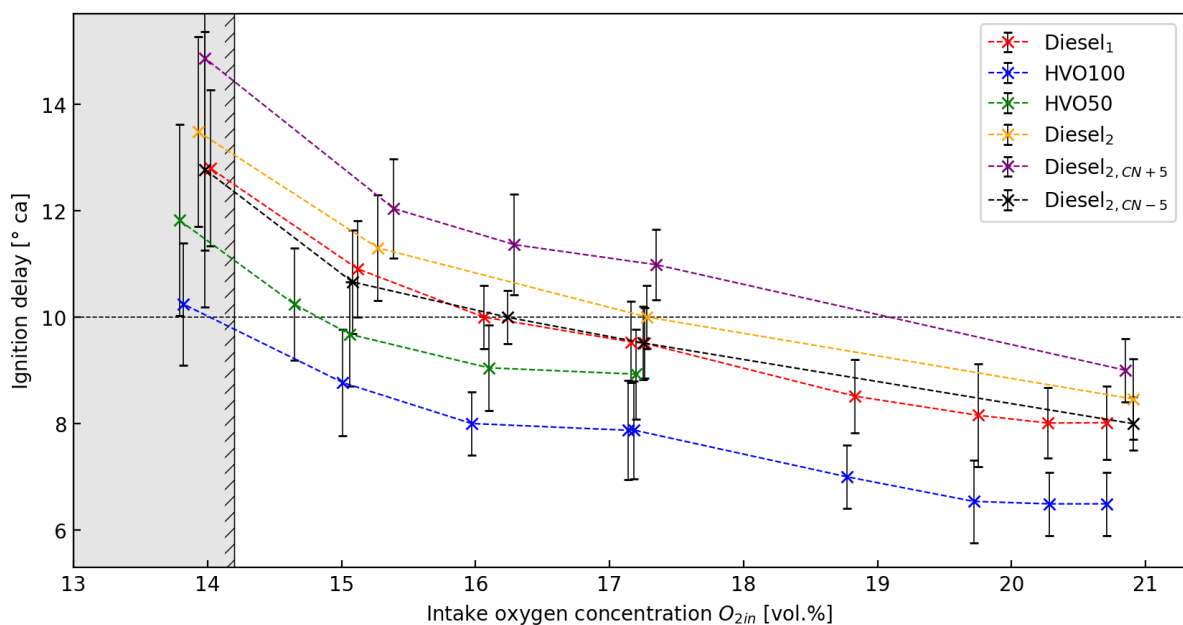
Figure 7.3: The measured ignition delay for fuels with a CN ranging from 89 - 43 under intake oxygen concentrations varying between 21% and 14% through the use of EGR.

The CN of the different blends ranges from 89.6 (blue curve) to 42.9 (purple curve). It is clear that the ID follows the tendency described in Section 6.1.3. Fuels with a higher CN exhibit a shorter ID, and their ID is less sensitive to a reduced intake oxygen concentration compared to lower CN fuels. To emulate the ASTM D613 method, ignition should be timed at TDC. The horizontal line indicates a constant ID of 10 °ca, resulting in ignition at TDC. Clearly, it was possible to control the engine to approximate this condition in a number of measurements, but a real-time calculation of the ID could make this easier in the future[1]. Figure 7.4 shows the pressure trace for HVO100, HVO50, and $Diesel_1$ at atmospheric conditions, and at an intake oxygen concentration to achieve ignition at TDC. It is apparent that by controlling the EGR rate, the ID can be controlled to a set value for various CN fuels. This illustrates that it is indeed possible to use EGR as a control input to an alternative cetane rating method in a production Diesel engine.
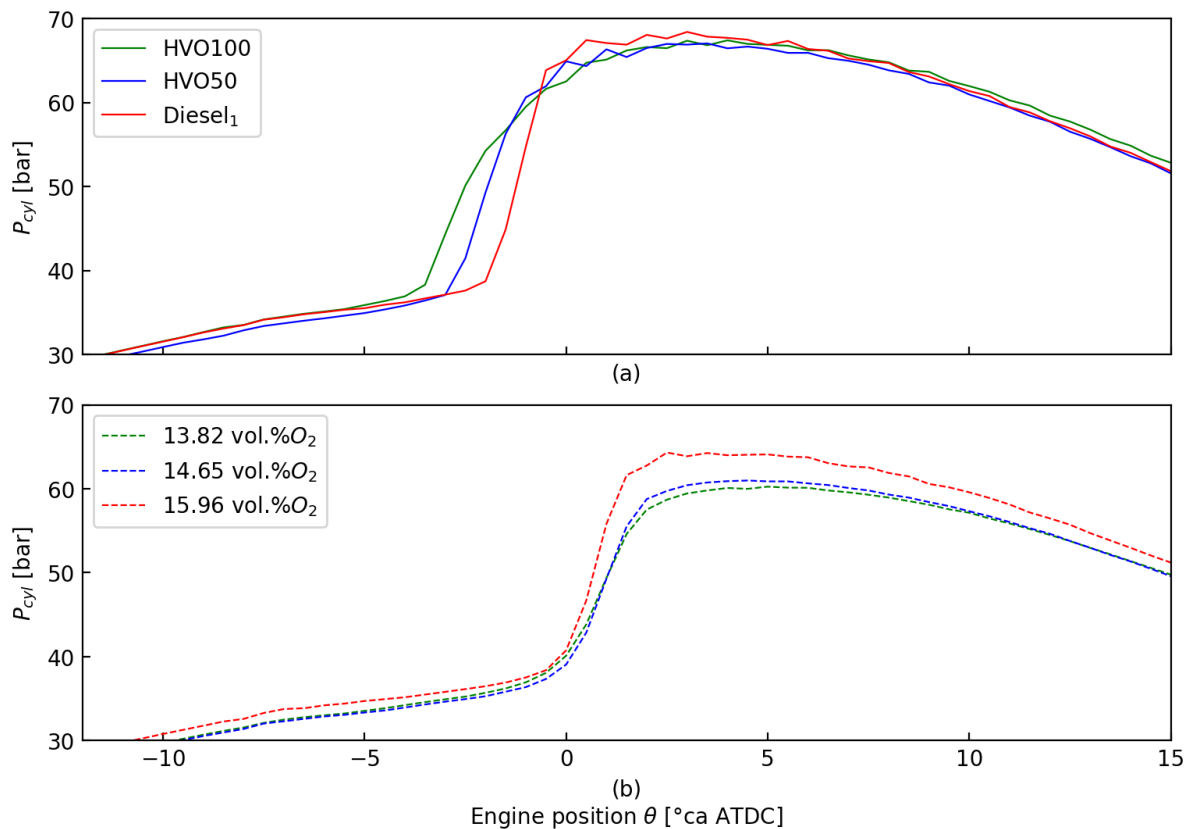
Figure 7.4: Pressure traces of Diesel 1, HVO100, and HVO50 at atmospheric conditions (a), and controlled to an ID of 10 °ca by means of EGR (b).

7.1.3 CN resolution and accuracy

The large difference in CN between HVO100, HVO50, and $Diesel_1$ allows a clear distinction in ID. For smaller changes in CN, this may not be the case. The crankshaft encoder limits the ID resolution to 0.5°ca. To estimate the CN resolution of the test engine, measurements are recorded using $Diesel_1$, $Diesel_2$, and $Diesel_{2,CN\pm5}$. The composition of these fuel blends can be found in Table 6.3. Figure 7.5 shows the ID under varying intake oxygen concentrations for these fuels. The ID of $Diesel_1$ appears to be indistinguishable from $Diesel_{2,CN-5}$, despite their difference of about 3.4 CN units. However, $Diesel_2$ and $Diesel_{2,CN\pm5}$ are clearly distinguishable

---

[1]Currently, the engine control software does not allow real-time calculation of the ID. This makes controlling the engine to a set ID a tedious task.

from each other, with a difference in ID of about $0.5°ca$, i.e. one encoder pulse. These four measurements would thus suggest a resolution between 3.4 and 5 CN units. However, the experiments be repeated to assure consistent results, and a more accurate estimation of the CN resolution can be obtained by testing blends with smaller CN differences.
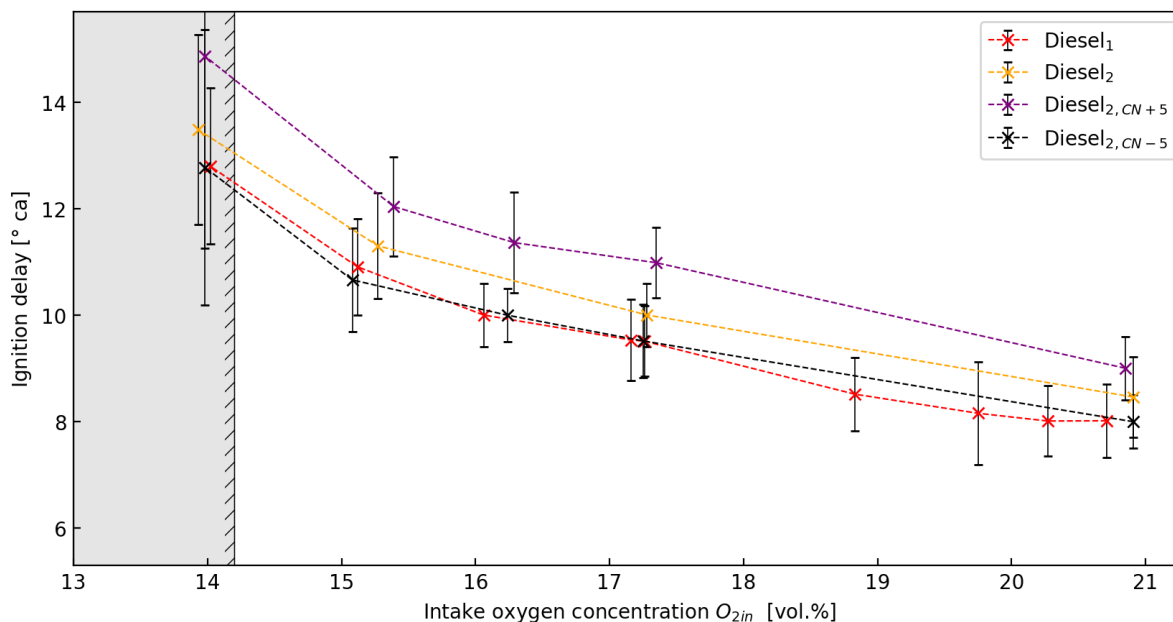
Figure 7.5: The effect of reduced intake oxygen using EGR on Diesel$_2$, and Diesel$_{2,CN\pm5}$.

The CN accuracy of the test differs from the CN resolution, as explained in Section 6.2.3. ID measurements are accurate within maximum $1°ca$. Inter-cycle variability further reduces the accuracy of the ID, and in extension of the CN. The ID difference between Diesel$_{2,CN-5}$ and Diesel$_{2,CN+5}$ is somewhat bigger than $1°ca$. This would suggest a CN accuracy of about 10 CN units. The relative position of the error bars on various measurements would confirm this conclusion.

7.2 Other factors influencing the ignition delay

The previous discussion shows that a reduced intake oxygen concentration, through the use of EGR, has the desired effect on the ID, and allows the implementation of an alternative cetane rating test. It is however important to recognize that EGR does not only influence the intake oxygen concentration. It should be examined how other engine parameters are affected by EGR, and how these would impact on the ID.

Figure 7.6 shows the effect of a reduced intake oxygen concentration, through EGR, on the outlet and inlet manifold temperatures for all tested fuels. It is clear that the stock EGR cooler cannot achieve a constant intake temperature given its limited size. The intake temperature increases almost linearly when the intake oxygen concentration is reduced, due to the introduction of hot exhaust gases. An increased intake temperature results in an increased temperature at SOI, resulting in a decreased ID. This decreases the sensitivity of the ID to the intake oxygen concentration, resulting in a lower CN measurement range of the test. The intake temperature also varies between measurements under similar conditions. This limits the accuracy of the cetane rating test. A closer control on the intake temperature would benefit both the CN measurement range and accuracy, and provide added flexibility.
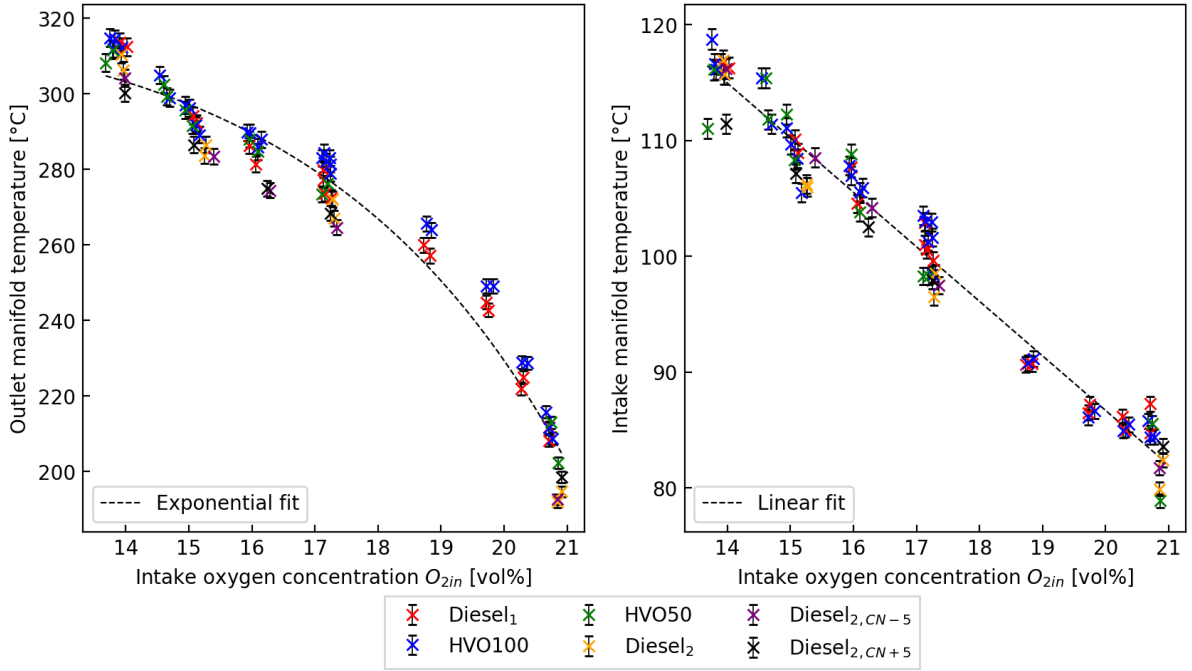
Figure 7.6: The effect of a reduced intake oxygen concentration (through EGR) on the outlet (left) and inlet manifold temperature (right) for different fuels.

Figure 7.7 shows the effect of a reduced oxygen concentration, through EGR, on the inlet manifold pressure for all tested fuels. Points located to the right of the black dotted line operate at a wide open throttle position. For these points, the inlet manifold pressure is relatively constant (atmospheric pressure). To the left of the black dotted line, the intake oxygen concentration is further reduced by gradually closing the throttle valve. This induces a decreased inlet pressure, and thus a decreased pressure at SOI, which would increase the ID. However, this effect is assumed to be negligible, as the pressure drop is minimal. The different colored lines represent different measurement runs of different fuels, recorded on different days. The offset in manifold pressures between both measurement runs is consistent with the different atmospheric pressure readings in the lab on those days.
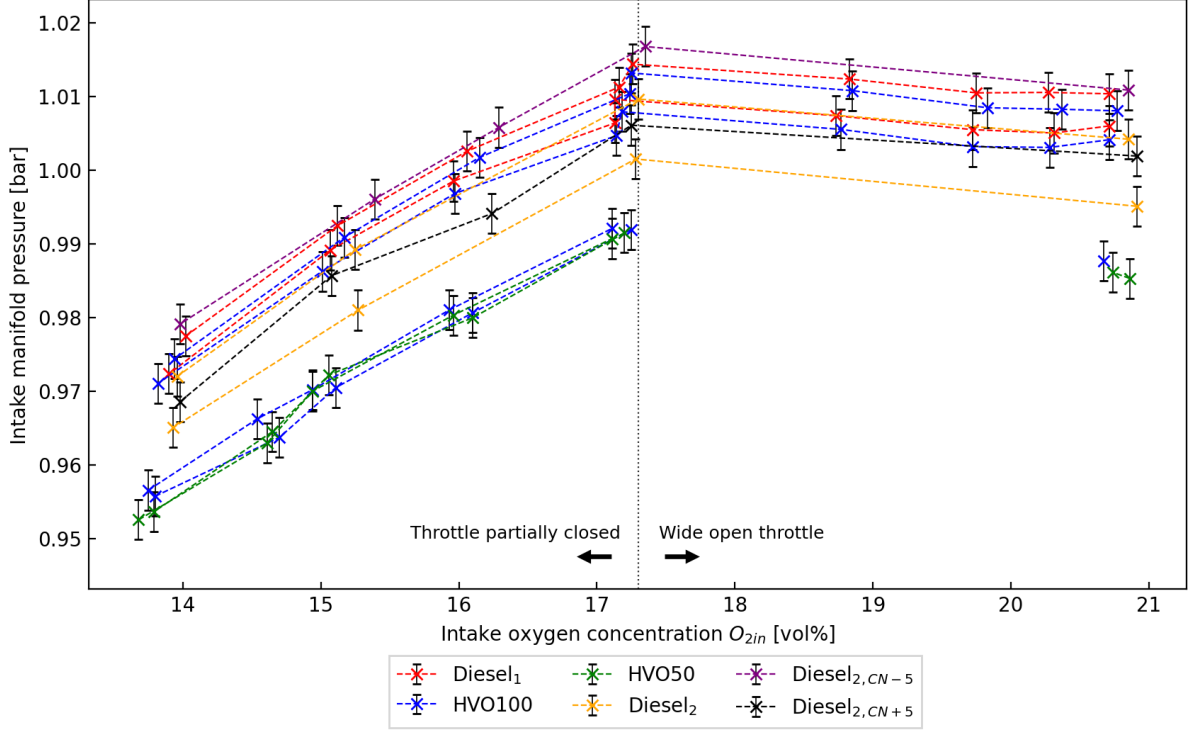
Figure 7.7: The effect of a reduced intake oxygen concentration (through EGR) on the inlet manifold pressure for different fuels.

Two more side effects can be identified. Firstly, it is important to acknowledge that the EGR composition depends on the chemical composition of the fuel sample and emission formation. The EGR composition, mainly its NOx content, can influence the ID [98], resulting in a misleading result of the test. Secondly, it should be remembered that the control system of the piezoelectric fuel injectors is calibrated for Diesel operation. This means that the required injection duration is mapped out as a function of the common rail pressure and desired fuel injection quantity. The use of different fuels with different physical properties, especially the density is of importance, has shown to influence the injected fuel mass. This would result in a deviation from the set operating conditions, specified in Table 6.1. However, this effect is seen to be minimal under single injection strategies and moderate speeds, as is the case here [77]. Also, the injected fuel mass has a negligible effect on the ID, as fuel which is injected after SOC can of course no longer influence the ID [99].

Chapter 8

Model proposition

A discussion of the measurements concluded that it is indeed possible to emulate the ASTM D613 method in a production Diesel engine using EGR. It was established that the CN resolution lies between 3.4 and 5 CN units, and it was shown that the intake temperature and pressure are also influenced by the use of EGR. It is expected that the increased intake temperature impacts the ID, and it is assumed that the changes in intake pressure have a negligible effect on the ID.

It is now attempted to model the alternative test method, i.e. form a mathematical model relating the intake oxygen concentration, CN, and ID. This may, in the end, be used to estimate the CN of a fuel sample based on measurements of the ID and corresponding intake oxygen concentration. It also provides insight in the test method, and can be used to decide on the optimal operation strategy of the test.

8.1   Model development

The empirical formula developed by Hardenberg and Hase [100], Eq. 8.1, estimates the ID (expressed in °ca) of a fuel with given CN at atmospheric oxygen concentrations, and is used as a starting point.

$$ID = (0.36 + 0.22M_{ps}) \cdot exp\left[\frac{618840}{CN + 25}\left(\frac{1}{RT_{TDC}} - \frac{1}{17190}\right) + \left(\frac{21.2}{p_{TDC} - 12.4}\right)^{0.63}\right] \qquad (8.1)$$

The ID also depends on the mean piston speed M_{ps} (m/s), and the temperature and pressure at top dead center: T_{TDC} (°C) and pressure p_{TDC} (bar) respectively. The universal gas constant $(8.3143 J/mol \cdot K)$ is denoted by R. The mean piston speed follows from the engine rpm n and engine stroke s: $M_{ps} = sn/30$. The values of T_{TDC} and p_{TDC} are estimated from the intake temperature and pressure, T_{in} and p_{in}, using a polytropic model of the compression process:

$$T_{TDC} = T_{in} \cdot r_v^{c-1} \qquad (8.2)$$

$$p_{TDC} = p_{in} \cdot r_v^{c} \qquad (8.3)$$

where c is the polytropic exponent (assumed to be 1.3) and r_v is the compression ratio. Substitution in Eq. 8.1 gives a model relating the ID to the CN, engine speed and intake conditions:

$$ID = f(CN, M_{ps}, T_{in}, p_{in})$$

As expected, the ID decreases exponentially for increasing CN under constant operating conditions.

Figures 6.2 and 7.3 show that the ID increases under a reduced intake oxygen concentration O_{2in}. Furthermore, this effect is coupled to the CN of the fuel: lower CN fuels show a higher sensitivity of the ID to O_{2in}. This effect may be modeled by including a term containing O_{2in} in Eq. 8.1. Equation 8.4 shows the proposed form of this extension to the correlation of Hardenberg and Hase, containing three fitting parameters: p_1, p_2, p_3.

$$ID = (p_1 + 0.22M_{ps}) \cdot$$
$$exp\left[\frac{p_2}{O_{2in} + p_3}\frac{618840}{CN + 25}\left(\frac{1}{RT_{TDC}} - \frac{1}{17190}\right) + \left(\frac{21.2}{p_{TDC} - 12.4}\right)^{0.63}\right] \tag{8.4}$$

Figure 7.6 shows that the intake temperature increases about linearly under reduced intake oxygen concentrations. A linear fit on the measurement data results in:

$$T_{in}\,(°C) = 182 - 4.78 \cdot O_{2in} \tag{8.5}$$

This can be used to eliminate T_{TDC} from Eq. 8.4 using Eq. 8.2. The intake manifold pressure p_{in} is not impacted significantly by EGR, and is therefore assumed constant and equal to the mean value recorded over all measurements (0.99 bar). This renders p_{TDC} constant as the polytropic exponent c is assumed constant as well. It should be noted that the ratio of specific heats γ is affected by EGR, resulting in a different p_{TDC}. The preceding reduces Eq. 8.4 to a relation between the parameters of interest:

$$ID = f\,(CN, O_{2in})$$

Fitting the measurements of Diesel$_2$, HVO100, and Diesel$_{2,CN-5}$ on this model using a non-linear least square fit yields the following parameters : $p_1 = 0.69$, $p_2 = 10.07$ and $p_3 = -7.77$. Figure 8.1 shows all measurements together with the fitted curves using the relevant CN, as listed in Table 6.3. The fuels used in the training data are plotted with a solid line, others are indicated by a dashed line. A coefficient of determination, R^2, of 95% was achieved with respect to all measurements. The model provides a reasonable prediction of the measurements using HVO50.
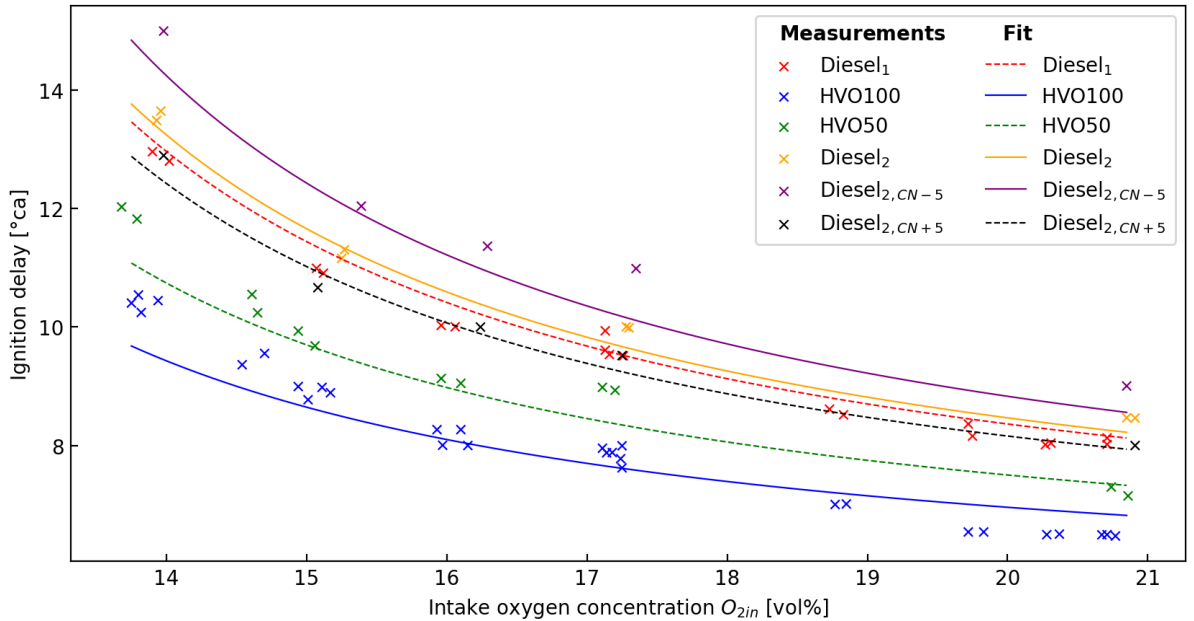
Figure 8.1: The measured and fitted ignition delay under varying intake oxygen concentrations for Diesel$_1$, HVO100, HVO50, Diesel$_2$, Diesel$_{2,CN-5}$ and Diesel$_{2,CN+5}$.

8.2 Calibration curves

The current model estimates the ID for a given CN and O_{2in}. As it is aimed to develop a cetane rating method, the inverse relationship is more interesting:

$$CN = f(ID, O_{2in})$$

Solving Eq. 8.4 for the CN results in Eq. 8.6. This allows to estimate the CN based on measurements of the ID and intake oxygen concentration O_{2in}, and can be used to create calibration curves for the alternative test.

$$CN = \frac{\frac{618840 \cdot p_2}{O_{2in} + p_3} \left(\frac{1}{RT_{TDC}} - \frac{1}{17190} \right)}{ln\left(\frac{ID}{p_1 + 0.22 \cdot M_{ps}} \right) - \left(\frac{21.2}{p_{TDC} - 12.4} \right)^{0.63}} - 25 \tag{8.6}$$

There are two possible approaches to generate calibration curves. EGR can be used to control the engine to a desired, fixed intake oxygen concentration. The ID measured under these conditions can be related to the CN of the fuel sample, forming a calibration curve $CN = f(ID)$. These curves curves are achieved by evaluating Eq. 8.6 at a constant value of O_{2in}, and correspond to an intersection of the lines in Figure 8.1 with a vertical.

On the other hand, EGR can be used to control the engine to operate at a desired, constant ID. The intake oxygen content required to achieve this can be related to the CN of the fuel sample, forming a calibration curve $CN = f(O_{2in})$. These curves are achieved by evaluating Eq. 8.6 at a constant value of the ID, and correspond to an intersection of the lines in Figure 8.1 with a horizontal.

8.2.1 Constant intake oxygen concentration

Figure 8.2 shows the relation $CN = f(ID)$ under constant intake oxygen concentrations of 20.8%, 17.2%, 15% and 13.7%. The measurements achieving these set values of O_{2in} were selected and added to the plot. The yellow dashed calibration curve indicates that these measurements fall within the zone of unstable engine operation. The general trend of the calibration curves is also represented in the measurements.
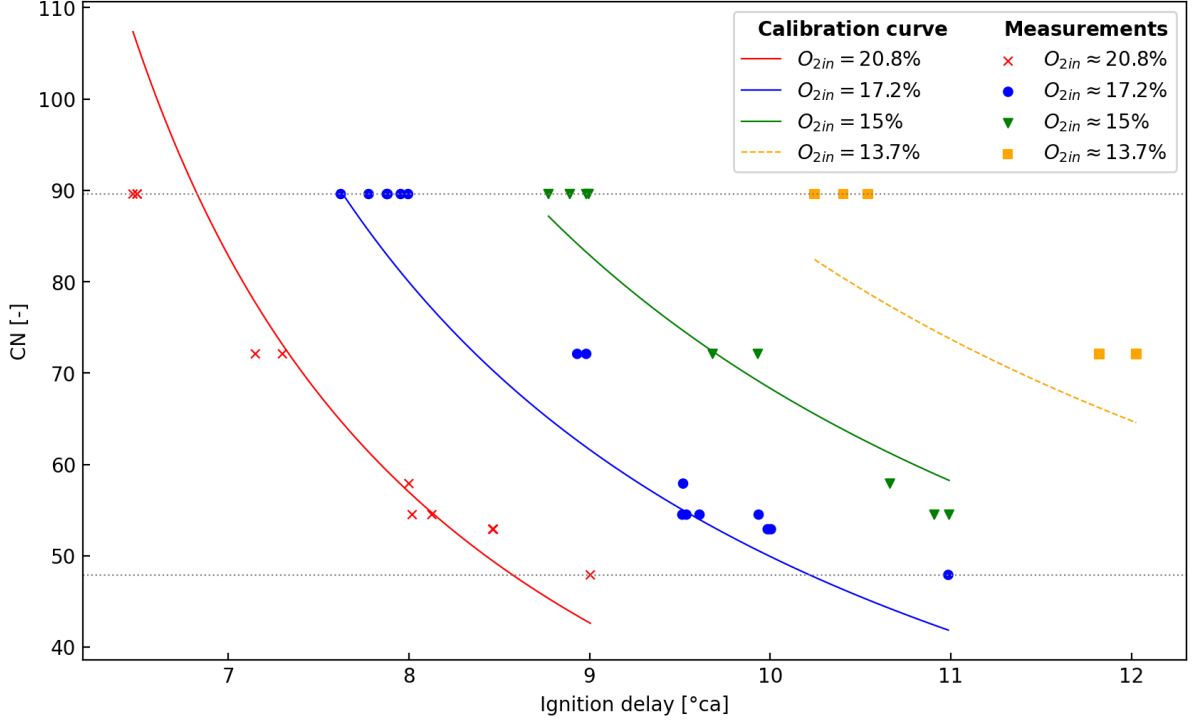
Figure 8.2: Calibration curves showing the relation between CN and ID under a constant intake oxygen concentration of 20.8%, 17.2%, 15% and 13.7%.

This representation shows the benefit of operating at reduced intake oxygen concentrations: the sensitivity of the ID to changes in CN is increased. This results in a higher measurement resolution and accuracy on the CN, given the limited measurement resolution and accuracy of the ID[1]. The black dotted lines show the minimum and maximum CNs that are tested. Operating at $O_{2in} = 17.2\%$ results in measurements where SOC occurs after TDC (i.e. $ID > 10°ca$) to span the current CN range. Temperature and pressure decreases after TDC, resulting in a further increase of the ID, making the comparison with other measurements difficult. Thus, achieving SOC before TDC forms a limit to the CN measurement range. This may be extended by an advanced injection timing.

At a given value of O_{2in}, the CN of a fuel sample can be estimated by evaluating the calibration curve in the measured ID: $CN_{calc} = f(ID_{measured})$. Figure 8.3 shows the relation of CN_{calc} to CN for the current measurements. Ideally, a unity relationship between CN and CN_{calc} is achieved, shown by the dotted line. This is however not the case due to discrepancies between the measurements and the fitted model shown in Figure 8.1, and due to spread in the results for repeated measurements of the same fuel. The coefficients of determination, R^2, are also given in Figure 8.3, from which it is concluded that the best CN estimation would be achieved at an O_{2in} of 17.2% or 15%. However, limitations with respect to achieving SOC before TDC should be taken into account.

---

[1]For a curve with a higher sensitivity of the ID to the CN (i.e. a flatter curve in Fig. 8.2), an interval ΔID on the horizontal axis results in a smaller interval ΔCN on the vertical axis.
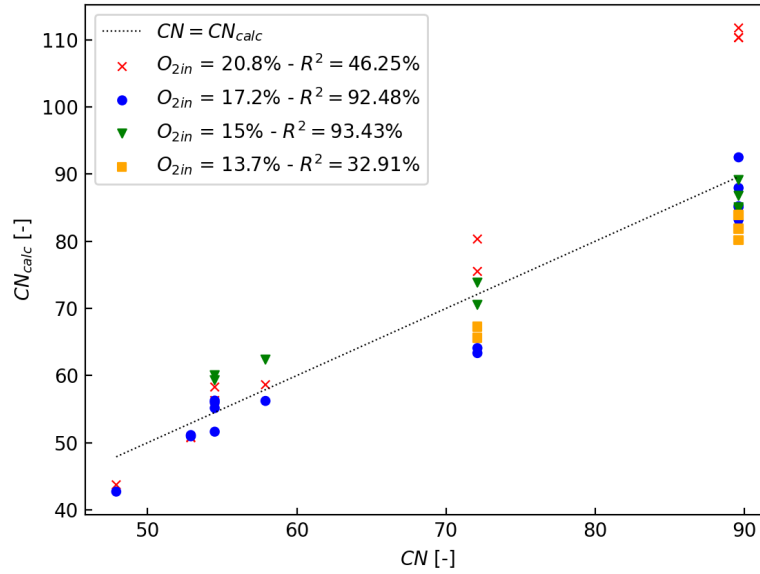
Figure 8.3: Comparing the actual CN of different tested fuels to the calculated CN using calibration curves at constant intake oxygen concentrations.

8.2.2 Constant ignition delay

Figure 8.4 shows the relation $CN = f(O_{2in})$ at constant values for the ID of 8°ca, 9°ca, and 10°ca. The measurements which achieve these IDs were selected and added to the plot. The shaded zone indicates where measurements are unstable. The general trend of the calibration curves is also represented in the measurements, and is as expected: a lower value of O_{2in} is required to control a higher CN fuel to a set ID.
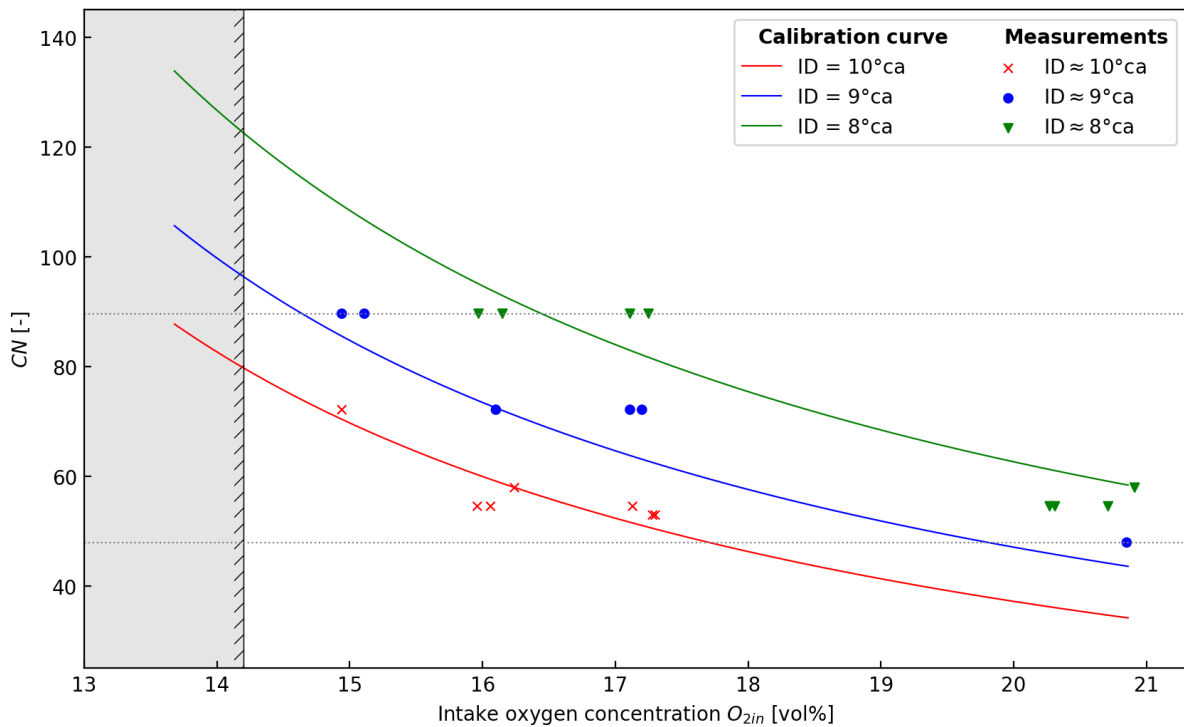
Figure 8.4: Calibration curves showing the relation between CN and the intake oxygen concentration to achieve a set ignition delay of 8°ca, 9°ca and 10°ca.

The black dotted lines show the minimum and maximum CNs that are tested. It is clear that, with an ID of 9°ca, the values of O_{2in} required to span this CN range stay within the stable zone. On the other hand, operating at an ID of 10°ca would require measurements in the unstable zone. It can be concluded that this unstable zone creates a relation between the chosen ID, and the CN measurement range of the test. Generally, a longer ID is more suited to test fuel samples with CNs in a lower range.

At a given value of the ID, the CN of a fuel sample can be estimated by evaluating the calibration curve in the measured O_{2in}: $CN_{calc} = f(O_{2in,measured})$. Figure 8.5 again shows the relation of CN_{calc} to CN. The values of R^2 would suggest an ID of 8°ca to provide the best CN estimations. Overall, the values of R^2 are lower than for operation at constant values of O_{2in}, but values between 70% and 90% would still suggest a relatively good fit. However, the difference between CN and CN_{calc} remains significant. For example, measurements at an ID of 8°ca resulted in a CN_{calc} between 82.9 and 95 for HVO100. These results may be improved with the use of more measurement data, an increased ID accuracy, or both.

Lastly, not only the current value of R^2 is important in selecting appropriate testing conditions. Figure 8.4 would suggest operation at an ID of 9°ca to be more favourable, as it allows to span the current CN range using the complete range of O_{2in}.
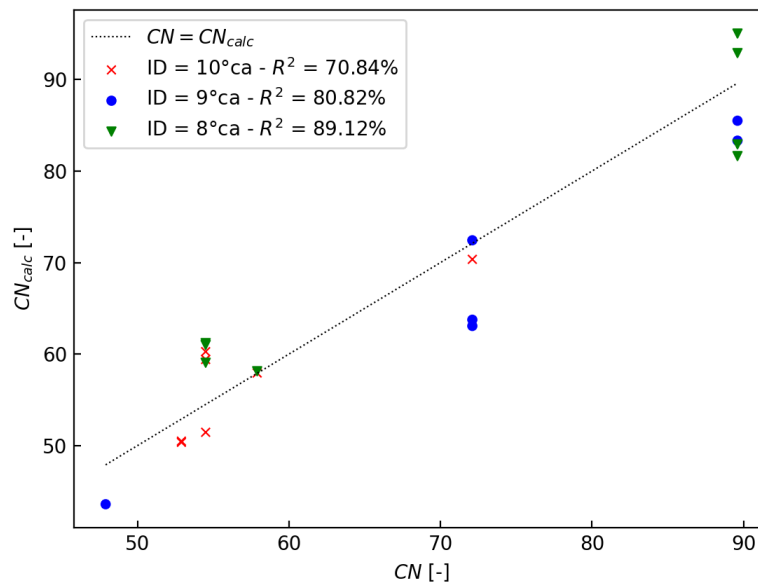
Figure 8.5: Comparing the actual CN of different tested fuels to the calculated CN using calibration curves at constant ID.

A comparison of Figures 8.3 and 8.5, based on R^2, suggests that operating under a constant-O_{2in}-strategy provides a better CN estimation. However, it is reasoned that operation under constant ID results in a better comparison of the fuels. In that case, different fuels undergo almost the same pressure and temperature trajectory during the ID. Therefore, the concept of constant ID yields the closest approximation to the ASTM D613 method. The constant-ID strategy also inherently avoids conditions in which SOC occurs after TDC. Further investigation with a more controlled set of fuel samples can give conclusion to this question.

8.3 Factors influencing the CN measurement range and resolution

The model fitted on the measurements can also be used to estimate the effect of other factors influencing the test method. Two factors will be discussed: the CN resolution and accuracy, and the effect of the intake temperature.

8.3.1 Estimating the CN resolution and accuracy

It was shown that the encoder resolution posed the largest limitation to the cetane accuracy. The calibration curves can be used to estimate the CN resolution and accuracy for a given encoder resolution. Figure 8.6 shows a calibration curve $CN = f(ID)$ at a constant intake oxygen concentration of 17%[2]. The black point indicates the CN of $Diesel_1$ and the corresponding ID. The red dotted lines indicate a window of $\pm 0.5°ca$, i.e. the smallest difference in ID that can be measured currently. This corresponds to a change of about 5 CN units according to the current model. Measurements using $Diesel_2$ and $Diesel_{2,CN\pm5}$, discussed in Section 7.1.3, led to the same conclusion. To conclude on the CN accuracy, the complete error margin on the ID should be considered. An error margin of $\pm 0.5°ca$ would result in a CN accuracy of 10 CN units. However, this ignores inter-cycle variability, which further reduces the accuracy.

Figure 8.6 also indicates a window of $\pm 0.2°ca$ around Diesel operation, indicated by green dotted lines. An encoder with upgraded resolution could improve the CN resolution to 2 CN units.
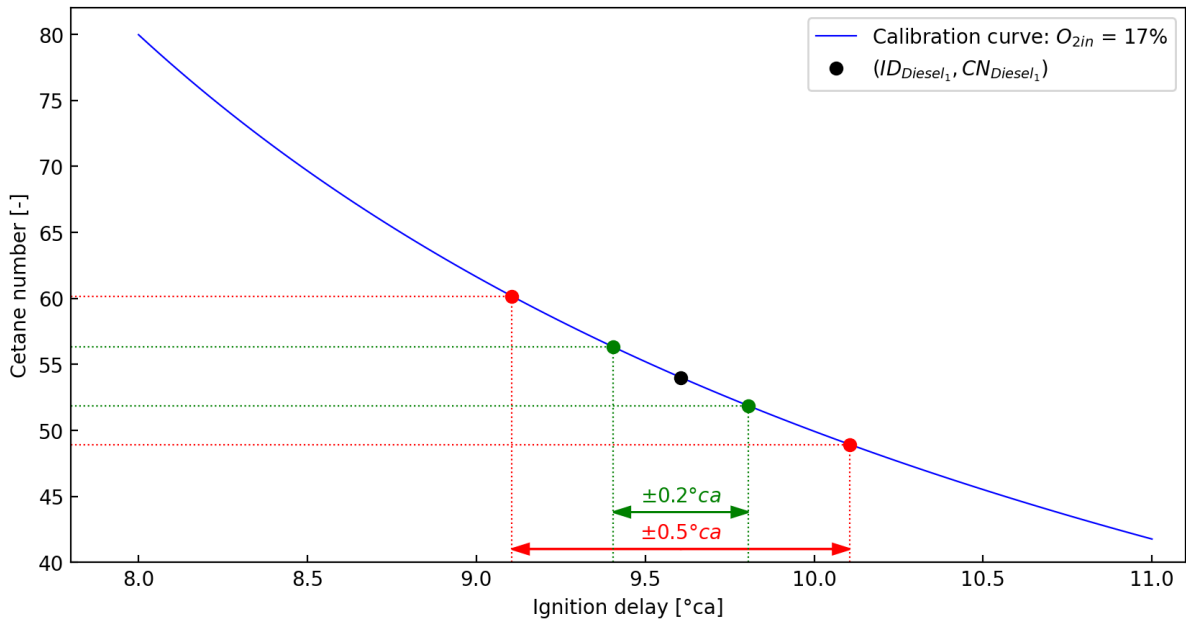
Figure 8.6: Using a modeled calibration curve $CN = f(ID)$ at $O_{2in} = 17\%$ to estimate the CN measurement resolution for an encoder resolution of $0.5°ca$ and $0.2°ca$.

8.3.2 Estimating the effect of an improved intake temperature control

The current model also allows to estimate the effect of an improved intake temperature control[3]. Currently, the intake temperature increase induced by EGR partially counteracts the increase

---

[2]It was chosen to show this calibration curve, as this allows the easiest interpretation. The same conclusions can be achieved with the use of a calibration curve $CN = f(O_{2in})$ at a constant ID.

[3]This holds under the assumption that the extension made to the correlation of Hardenberg and Hase (Eq. 8.4) has maintained a good prediction of temperature effects. This was not validated in itself.

in ID due to the reduced intake oxygen concentration. As can be expected, a constant intake temperature allows a higher CN measurement range.

Current operating conditions allows to test fuels with a CN ranging from 48 to 90. Fuels with CNs well above 90 are encountered little in practise and the current CN measurement range should suffice. It is thus actually desirable to have an increasing intake temperature with increasing EGR rates. However, a better control over the intake temperature may benefit the repeatability and accuracy of the test.

Chapter 9

Conclusion and future perspectives

9.1 Conclusion

The above-mentioned thesis work and research yielded some promising results and valuable insights. It is aimed to develop an alternative cetane rating method using a production CRDI Diesel engine, to serve sustainable fuel development. First and foremost, a thorough understanding of the cetane number and its test methods is attained. The ASTM D613 is the only standardized cetane test which operates under engine conditions, and is the standard up to this day. Three alternatives to emulate the variable compression ratio of the CFR engine, used in this standard, are investigated. A conclusion is formed based on information found in literature and our own hands-on experience.

The use of a throttle valve to emulate the effect of a decreased compression ratio is investigated in literature, where only a limited CN measurement range was achieved. On the other hand, using a variable geometry turbocharger (VGT) could allow a higher CN measurement range, while providing a better emulation of the CFR engine's variable compression ratio. However, a sufficiently high engine speed and load are required to influence the ID significantly. It is hypothesized that higher engine speeds result in more frequent software instabilities during measurement logging. Moreover, stronger oscillations of the cylinder pressure are observed under the investigated load points, resulting in a less reliable estimation of the start of combustion (SOC). The ignition delay forms the basis of a cetane rating method, and needs to be determined in an accurate and reliable way. Several metrics to estimate SOC are investigated, from which the maximum of the second-order derivative of the pressure signal is chosen. This proves to be a robust metric, and its low number of assumptions reduces the amount of uncertainty compared to metrics based on HRR-calculations.

Because of the practical difficulties related to using the VGT to influence the ignition delay, exhaust gas recirculation (EGR) is considered as a third, alternative option. EGR decreases the intake oxygen concentration (O_{2in}), resulting in an increased ignition delay. Also, the difference in ID between fuels with a different CN is amplified at reduced intake oxygen concentrations, making it easier to distinguish between fuels. The CN measurement range is also not bound by the engine load point, as is the case for VGT operation.

Experiments are conducted using blends of Diesel, HVO, iso-octane and n-dodecane with a cetane number ranging from 48 to 90. The use of cooled EGR allows to increase the ignition delay by 5°ca under Diesel operation, which is about twice the range obtained with the VGT. Further experiments show that EGR indeed allows to control fuels with a wide CN range to manifest the same ignition delay. This proves that EGR may serve as a valuable alternative control input to the cetane rating test developed in this work.

The limited size of the EGR cooler results in an increased intake temperature with increasing EGR rate. It is expected that this influences the ignition delay in its turn, limiting the CN measurement range. The intake manifold pressure is almost unaffected by EGR, and is assumed to have a negligible effect on the ignition delay.

The measurement data is used to build a model of the test method, relating the cetane number to the ignition delay and intake oxygen concentration: $CN = f(ID, O_{2in})$. This model can be used to inter- and extrapolate between results, and decide on the optimal operation strategy of the test. The alternative cetane rating test can be conducted using two operation strategies: by maintaining either a constant value of the ID, or O_{2in}.

The engine can be controlled to a fixed intake oxygen concentration O_{2in}, which directly relates the measured ID to the CN of a fuel sample: $CN = f(ID)$. Under reduced intake oxygen concentrations, the sensitivity of the ID to changes in the CN is increased. This provides a higher CN measurement accuracy given the limited ID accuracy. Thus, the use of EGR shows its benefit for the development of an alternative cetane rating test. However, current measurements under a constant value of O_{2in} achieved ignition after TDC for fuels with a lower CN. It should be ensured that SOC remains before TDC, as otherwise, comparison with other fuels is difficult. Therefore achieving SOC before TDC poses a limit to the CN measurement range, when operating under constant O_{2in}.

On the other hand, EGR can be used to control the engine to operate at a desired, fixed ignition delay. This eliminates conditions where SOC occurs after TDC. The required intake oxygen content is then directly related to the CN of the fuel sample: $CN = f(O_{2in})$. Under constant ID, the CN measurement range is limited by the minimum achievable intake oxygen concentration at which stable engine operation is maintained. Both the measurements and the model suggest operation at a constant ID of 9°ca, as this allows CNs ranging from 45 to 90 to be tested.

A comparison of CN and CN_{calc}, based on R^2, would advice to operate the test under a constant-O_{2in}-strategy. However, the authors hypothesize that operation under a constant ID results in a better comparison of the fuels. In this case, different fuels undergo almost the same history of pressure and temperature during the ignition delay. This provides the closest approximation of the ASTM D613 method. Further investigation with a more controlled set of fuel samples can give conclusion to this question.

The CN measurement resolution and accuracy have been estimated, based both on measurements and the developed model. Measurements suggest a CN resolution between 3.4 and 5 CN units, while the model predicts a resolution of 5 CN units. The CN accuracy should take into account the limits of the ID resolution and inter-cycle variability. Both measurements and model predictions estimate a CN accuracy of about 10 CN units. It is shown that the limited encoder resolution accounts for about 60% of the ID uncertainty, making this a strong constraint on the accuracy of the developed CN test. Lastly, it is established that an upgraded EGR cooler is not required in terms of CN measurement range. However, an improved intake temperature control would benefit the accuracy of the test.

9.2 Future perspectives

The work through the year has led to several modifications of the test bench. This includes enabling control of the EGR and throttle valves, making the sensor connections required to record measurements, and building a Python-based post processing framework. However, unreliable behaviour of the engine control and DAQ system results in frequent engine stalls when recording a measurement. This posed the largest limitation to the amount of experimental data that could be collected. The source of the problem was not identified clearly. Improving the software

stability during measurements is paramount for conducting further experimental work on this engine test bench. A solution may come in the form of a separate LabVIEW script, parallel to the current engine control system, responsible for measurement logging only. Currently, the engine control software does not allow a real-time calculation of the ID. This functionality may be included in the secondary LabVIEW script.

The above-mentioned adaptations may largely improve the workflow for the alternative cetane rating test. Currently, a comparison of CN to CN_{calc}, based on the value of R^2, would advice to operate the test under constant values of O_{2in}. As no real-time calculation of the ID was possible this year, measurements were conducted under a selection of EGR and throttle valve positions, resulting in an almost constant set of intake oxygen concentrations. It is simply possible that higher values of R^2 are achieved under constant O_{2in} due to the availability of more measurements. Measurement data using a more controlled set of fuel blends and a real-time calculation of the ID may improve the predicted CN under a constant ID-strategy.

However, the largest limitation to the CN accuracy originates from the limited encoder resolution. Upgrading the current encoder would largely improve the CN accuracy. Also an improved intake temperature control may be a worthwhile adaptation to the setup.

It is important to note that it should be further examined what the lowest CN is at which the engine can operate, as this forms the practical lower limit to the CN measurement range.

Part III

Appendices

Appendix A

Error analysis

Error calculations for measured and calculated quantities are covered in this appendix. The error on a measured quantity can be depicted as in Eq. A.1. A particular quantity, such as pressure, temperature, etc., is denoted by the symbol X. Every sensor's measured value differs from the actual value, due to noise or environmental factors, by a very small margin δX.

$$X_{actual} = X_{measured} + \delta X \tag{A.1}$$

A.1 Measured quantities

A.1.1 In-cylinder pressure signal

The in-cylinder pressure signal undergoes several conversion processes before they are transmitted to the PC. Figure A.1 schematically shows these steps, along with the corresponding unit of the signal at that time. The AVL GH13P piezoelectric pressure sensor generates an electrical charge (in the order of pC) proportional to the in-cylinder pressure. This signal is converted to a voltage (0-10V) by the AVL Microifem amplifier, which is finally converted to a digital signal by the PXI-6123 module and sent to the PC. The following sections discuss the signal error through the different stages, to finally estimate the error on the cylinder pressure signal. Table A.1 lists the values of the relative and absolute errors of the different components in the signal chain of cylinder and manifold pressures.
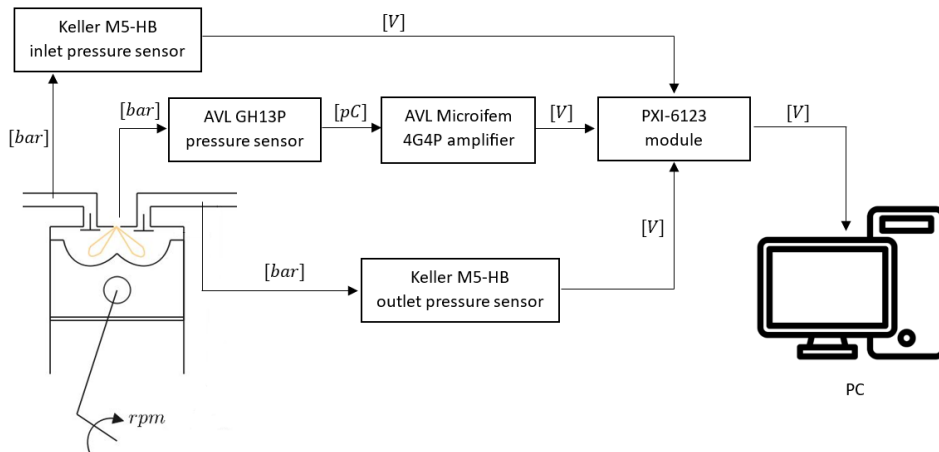
Figure A.1: A schematic representation of the signal path of the different pressure sensors.

Table A.1: Absolute and relative errors on the pressure measurement components, FS = full scale.

Source X	AE$_\mathbf{X}$	RE$_\mathbf{X}$
AVL GH13P	$\pm 0.09\% FS$	-
AVL MICROIFEM	1mV + 0.01%FS	-
NI PXI-6123	3 mV	0.02%
Intake Keller M5-HB	0.027%FS	-
Outlet Keller M5-HB	0.053%FS	-

A.1.1.1 In-cylinder pressure sensor

Instead of a direct voltage reading, the in-cylinder pressure sensor converts the pressure signal into an electric charge. The sensitivity and error of the sensor are dependent on the temperature and pressure it operates at. Figure A.2 shows the sensor's configuration, as shown in the AVL Indisignal software. The pressure range is set to 250 bar. The manufacturer determined the sensitivity to be 15.74 $\frac{pC}{bar}$, at 230 °C and 150 bar respectively. For these settings, the error on the sensitivity is $\pm$ 0.09 $\%FS$.
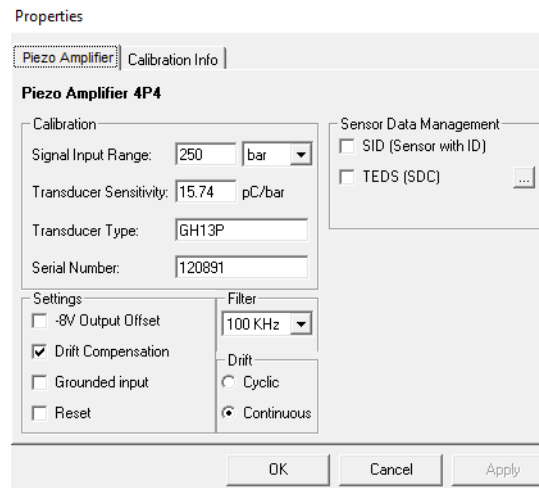
Figure A.2: Calibration properties AVL GH13P pressure sensor.

Figure A.3 gives a graphical representation of the sensitivity error of the sensor if a measurement range of 250 bar is chosen. The error on the $FS = 15.74 \frac{pC}{bar} \cdot 250 \ bar = 3935 \ pC$ is thus $\pm 3.54 \ pC$.
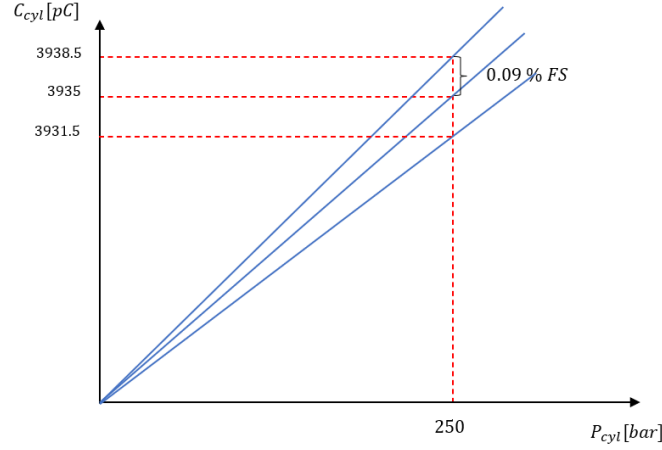
Figure A.3: The sensitivity and error of the AVL GH13P pressure sensor.

The charge generated by the AVL G13P C_{cyl}, and the absolute error, is given by Eq. A.2.

$$C_{cyl} = x\ bar \cdot\ 15.74\ \frac{pC}{bar}\ \pm\ 3.54\ pC \tag{A.2}$$

A.1.1.2 Microifem amplifier

The Microifem amplifier converts the electric charge from the in-cylinder sensor into a voltage that is readable for the PC. The output is a voltage between 0 and 10 V, which gives a conversion factor of $\frac{10}{3935}\ \frac{V}{pC}$. The datasheet [101] lists a fixed AE of $1\ mV + 0.1\% FS$, resulting in an AE of $2\ mV$. The error of the pressure sensor is passed on to the amplifier. The accumulated error on the cylinder pressure signal, after the amplifier, is given by Eq. A.3.

$$V_{cyl} = [x\ bar \cdot\ 15.74\ \frac{pC}{bar}\ \pm\ 3.54\ pC]\ \cdot \frac{10}{3935}\ \frac{V}{pC}\ \pm\ 2\ mV \tag{A.3}$$

A.1.1.3 PXI-6123

Finally, the PXI-6123 module performs an analog-to-digital conversion on the signal, and communicates the data to the PC. This module has both an absolute error, and a relative error. The datasheet [102] provides an explanation on how to calculate the error, resulting in an error of $4.96\ mV$. The total error on the in-cylinder pressure is given by Eq. A.4.

$$V_{cyl} = \left[\left[x\ bar \cdot\ 15.74\ \frac{pC}{bar}\ \pm\ 3.54\ pC\right]\ \cdot\frac{10}{3935}\ \frac{V}{pC}\ \pm\ 0.002\ V\right] \pm\ 0.00496\ V$$
$$= x\ bar \cdot 0.04\ \frac{V}{bar} \pm 0.01596\ V \quad \text{(A.4)}$$

As the signal of the cylinder pressure is pegged with the pressure of the inlet manifold, the total error on the pressure signal is the sum of both signals. Multiplication with the corresponding conversion factor gives the total error on the pressure signal depicted in Eq. A.5.

$$\delta P_{cyl,tot} = (\delta P_{cyl} + \delta P_{inlet}) = (\delta V_{cyl} \cdot 25 \, \frac{bar}{V}) + (\delta V_{inlet} \cdot 1 \, \frac{bar}{V})$$
$$= (0.399 \, bar + 0.00766 \, bar) = \pm \, 0.4066 \, bar \quad \text{(A.5)}$$

A.1.2 Manifold pressures

The inlet and outlet manifold pressures are measured by two Keller M5-HB piezoelectric pressure transducers. The datasheets state an absolute error (AE) of 0.027%FS and 0.053%FS for the inlet and outlet respectively. The sensor generates a voltage between 0 and 10V, proportional to the manifold pressure, resulting in a conversion factor of $1 \, \frac{V}{bar}$. Eq. A.6 gives the absolute error on the inlet and outlet manifold pressure signal.

$$\begin{cases} V_{inlet} = x \, bar \, \cdot \, 1 \, \frac{V}{bar} \, \pm 0.0027 \, V \\ V_{outlet} = x \, bar \, \cdot \, 1 \, \frac{V}{bar} \, \pm 0.0053 \, V \end{cases} \quad \text{(A.6)}$$

The manifold pressure sensors are also transmitted to the PC, through the PXI-6123 module. Therefore, the error of the data acquisition unit is also added to the manifold sensor voltage. The total error on the manifold pressures given by Eq. A.7.

$$\begin{cases} V_{inlet} = [x \, bar \cdot 1 \, \frac{V}{bar} \, \pm \, 0.0027 \, V \,] \, \pm \, 0.00496 \, V = x \, bar \cdot 1 \, \frac{V}{bar} \, \pm \, 0.00766 \, V \\ V_{outlet} = [x \, bar \cdot 1 \, \frac{V}{bar} \, \pm \, 0.0053 \, V \,] \, \pm \, 0.00496 \, V = x \, bar \cdot 1 \, \frac{V}{bar} \, \pm \, 0.01026 \, V \end{cases} \quad \text{(A.7)}$$

Using the unity conversion factor between sensor voltage and pressure, the error on the inlet and outlet manifold pressure sensors are $\pm 0.007 bar$ and $\pm 0.01 bar$ respectively.

A.1.3 Manifold temperatures

Two K-type thermocouples are used to measure the intake and exhaust manifold temperatures. The error on a K-type thermocouple at high temperatures is about 0.75% of the measured value [103].

$$\frac{\delta T_i}{T_i} = 0.0075 \quad \text{(A.8)}$$

A.1.4 Engine speed

The engine speed is calculated by the NI-CAS software, based on the Kistler type 2614C11 optical encoder. However, the fluctuating load of the hydraulic dynamometer results in engine speed variations during measurements. This variation is dominant over the accuracy of the speed calculation done by the software. Therefore, the error on the engine speed is calculated by the peak-to-peak variation, which was maximum 25 rpm over all used measurements. The resulting abolute error on the engine speed is half of this:

$$\delta n[rpm] = \frac{25}{2} = 12.5 \quad \text{(A.9)}$$

A.2 Calculated quantities

The measured quantities can be used to calculate other, derived, quantities. One can determine the error on a these quantities by using the standard error propagation formula, shown in Eq. A.10, and the errors on the measured quantities.

$$\delta X(x,y) = \sqrt{(\frac{\partial X}{\partial x})^2 \cdot (\delta x)^2 + (\frac{\partial X}{\partial y})^2 \cdot (\delta y)^2} \tag{A.10}$$

A.2.1 Pegged cylinder pressure

Each engine cycle, the cylinder pressure signal is pegged to the inlet manifold pressure signal around inlet valve closure. This results in an accumulation of the error of both pressure signals:

$$\delta P_{cyl,peg} = \delta P_{cyl} + \delta P_{inlet} \tag{A.11}$$

A.2.2 Heat release rate

The equation for the HRR is repeated for simplicity as it was derived in Section 5.2.2.

$$\frac{dQ_n}{d\theta} = \frac{\gamma}{\gamma - 1} p_{cyl} \frac{dV}{d\theta} + \frac{1}{\gamma - 1} V \frac{dp_{cyl}}{d\theta} \tag{A.12}$$

The standard error propagation formula (Eq. A.10) is applied to the HRR.

$$\delta \frac{dQ_n}{d\theta}(P_{cyl}, \gamma, V) = \left\{ (\frac{\delta \frac{dQ_n}{d\theta}(P_{cyl}, \gamma, V)}{\delta P_{cyl}})^2 \cdot (\delta P_{cyl})^2 + (\frac{\delta \frac{dQ_n}{d\theta}(P_{cyl}, \gamma, V)}{\delta \gamma})^2 \cdot (\delta \gamma)^2 + \right.$$
$$\left. (\frac{\delta \frac{dQ_n}{d\theta}(P_{cyl}, \gamma, V)}{\delta V})^2 \cdot (\delta V)^2 \right\}^{1/2} \tag{A.13}$$

The error δP_{cyl} equals $\delta P_{cyl,peg}$. The specific heat ratio γ is assumed constant at 1.3 during the calculations in Section 5.2.2. However, the value is significantly impacted by the combustion process. Heywood discovered that during combustion, γ varies between 1.3 and 1.35, such that $\delta \gamma = 0.05$ [29]. The volume of the cylinder varies over the period of a cycle. The volume change error should be small and is neglected ($\delta V = 0$). The elaborated error on the HRR is shown in Eq. A.14.

$$\delta \frac{dQ_n}{d\theta} = \left\{ (\frac{\gamma}{\gamma - 1} \frac{dV}{d\theta})^2 \cdot (\delta P_{cyl})^2 + (\frac{1}{\gamma - 1} V)^2 \cdot (\delta \frac{dP_{cyl}}{d\theta})^2 + \right.$$
$$\left. (\frac{P_{cyl}}{\gamma - 1} \frac{dV}{d\theta} - \frac{\gamma}{(\gamma - 1)^2} P_{cyl} \frac{dV}{d\theta} - \frac{V}{(\gamma - 1)^2} \frac{P_{cyl}}{d\theta})^2 \cdot (\delta \gamma)^2 \right\}^{1/2} \tag{A.14}$$

Figure A.4 shows the HRR of a cycle around TDC with the corresponding error margins as calculated in Eq. A.14. The SOI is shown by the black line. The pressure signal values are low before combustion occurs, resulting in a relatively high error on the HRR. The error relative to the HRR decreases during combustion, as the pressure signals and released heat are orders of magnitude greater and impact of errors is decreased.
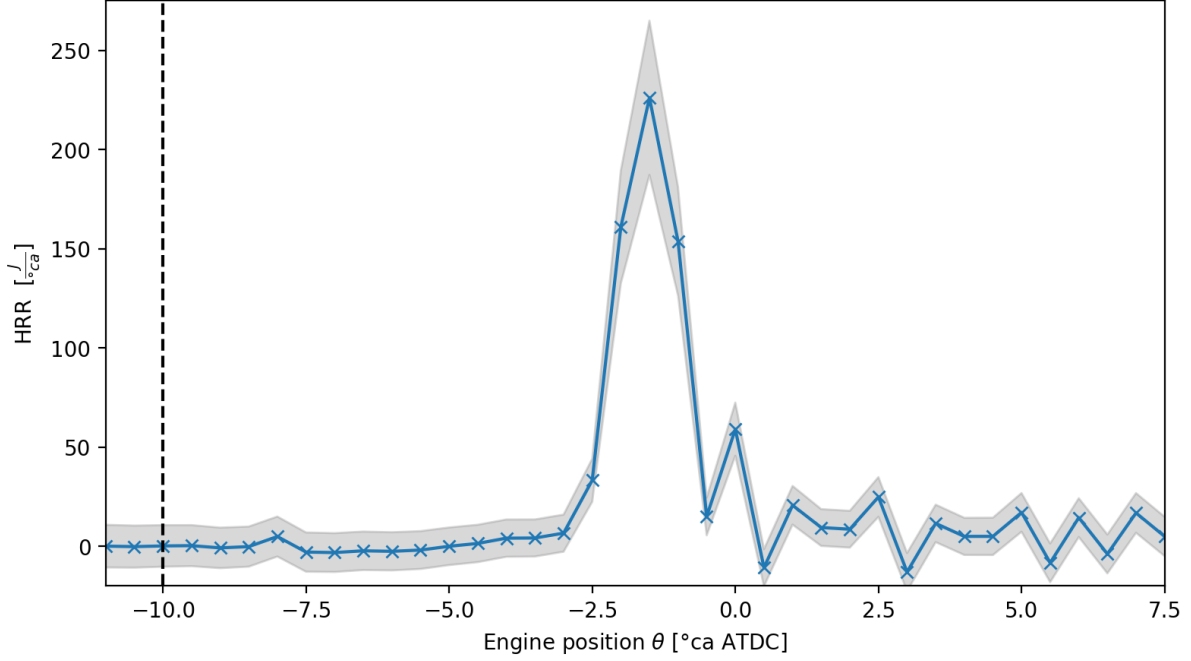
Figure A.4: The HRR, and SOI (black dashed line), with error margins around TDC under the alternative cetane rating method operating conditions using Diesel.

A.2.3 Mass fraction burned

The MFB follows from an integration of the HRR, resulting in an accumulation of the error on the HRR.

Calculation of error on MFB is done by summation of the error on the HRR.

$$\delta MFB \approx \sum_{\theta=\theta_{SOI}} \frac{dQ_n}{d\theta} \tag{A.15}$$

Due to the large relative $\delta \frac{dQ_n}{d\theta}$ before combustion, the error on MFB accumulates very rapidly from SOI onwards. As a result, the MFB metric's level of uncertainty increases to the point where it is no longer considered a reliable way to calculate SOC. As an alternative starting point, one could consider the minimum of the MFB curve. Figure A.5 shows the error on MFB around the moment at which a flammable mixture is formed. The orange lines indicate CA2, 5, and 10 respectively. Since the point at which the MFB reaches its minimum value is not consistent between cycles, this method cannot be considered measurement-independent. Therefore, it was opted to use DP-metrics to estimate SOC.
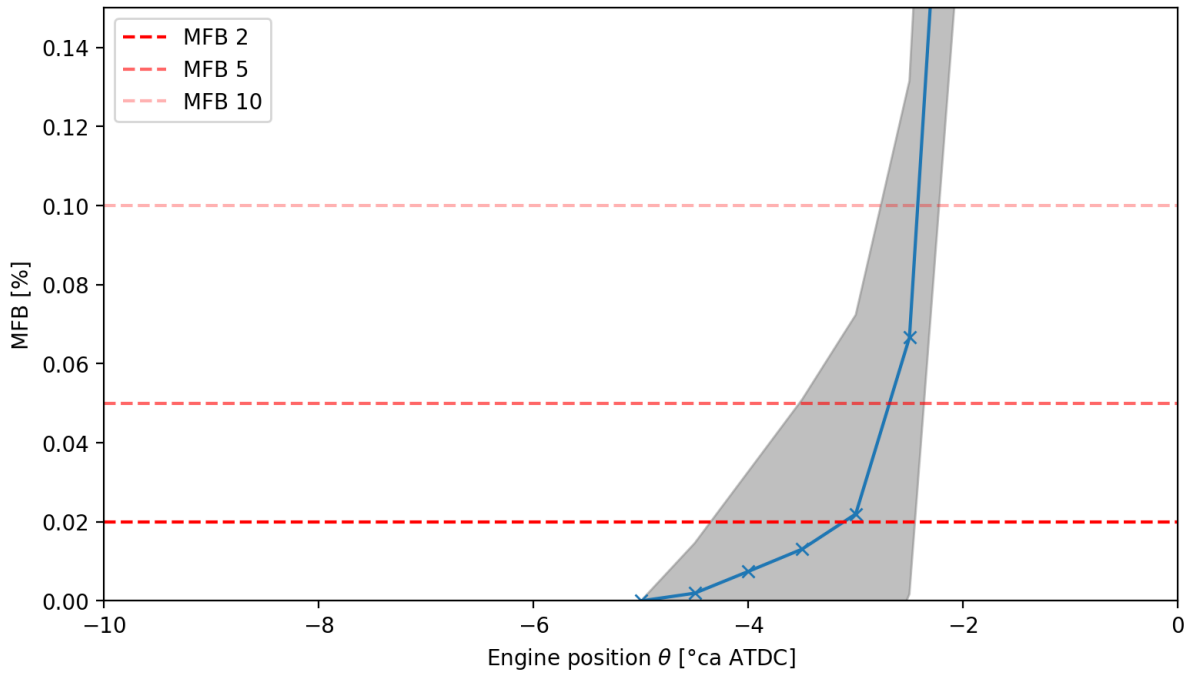
Figure A.5: MFB around TDC with CA2, 5 ,10 indicated by dashed orange lines, under the alternative cetane rating method operating conditions using Diesel.

Appendix B

Determining SOC based on pressure derivatives

The start of combustion is determined in post-processing, by detecting the location of strong increase in pressure, i.e. by detecting large peaks in pressure derivatives. The Python package `Scipy` contains a function `find_peaks` to detect peaks in a signal. To avoid a faulty detection of SOC due to measurement noise, only peaks which occur after SOI and surpass a set threshold value are considered as valid. The threshold values are set to a certain percentage of the maximum of the corresponding signal and can be altered manually in the function `get_soc_dp`. Figure B.1 shows the pressure trace and its first three derivatives for one of the cycles of Diesel operation under conditions similar to those in the cetane rating test. The SOI is indicated with a red dashed line, the threshold values are marked by grey dotted lines. The figure also shows a crank angle position θ_{start}. This value can be set manually, such that only peaks after θ_{start} will be considered. It is clear that with the current threshold values, SOC would not be detected correctly based on the third order derivative if peaks are detected from SOI. Raising the relevant threshold value would relieve the problem in this measurement cycle, but may induce faulty SOC detection in other cycles. This is because the height of signal and noise peaks vary between cycles. The manual specification of θ_{start} allows to achieve a minimum of inter-cycle variability in the SOC detection.
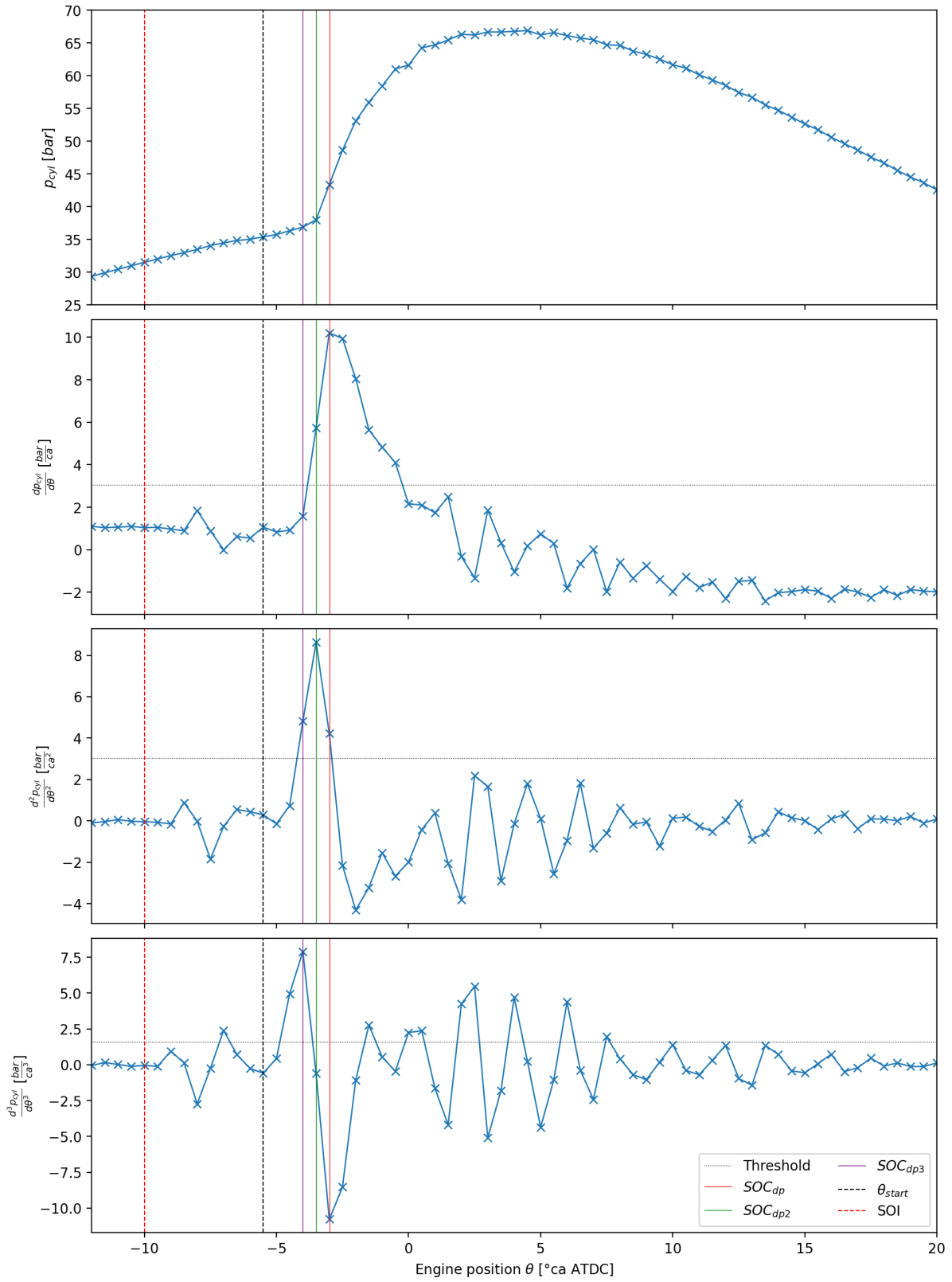
Figure B.1: Pressure traces of a measurement cycle of Diesel operation under conditions similar to those in the cetane rating test. An illustration of the SOC detection using pressure derivatives.

Appendix C

Estimating the intake oxygen content

The intake oxygen concentration can also be estimated through measurements of the intake gas flow rate and manifold temperatures and pressures. This may yield a good approximation for tests in the absence of a gas analyzer. The model assumes that a decrease in volumetric intake flow rate is compensated by an equal volume of EGR, and has been proposed by Dierickx and Huyghebaert [104]. These calculations were implemented, giving satisfactory results. The model was not further studied as the gas analyzer was used for further tests, but it remains interesting for future work.

The EGR flow rate $\dot{m}_{EGR}$ follows from the decrease in intake volumetric flow rate ΔQ_{in}, as shown in Eq. C.1.

$$\dot{m}_{EGR} = \rho_{EGR} \cdot \Delta Q_{in} \tag{C.1}$$

Comparing the current volumetric intake flow rate Q_{in} to the intake flow rate in absence of EGR $Q_{in,0}$ gives $\Delta Q_{in} = Q_{in,0} - Q_{in}$. The measured intake mass flow rate is converted to a volumetric flow rate using the air density resulting from air as an ideal gas on the measured ambient lab conditions. The EGR density ρ_{EGR} is calculated using the ideal gas law, Eq. C.2, with p_{EGR} and T_{EGR} being the pressure and temperature measured in the exhaust manifold.

$$\rho_{EGR} = \frac{p_{EGR}}{R_{EGR} \cdot T_{EGR}} \tag{C.2}$$

The gas constant of the EGR gas mixture R_{EGR} is derived from the combustion equation. Equation C.3 considers lean combustion of dodecane as a representation for Diesel operation. The equivalence ratio λ is measured in the exhaust line.

$$\mathrm{C_{12}H_{26}} + \lambda\frac{37}{2}(\mathrm{O_2} + \frac{79}{21}\mathrm{N_2}) \longrightarrow 12\mathrm{CO_2} + 13\mathrm{H_2O} + \lambda\frac{37}{2}\frac{79}{21}\mathrm{N_2} + (\lambda - 1)\frac{37}{2}\mathrm{O_2} \tag{C.3}$$

This approximation of the exhaust gas composition allows to estimate its molar mass MW_{EGR} and gas constant R_{EGR} using Equations C.4 and C.5. The molar fractions of all exhaust species are denoted with y.

$$MW_{EGR} = y_{\mathrm{H_2O}} \cdot MW_{\mathrm{H_2O}} + y_{\mathrm{CO_2}} \cdot MW_{\mathrm{CO_2}} + y_{\mathrm{O_2}} \cdot MW_{\mathrm{O_2}} + y_{\mathrm{N_2}} \cdot MW_{\mathrm{N_2}} \tag{C.4}$$

$$R_{EGR} = y_{\mathrm{H_2O}} \cdot R_{\mathrm{H_2O}} + y_{\mathrm{CO_2}} \cdot R_{\mathrm{CO_2}} + y_{\mathrm{O_2}} \cdot R_{\mathrm{O_2}} + y_{\mathrm{N_2}} \cdot R_{\mathrm{N_2}} \tag{C.5}$$

Subsequently, the intake oxygen concentration follows from a mixing of two molar flow rates, according to Equation C.6. The oxygen concentration of the intake air $y_{O_2,intake}$ equal approximately 21%. The molar flow rates of the intake air, $\dot{n}_{air,in}$, and EGR stream, $\dot{n}_{EGR}$, follow by dividing the relevant mass flow rate by its molar mass.

$$y_{O_2,intake} = \frac{y_{O_2,air} \cdot \dot{n}_{air,in} + y_{O_2,EGR} \cdot \dot{n}_{EGR}}{\dot{n}_{in} + \dot{n}_{EGR}} \tag{C.6}$$

Figure C.1 shows the calculated intake oxygen concentration for some measurements, compared to the measured intake oxygen concentration. The calculated values only deviate by maximum 1 vol%-unit over the whole range. When the Ultramat 23 is set to a measurement range of 0 - 25 vol% O_2, a measurement accuracy of 0.25 vol% is obtained as well, making this calculation a usable estimation. Figure C.1 also shows results for HVO and HVO50. The results remain close to those of Diesel, since HVO has an air-to-fuel ratio and C/H ratio close to those of Diesel. Fuels with significantly different air-to-fuel ratios are expected to provide lower quality estimations. The model can be further extended to arbitrary C/H-ratios.
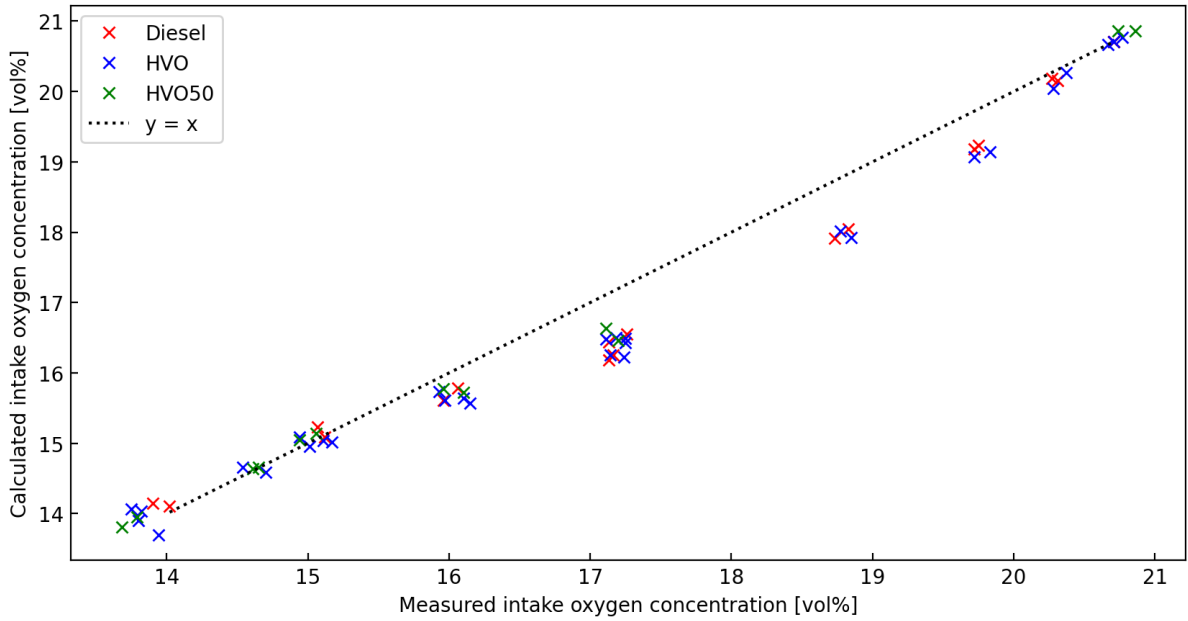
Figure C.1: Comparing the calculated intake oxygen concentration to direct measurements for Diesel, HVO and HVO50 under conditions of the alternative cetane rating test and reduced intake oxygen concentrations.

Appendix D

Calculated ignition delay for all recorded measurements
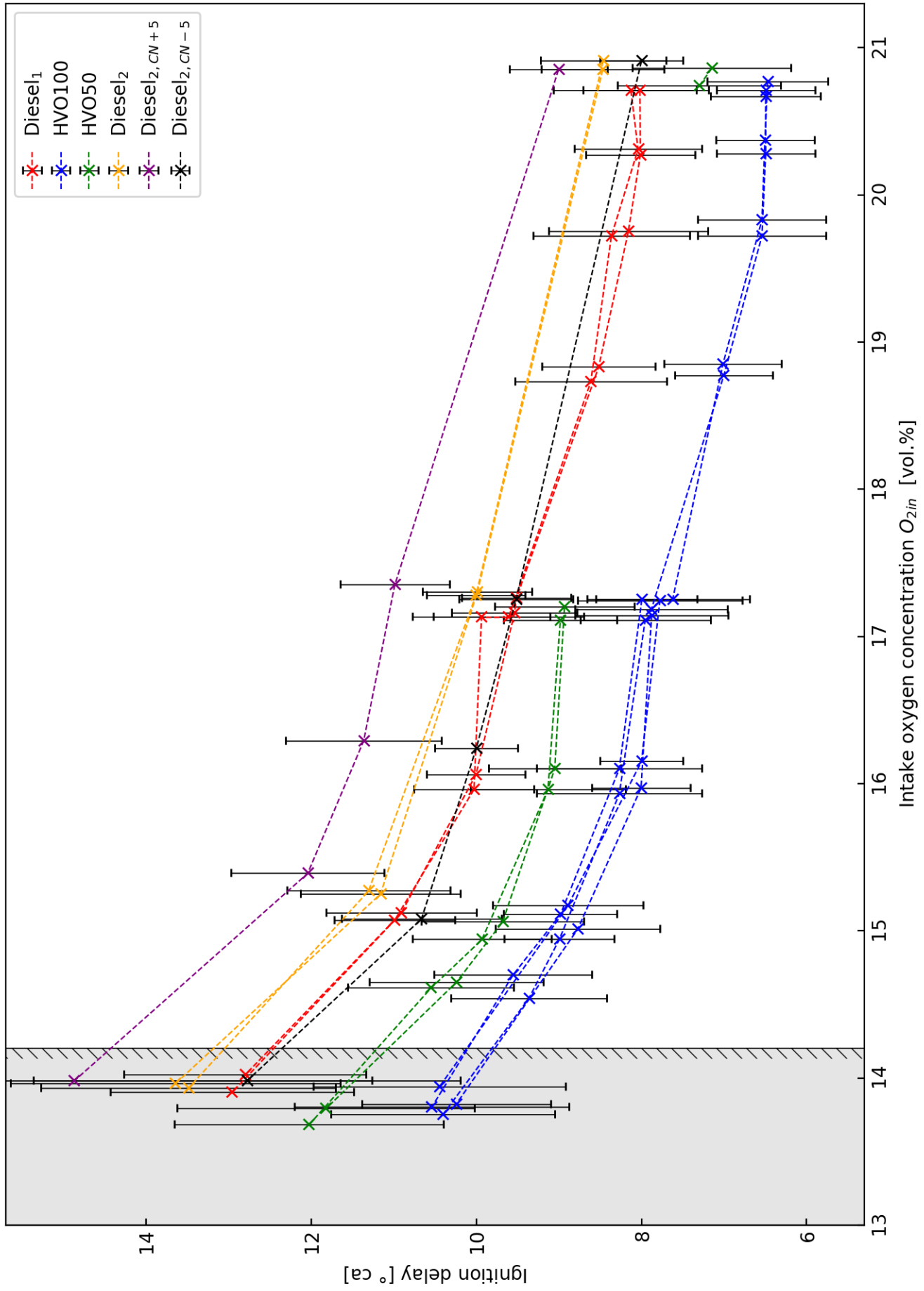
Figure D.1: The effect of a reduced intake oxygen concentration using EGR on the ignition delay for different fuels - all recorded measurements.

Appendix E

Measurement data

Diesel Batch 1

Date measurement	5/04/2023	5/04/2023	5/04/2023	5/04/2023	5/04/2023	5/04/2023	5/04/2023	5/04/2023	5/04/2023	6/04/2023	6/04/2023	6/04/2023	6/04/2023	6/04/2023	6/04/2023	6/04/2023	6/04/2023	6/04/2023
Environmental conditions																		
Patm [hPa]	1017.9	1017.7	1017.6	1017.4	1017.4	1017.2	1017	1016.9	1016.9	1012.8	1012.8	1012.8	1012.8	1012.6	1012.6	1012.5	1012.4	1012.3
Tatm [°C]	20.7	20.8	20.9	21	21.1	21.1	21.1	21.1	21.2	20.8	20.9	20.9	20.8	21.1	21.2	21.2	21.1	21.2
Relative humidity [%]	21.4	21.5	21.5	20.7	20.7	20.9	20.9	21.1	21.1	31.1	31.4	31.6	32.2	32.4	33.2	32.7	34.2	34.1
Parameters held constant																		
SOI [°ca BTDC]	10	10	10	10	10	10	10	10	10	10	10	10	10	10	10	10	10	10
Pedal stand [%]	7	7	7	7	7	7	7	7	7	7	7	7	7	7	7	7	7	7
Injection pressure [bar]	900	900	900	900	900	900	900	900	900	900	900	900	900	900	900	900	900	900
Variable parameters																		
EGR valve [%open]	0	20	30	40	100	100	100	100	100	0	20	30	40	100	100	100	100	100
Intake throttle valve [%open]	100	100	100	100	100	50	30	20	10	100	100	100	100	100	50	30	20	10
Measured conditions																		
Speed [rpm]	1293	1301	1296	1301	1301	1294	1298	1302	1311	1297	1300	1301	1293	1296	1296	1292	1316	1326
Tinlet [°C]	87.28	86.18	87.24	90.71	99.63	100.60	104.55	108.92	116.29	84.75	85.03	86.52	90.67	101.03	102.93	107.68	110.09	116.60
Pinlet [bar]	1.01	1.01	1.01	1.01	1.01	1.01	1.00	0.99	0.98	1.01	1.01	1.01	1.01	1.01	1.01	1.00	0.99	0.97
O2 - intake [%]	20.71	20.27	19.75	18.83	17.26	17.16	16.06	15.12	14.02	20.71	20.31	19.72	18.73	17.13	17.13	15.96	15.07	13.90
CO2 - intake [%]	0.04	0.37	0.75	1.42	2.53	2.6	3.38	4.05	4.83	0.05	0.34	0.77	1.49	2.62	2.61	3.44	4.07	4.91
CO - intake [%]	0.004	0.005	0.006	0.006	0.011	0.012	0.017	0.026	0.047	0.003	0.002	0.003	0.004	0.014	0.013	0.018	0.026	0.049
NO - intake [vpm]	11	95	146	187	157	143	125	77	28	30	104	182	208	170	152	141	92	32
O2 - exhaust [%]	13.14	12.81	12.13	11.13	9.66	9.36	8.52	7.6	5.37	12.99	12.72	12.09	10.98	9.49	9.27	8.52	7.57	5.21
CO2 - exhaust [%]	5.39	5.64	6.14	6.89	7.93	8.16	8.74	9.41	11.02	5.54	5.72	6.18	6.97	8.05	8.2	8.77	9.43	11.14
CO - exhaust [%]	0.017	0.018	0.017	0.019	0.028	0.030	0.038	0.049	0.090	0.015	0.013	0.015	0.018	0.029	0.032	0.039	0.053	0.093
NO - exhaust [vpm]	989	953	889	754	497	447	318	186	51	1272	1189	1082	860	526	472	351	196	66
Calculated conditions																		
O2 - intake [%]	20.71	20.19	19.23	18.05	16.55	16.26	15.78	15.09	14.11	20.71	20.16	19.18	17.92	16.44	16.18	15.62	15.24	14.15
massflow - EGR [kg/h]	0.00	1.51	4.15	7.12	10.45	11.04	11.93	13.11	14.53	0.00	1.61	4.30	7.47	10.70	11.21	12.27	12.89	14.54
IMEP [bar]	4.32	4.30	4.43	4.42	4.46	4.42	4.47	4.45	4.50	4.34	4.46	4.43	4.41	4.44	4.37	4.47	4.41	4.45
ID - DP1 [°ca]	8.72	8.72	8.95	9.28	10.18	10.36	10.68	11.58	13.65	8.92	8.75	9.02	9.43	10.42	10.50	10.73	11.66	13.90
ID - DP2 [°ca]	8.02	8.01	8.16	8.52	9.51	9.54	10.00	10.91	12.80	8.13	8.04	8.36	8.61	9.61	9.94	10.03	10.99	12.96
ID - DP3 [°ca]	7.50	7.50	7.53	8.00	9.00	9.00	9.50	10.27	12.01	7.52	7.50	7.62	8.01	9.00	9.24	9.50	10.35	12.24
ID - CA2 [°ca]	7.58	7.53	7.58	7.70	8.33	8.42	8.57	9.01	9.94	7.49	7.41	7.54	7.83	8.27	8.45	8.62	9.09	10.00
ID - CA5 [°ca]	8.00	7.98	8.06	8.33	9.12	9.18	9.54	10.20	11.72	8.05	7.99	8.10	8.41	9.19	9.33	9.62	10.32	11.88
ID - CA10 [°ca]	8.18	8.19	8.30	8.64	9.55	9.61	10.01	10.75	12.50	8.26	8.20	8.39	8.68	9.74	9.74	10.07	10.84	12.69

Diesel Batch 2

Date measurement	14/04/2023	14/04/2023	14/04/2023	14/04/2023	20/04/2023	20/04/2023	20/04/2023	20/04/2023
Environmental conditions								
Patm [hPa]	1005.2	1005.3	1005.2	1005.2	1014.1	1013.9	1013.6	1013.6
Tatm [°C]	23	22.9	22.6	22.5	20.2	21	21.2	21.2
Relative humidity [%]	26.2	26.5	26.9	27.1	31.1	29.7	29.3	29
Parameters held constant								
SOI [°ca BTDC]	10	10	10	10	10	10	10	10
Pedal stand [%]	7	7	7	7	7	7	7	7
Injection pressure [bar]	900	900	900	900	900	900	900	900
Variable parameters								
EGR valve [%open]	0	100	100	100	100	100	100	100
Intake throttle valve [%open]	100	100	40	30	10	20	30	40
Measured conditions								
Speed [rpm]	1304	1288	1298	1318	1298	1298	1299	1302
Tinlet [°C]	82.45	96.49	106.00	116.91	79.93	98.56	106.26	115.71
Pinlet [bar]	1.00	1.00	0.98	0.97	1.00	1.01	0.99	0.97
O2 - intake [%]	20.91	17.28	15.27	13.93	20.85	17.30	15.25	13.96
CO2 - intake [%]	0.01	2.64	4.05	4.95	0.03	2.58	4.01	4.92
CO - intake [%]	0	0.01	0.023	0.045	0	0.011	0.026	0.048
NO - intake [vpm]	3	155	75	19	7	162	84	26
O2 - exhaust [%]*	/	/	/	/	/	/	/	/
CO2 - exhaust [%]*	/	/	/	/	/	/	/	/
CO - exhaust [%]*	/	/	/	/	/	/	/	/
NO - exhaust [vpm]*	/	/	/	/	/	/	/	/
Calculated conditions								
O2 - intake [%]	20.91	16.40	15.00	14.09	20.85	16.52	15.14	13.88
massflow – EGR [kg/h]	0.00	10.94	13.42	14.59	0.00	10.59	13.07	14.84
IMEP [bar]	4.23	4.43	4.26	4.32	4.23	4.31	4.25	4.29
ID - DP1 [°ca]	9.09	10.57	11.96	14.37	9.07	10.50	11.86	14.55
ID - DP2 [°ca]	8.46	10.00	11.30	13.49	8.47	9.99	11.16	13.65
ID - DP3 [°ca]	7.84	9.49	10.64	12.66	7.82	9.41	10.53	12.81
ID - CA2 [°ca]	7.69	8.53	8.97	10.10	7.68	8.45	9.03	10.03
ID - CA5 [°ca]	8.17	9.46	10.49	12.21	8.17	9.38	10.39	12.28
ID - CA10 [°ca]	8.49	9.92	11.10	13.11	8.48	9.82	10.99	13.22

* The emissions in the exhaust were not measured as this was not further used in this work

HVO50 Batch

Date measurement	12/04/2023	12/04/2023	12/04/2023	12/04/2023	12/04/2023	12/04/2023	12/04/2023	12/04/2023	12/04/2023	12/04/2023	12/04/2023	12/04/2023
Environmental conditions												
Patm [hPa]	995.7	995.5	995.5	995.3	995.5	995.7	995.7	995.5	995.7	995.7	996.6	995.5
Tatm [°C]	21	21.1	21.1	21.2	21.1	21.2	21.1	21.1	21.1	21.1	21.2	21.1
Relative humidity [%]	34.4	32.1	34.1	33.9	33.8	33.6	33.4	31.6	33.1	33	32.9	32.3
Parameters held constant												
SOI [°ca BTDC]	10	10	10	10	10	10	10	10	10	10	10	10
Pedal stand [%]	7	7	7	7	7	7	7	7	7	7	7	7
Injection pressure [bar]	900	900	900	900	900	900	900	900	900	900	900	900
Variable parameters												
EGR valve [%open]	0	0	100	100	100	100	100	100	100	100	100	100
Intake throttle valve [%open]	100	100	0	20	30	40	100	100	40	30	20	0
Measured conditions												
Speed [rpm]	1293	1313	1297	1296	1288	1287	1298	1293	1299	1289	1294	1302
Tinlet [°C]	98.30	78.89	85.80	98.28	103.84	108.35	111.82	116.11	111.03	115.42	112.26	108.85
Pinlet [bar]	0.99	0.99	0.99	0.98	0.97	0.96	0.95	0.95	0.96	0.97	0.98	0.99
O2 - intake [%]	20.86	20.74	17.2	16.1	15.06	14.65	13.79	13.68	14.61	14.94	15.96	17.11
CO2 - intake [%]	0.02	0.03	2.62	3.4	4.11	4.4	4.95	5.02	4.39	4.11	3.43	2.64
CO - intake [%]	0	0.001	0.006	0.009	0.015	0.02	0.047	0.051	0.022	0.017	0.011	0.008
NO - intake [vpm]	9	19	147	121	78	47	24	29	44	76	114	150
O2 - exhaust [%]*	—	—	—	—	—	—	—	—	—	—	—	—
CO2 - exhaust [%]*	—	—	—	—	—	—	—	—	—	—	—	—
CO - exhaust [%]*	—	—	—	—	—	—	—	—	—	—	—	—
NO - exhaust [vpm]*	—	—	—	—	—	—	—	—	—	—	—	—
Calculated conditions												
O2 - intake [%]	20.86	20.74	17.20	16.10	15.06	14.65	13.79	13.68	14.61	14.94	15.96	17.11
massflow - EGR [kg/h]	0.00	0.00	10.56	11.84	12.77	13.47	14.39	14.60	13.42	12.82	11.61	10.10
IMEP [bar]	4.29	4.28	4.39	4.40	4.35	4.38	4.32	4.34	4.29	4.34	4.34	4.38
ID - DP1 [°ca]	8.01	8.05	9.50	9.78	10.39	11.00	12.61	12.85	11.26	10.51	9.82	9.51
ID - DP2 [°ca]	7.15	7.30	8.93	9.05	9.68	10.24	11.82	12.03	10.55	9.93	9.13	8.98
ID - DP3 [°ca]	6.64	7.84	8.12	8.47	9.03	9.67	11.08	11.11	9.91	9.26	8.52	8.18
ID - CA2 [°ca]	6.55	6.89	7.64	7.91	8.29	8.53	9.09	8.97	8.62	8.38	8.09	7.62
ID - CA5 [°ca]	7.15	7.23	8.45	8.63	9.12	9.57	10.69	10.76	9.78	9.25	8.69	8.45
ID - CA10 [°ca]	7.44	7.54	8.82	9.07	9.61	10.17	11.48	11.63	10.39	9.77	9.12	8.85

* The emissions in the exhaust were not measured as this was not further used in this work

HVO100 Batch (a)

Date measurement	6/04/2023	6/04/2023	6/04/2023	6/04/2023	6/04/2023	6/04/2023	6/04/2023	6/04/2023	6/04/2023	7/04/2023	7/04/2023	7/04/2023	7/04/2023	7/04/2023	7/04/2023	7/04/2023	7/04/2023	7/04/2023
Environmental conditions																		
Patm [hPa]	1011.1	1011.1	1011.1	1011	1010.9	1010.8	1010.8	1010.8	1010.7	1015.9	1016.1	1016.2	1016.4	1016.5	1016.6	1016.6	1016.7	1016.7
Tatm [°C]	21.7	21.7	21.6	21.7	21.7	21.8	21.7	21.8	21.9	21.3	22.7	22.7	22.7	22.7	22.8	22.3	22.2	22.1
Relative humidity [%]	35.4	35.9	36.5	36.8	36	36.1	37.2	36.8	36.9	32.5	33.3	33.3	33.6	33.4	33.6	34.3	34.5	34.6
Parameters held constant																		
SOI [°ca BTDC]	10	10	10	10	10	10	10	10	10	10	10	10	10	10	10	10	10	10
Pedal stand [%]	7	7	7	7	7	7	7	7	7	7	7	7	7	7	7	7	7	7
Injection pressure [bar]	900	900	900	900	900	900	900	900	900	900	900	900	900	900	900	900	900	900
Variable parameters																		
EGR valve [%open]	0	20	30	40	100	100	100	100	100	0	20	30	40	100	100	100	100	100
Intake throttle valve [%open]	100	100	100	100	100	50	30	20	10	100	100	100	100	100	50	30	20	10
Measured conditions																		
Speed [rpm]	1307	1301	1299	1314	1303	1302	1294	1295	1310	1304	1315	1300	1299	1297	1302	1295	1314	1307
Tinlet [°C]	84.39	84.97	86.11	90.82	101.26	103.03	106.98	109.66	116.13	84.42	85.48	86.66	91.18	101.65	102.96	105.92	105.51	115.73
Pinlet [bar]	1.00	1.00	1.00	1.01	1.01	1.00	1.00	0.99	0.97	1.01	1.01	1.01	1.01	1.01	1.01	1.00	0.99	0.97
O2 - intake [%]	20.71	20.28	19.72	18.77	17.18	17.14	15.97	15.01	13.82	20.77	20.37	19.83	18.85	17.25	17.24	16.15	15.17	13.94
CO2 - intake [%]	0.04	0.35	0.77	1.46	2.55	2.57	3.36	4.02	4.83	0.04	0.34	0.75	1.45	2.53	2.53	3.32	3.96	4.8
CO - intake [%]	0.004	0.004	0.005	0.006	0.009	0.008	0.011	0.016	0.054	0.004	0.005	0.006	0.008	0.010	0.009	0.008	0.012	0.045
NO - intake [vpm]	55	112	169	192	148	133	116	79	26	52	104	166	187	158	140	119	74	21
O2 - exhaust [%]	12.93	12.74	12	10.97	9.39	9.04	8.29	7.22	4.88	13.17	12.9	12.11	11.15	9.5	9.18	8.39	7.43	5.05
CO2 - exhaust [%]	5.37	5.54	6.05	6.67	7.87	8.13	8.65	9.39	10.99	5.26	5.46	6	6.68	7.83	8.04	8.58	9.27	10.9
CO - exhaust [%]	0.014	0.013	0.014	0.015	0.018	0.019	0.023	0.029	0.100	0.012	0.014	0.015	0.016	0.019	0.019	0.022	0.025	0.085
NO - exhaust [vpm]	1152	1063	953	736	445	400	284	174	56	1110	1066	952	730	459	415	305	169	53
Calculated conditions																		
O2 - intake [%]	20.71	20.05	19.07	18.02	16.50	16.25	15.61	14.95	14.03	20.77	20.27	19.14	17.93	16.43	16.23	15.57	15.02	13.70
massflow - EGR [kg/h]	0.00	1.92	4.58	7.18	10.51	11.00	12.22	13.36	14.68	0.00	1.48	4.58	7.58	10.82	11.23	12.46	13.46	15.37
IMEP [bar]	4.42	4.40	4.43	4.51	4.50	4.54	4.51	4.47	4.48	4.45	4.49	4.49	4.52	4.55	4.52	4.52	4.47	4.43
ID - DP1 [°ca]	7.07	7.10	7.42	7.79	8.57	8.58	8.85	9.50	10.96	7.07	7.21	7.40	7.73	8.54	8.53	8.86	9.53	11.21
ID - DP2 [°ca]	6.50	6.50	6.54	7.00	7.88	7.88	8.00	8.77	10.25	6.47	6.50	6.54	7.01	7.62	7.78	8.00	8.89	10.45
ID - DP3 [°ca]	5.96	5.97	6.00	6.49	7.06	7.07	7.41	8.03	9.57	5.92	5.98	6.00	6.42	7.00	7.01	7.36	8.10	9.70
ID - CA2 [°ca]	6.10	6.04	6.08	6.45	6.92	6.82	7.17	7.58	8.36	5.94	5.99	6.19	6.37	6.84	6.60	7.11	7.62	8.41
ID - CA5 [°ca]	6.56	6.56	6.67	7.06	7.63	7.62	7.79	8.32	9.40	6.52	6.59	6.66	6.95	7.55	7.49	7.76	8.36	9.54
ID - CA10 [°ca]	6.78	6.79	6.99	7.34	8.02	8.02	8.18	8.78	10.07	6.74	6.84	6.97	7.25	7.92	7.97	8.15	8.83	10.23

HVO100 Batch (b)

Date measurement	12/04/2023	12/04/2023	12/04/2023	12/04/2023	12/04/2023	12/04/2023	12/04/2023	12/04/2023	12/04/2023	12/04/2023	12/04/2023
Environmental conditions											
Patm [hPa]	996	995.8	995.9	995.9	996	996	995.9	996	996	996	996
Tatm [°C]	21.3	21.5	21.2	21	21	21.2	21.1	21.2	21.2	21.3	21.3
Relative humidity [%]	37.5	38	38.6	39.1	38.7	38.4	38.3	38.2	38.1	37.7	37.5
Parameters held constant											
SOI [°ca BTDC]	10	10	10	10	10	10	10	10	10	10	10
Pedal stand [%]	7	7	7	7	7	7	7	7	7	7	7
Injection pressure [bar]	900	900	900	900	900	900	900	900	900	900	900
Variable parameters											
EGR valve [%open]	0	100	100	100	100	100	100	100	100	100	100
Intake throttle valve [%open]	100	100	40	30	20	10	10	20	30	40	100
Measured conditions											
Speed [rpm]	1304	1300	1292	1299	1305	1301	1298	1293	1307	1303	1298
Tinlet [°C]	84.39	98.40	105.56	108.46	111.43	116.62	118.75	115.41	111.11	107.82	103.53
Pinlet [bar]	0.99	0.99	0.98	0.97	0.96	0.96	0.96	0.97	0.97	0.98	0.99
O2 - intake [%]	20.67	17.25	16.10	15.11	14.70	13.80	13.75	14.54	14.94	15.93	17.11
CO2 - intake [%]	0.03	2.57	3.34	4.01	4.28	4.87	4.88	4.35	4.02	3.37	2.56
CO - intake [%]	0	0.004	0.004	0.005	0.006	0.009	0.004	0.005	0.006	0.008	0.010
NO - intake [vpm]	9	55	112	169	192	148	52	104	166	187	158
O2 - exhaust [%]*	/	/	/	/	/	/	/	/	/	/	/
CO2 - exhaust [%]*	/	/	/	/	/	/	/	/	/	/	/
CO - exhaust [%]*	/	/	/	/	/	/	/	/	/	/	/
NO - exhaust [vpm]*	/	/	/	/	/	/	/	/	/	/	/
Calculated conditions											
O2 - intake [%]	20.67	16.49	15.64	15.04	14.59	13.90	14.06	14.66	15.09	15.74	16.48
massflow - EGR [kg/h]	0.00	10.17	11.71	12.71	13.38	14.29	14.01	13.19	12.55	11.47	10.10
IMEP [bar]	4.31	4.44	4.34	4.33	4.33	4.31	4.32	4.33	4.36	4.37	4.37
ID - DP1 [°ca]	8.68	8.74	9.00	9.55	10.26	11.28	11.03	10.01	9.70	9.01	8.68
ID - DP2 [°ca]	7.95	8.00	8.27	8.98	9.55	10.54	10.40	9.36	9.00	8.27	7.95
ID - DP3 [°ca]	7.15	7.26	7.52	8.37	8.92	9.77	9.72	8.69	8.40	7.52	7.15
ID - CA2 [°ca]	7.12	6.89	7.34	7.54	7.96	8.31	8.26	7.88	7.62	7.43	7.12
ID - CA5 [°ca]	7.67	7.67	7.95	8.43	8.89	9.58	9.46	8.69	8.52	8.00	7.67
ID - CA10 [°ca]	8.06	8.08	8.32	8.93	9.46	10.31	10.15	9.24	9.00	8.37	8.06

* The emissions in the exhaust were not measured as this was not further used in this work

	Diesel - Iso Octane					Diesel - Dodecane				
Date measurement	21/05/2023	21/05/2023	21/05/2023	21/05/2023	21/05/2023	21/05/2023	21/05/2023	21/05/2023	21/05/2023	21/05/2023
Environmental conditions										
Patm [hPa]	1019.8	1019.8	1019.8	1019.8	1019.7	1009.6	1009.3	1009.3	1009.3	1009.3
Tatm [°C]	20.3	20.3	20.4	20.5	20.4	20.3	20.2	20.2	20.2	20.5
Relative humidity [%]	61.6	61.8	61.3	59.4	59.8	62.6	64.3	65.3	65.8	64.3
Parameters held constant										
SOI [°ca BTDC]	10	10	10	10	10	10	10	10	10	10
Pedal stand [%]	7	7	7	7	7	7	7	7	7	7
Injection pressure [bar]	900	900	900	900	900	900	900	900	900	900
Variable parameters										
EGR valve [%open]	0	100	100	100	100	0	100	100	100	100
Intake throttle valve [%open]	100	100	30	20	10	100	100	30	20	10
Measured conditions										
Speed [rpm]	1309	1311	1308	1286	1280	1293	1300	1304	1295	1316
Tinlet [°C]	81.75	97.51	104.21	108.53	116.19	83.62	97.93	102.54	107.18	111.44
Pinlet [bar]	1.01	1.02	1.01	1.00	0.98	1.00	1.01	0.99	0.99	0.97
O2 - intake [%]	20.85	17.35	16.29	15.39	13.98	20.91	17.25	16.24	15.08	13.98
CO2 - intake [%]	0.02	2.55	3.3	3.92	4.92	0.02	2.6	3.34	4.13	4.92
CO - intake [%]	0.003	0.014	0.022	0.03	0.057	0	0.008	0.012	0.019	0.042
NO - intake [vpm]	5	127	95	65	18	7	138	110	73	21
O2 - exhaust [%]*	/	/	/	/	/	/	/	/	/	/
CO2 - exhaust [%]*	/	/	/	/	/	/	/	/	/	/
CO - exhaust [%]*	/	/	/	/	/	/	/	/	/	/
NO - exhaust [vpm]*	/	/	/	/	/	/	/	/	/	/
Calculated conditions										
O2 - intake [%]	20.85	16.46	15.72	14.96	13.54	20.91	16.66	15.86	15.20	14.15
massflow - EGR [kg/h]	0.00	10.89	12.25	13.52	15.52	0.00	10.25	11.73	12.80	14.34
IMEP [bar]	4.21	4.29	4.28	4.30	4.38	4.21	4.46	4.35	4.39	4.42
ID - DP1 [°ca]	9.56	11.51	12.00	12.70	15.98	8.60	10.31	10.66	11.37	13.75
ID - DP2 [°ca]	9.00	10.99	11.36	12.04	14.87	8.00	9.52	10.00	10.66	12.78
ID - DP3 [°ca]	8.43	10.26	10.57	10.46	5.64	7.49	8.99	9.45	9.85	8.57
ID - CA2 [°ca]	8.08	8.96	9.18	9.32	10.49	7.43	8.24	8.42	8.70	9.44
ID - CA5 [°ca]	8.63	10.21	10.59	11.08	13.30	7.85	9.11	9.48	9.95	11.54
ID - CA10 [°ca]	8.97	10.73	11.14	11.75	14.43	8.11	9.57	9.97	10.53	12.49

* The emissions in the exhaust were not measured as this was not further used in this work

Appendix F

Illustration of unstable operating conditions
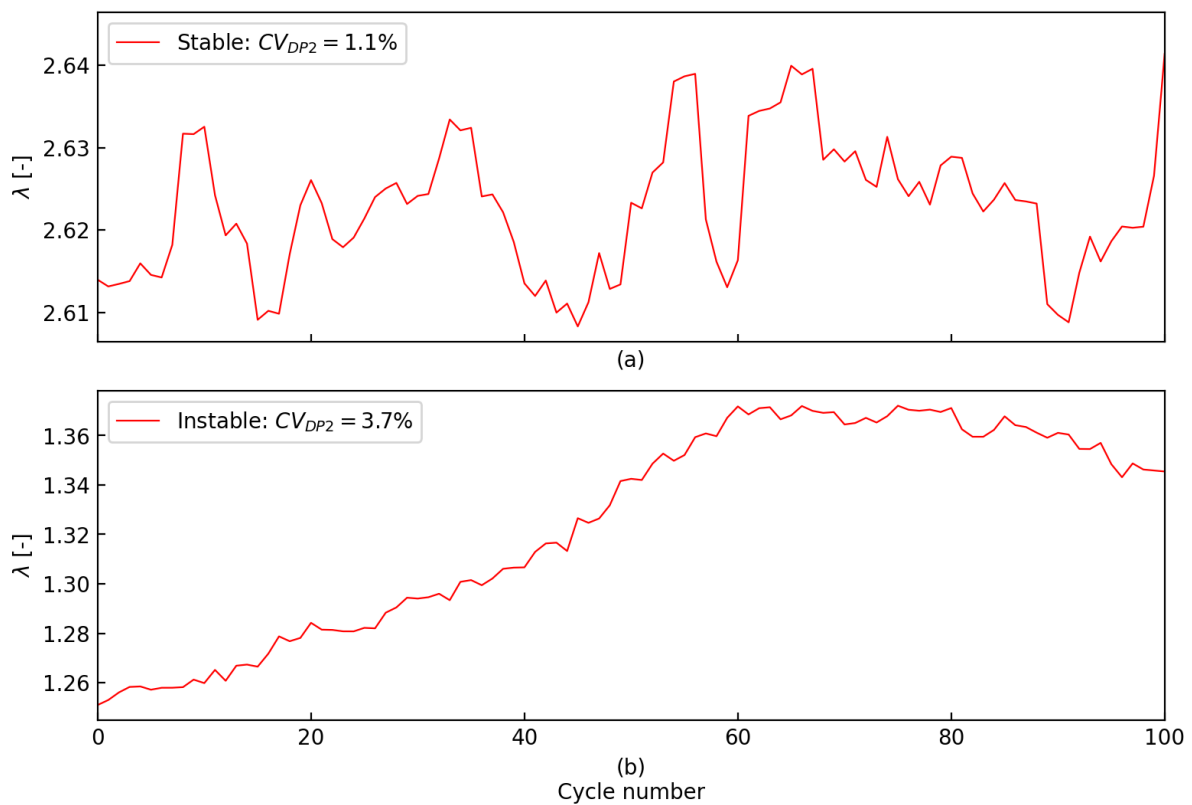
Figure F.1: Measurements of lambda over 100 consecutive engine cycles for a stable load point (a) and an unstable load point (b). The unstable operation is indicated by the variation in lambda, and the coefficient of variance of the ignition delay CV_{DP2}.

Appendix G

Engine control and DAQ system adaptations

G.1 New thermocouple converter modules

The two K-type thermocouples which measure the manifold temperatures were originally connected to the NI 9213 control module. The sensor values were not registered in the NI-CAS softwere however. Two new Crouzet K-type thermocouples [105] were installed. Their output signals can be connected to the BNC rack to allow sensor logging.

G.2 Logging sensor measurements

For this thesis work it is needed to log sensor readings over a number of cycles in a reliable way to perform combustion analysis. The Raw File Save vi allows to save a selected set of sensor readings to a .tdms file. This file contains measurements of the sensors connected to the BNC rack paired with the encoder pulses. Initially, only the cylinder pressure sensor was connected. This Sync Analog Channels Setup vi, shown in Figure G.1 allows to configure how the sensors connected to the BNC rack are logged in the .tdms file. The Physical Channels corresponds to the position on the BNC rack.
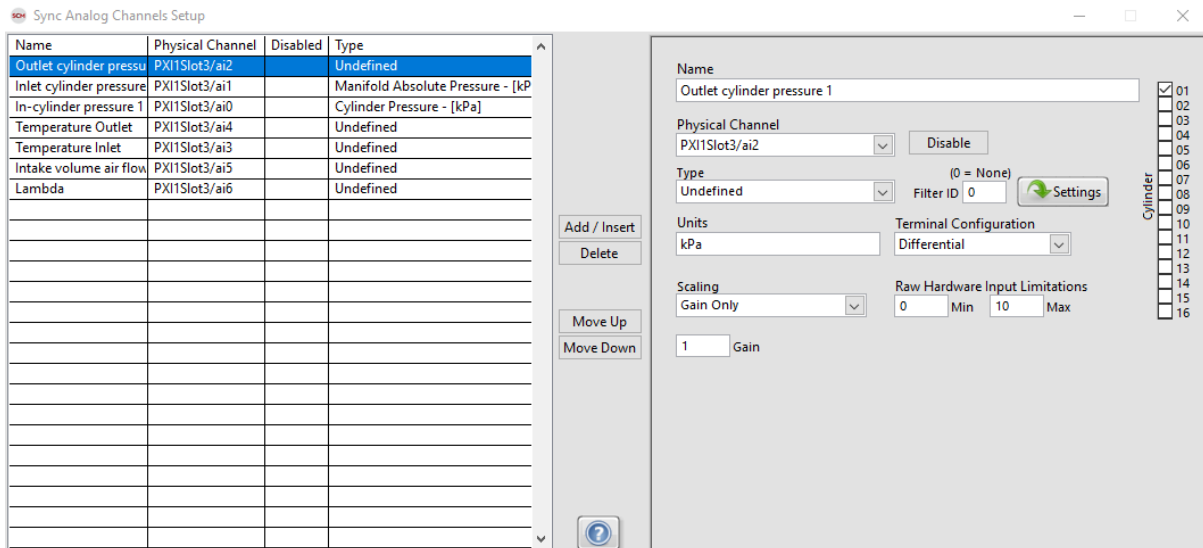
Figure G.1: The Sync Analog Channels Setup vi allows to configure logging settings for the sensors connected to the BNC rack.

A measurement can be made using the Raw File Save vi. The process of recording measurements has proven to be rather unreliable, often resulting in engine stall when doing so. In the past, an upgraded CPU has been installed in the test bench PC as advised by National Instruments. This has not yet remedied the problem yet. High CPU usage is still observed, which probably results in these engine stalls. The Windows Search Indexer has been deactivated to lower CPU usage. Raw file saves can be read and processed using Python scripts and the nptdms package [106].

G.3 Throttle valve control

The position of the EGR and throttle valves can be controlled manually in the using the EGR control vi, shown in Figure G.2. The position of both valves can be controlled by a customizable engine map if desired, but are under manual control at this moment. The High Pressure EGR Position signifies the control of the EGR valve. It can be set to a desired position using the HighPEGRPsn_Man field. The throttle valve can be controlled in the Low Pressure EGR Position part of the vi, by changing the LowPEGRPsn_Man field.
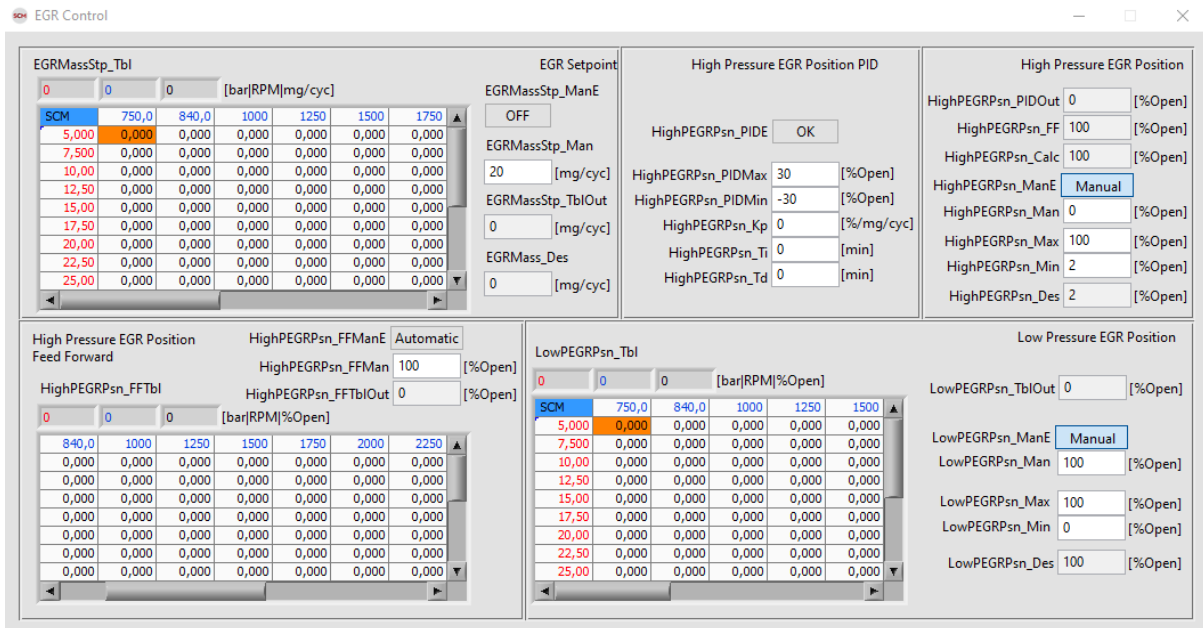
Figure G.2: The EGR control vi, which controls the EGR and throttle valves.

Initially, only the EGR valve control was operational. Both valves are controlled through the NI 9759 control module, which contains two H-bridge driver channels to each drive a typical passenger car electronic throttle body [107]. The control module generates a PWM signal driving the servo motor in the throttle body. This generates a force opposing the returning spring force, controlling the pedal to a constant position. A classical throttle body feeds back its own position through a voltage divider circuit using a potentiometer connected to the valve plate. This position feedback is fed back to a PID controller to control the valve in a closed-loop manner. This controller can be set up in the 'NI 9759 (Throttle) Setup' window, where the first and second channel (two tabs on the left side) correspond to the EGR and throttle valve respectively.
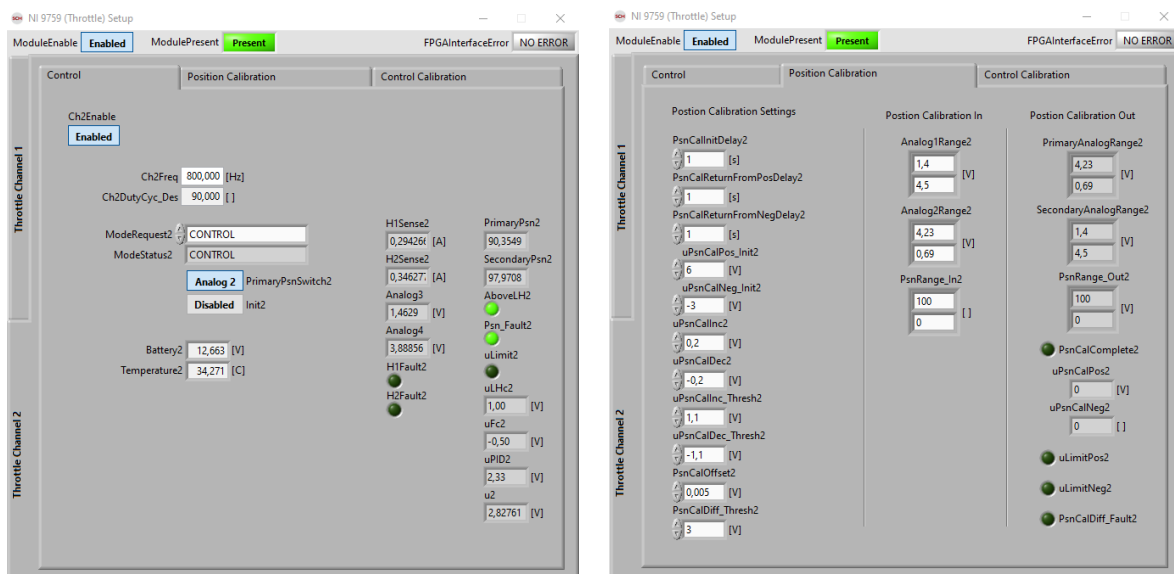
Figure G.3: The Control (left) and Position Calibration (right) tabs of the NI 9759 Throttle driver setup.

The Control panel allows to place the controller in Control mode, Position Calibration mode or Control Calibration mode. The throttle driver can be deactivated by switching the Init2 to Enabled. The Analog3 value shows the measured voltage in the potentiometer circuit of the valve. This voltage is proportional to the valve position. The Position Calibration tab allows to relate this voltage to any desired proportional quantity. The valve position has currently been expressed as $\% open$, as shown in the EGR control vi (see Fig. G.2): a voltage of $1.4V$ corresponds to $100\% open$, a voltage of $4.5V$ corresponds to a completely closed position of the valve. This calibration can be done by manually altering the valve position after removing the inlet air tubing and monitoring the received voltage in the Control tab. Once this position calibration has been set up, the PID constants can be set in the Control Calibration tab shown in Figure G.4. The controller can be made to behave non-linearly, i.e. different PID-constants for forward (KRPos2, TIPos2, TDPos2) and reverse (KRNeg2, TINeg2, TDNeg2) movement of the valve. This allows to compensate for the spring force resisting movement in the forward direction and aiding movement in the reverse direction. The proportional control constants should be negative as the H-bridge circuit requires a positive motor voltage to close the valve against its returning spring force. The controller was tuned manually until a stable control response was observed, the motor resistance was measured manually on the terminals of the servo motor.
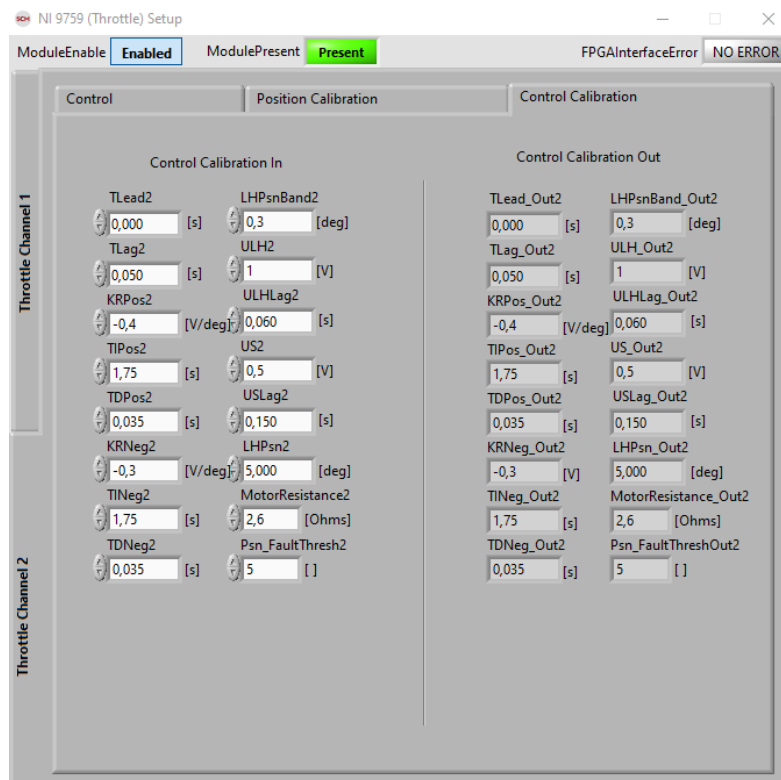
Figure G.4: The Control Calibration tab of the NI 9759 Throttle driver setup.

G.4 Starting the engine

Initially, the engine did not start smoothly. It seemed that the engine would not start using its mapped Fuel Command. This engine map controls the injected fuel quantity (IQ) as a function of the engine rpm (horizontal axis) and pedal stand (vertical axis). The engine can be started more easily by controlling the fuel injection manually to $25\,mg/cycle$ during startup, and switching to automatic control once the engine starts.
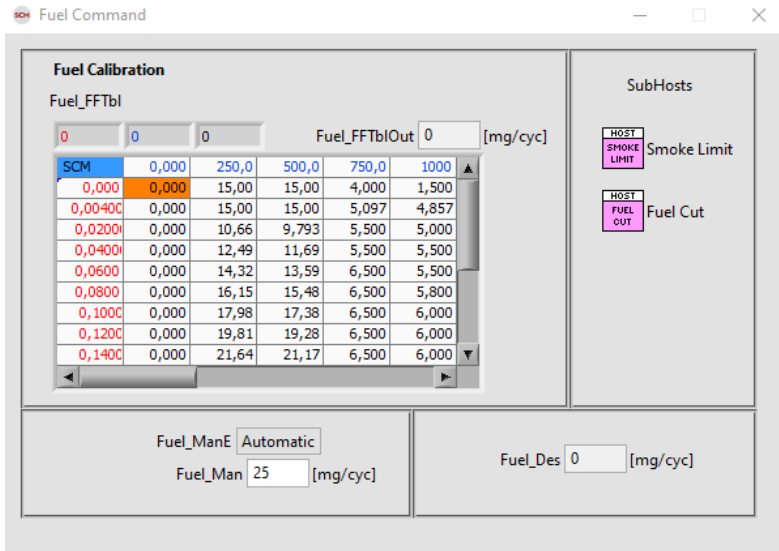
Figure G.5: The Fuel Command vi. allows to alter the fuel command engine map and toggle to manual control.

Bibliography

[1] H.-O. Pörtner, D.C. Roberts, H. Adams, I. Adelekan, C. Adler, R. Adrian, P. Aldunce, E. Ali, R. Ara Begum, B. Bednar Friedl, R. Bezner Kerr, R. Biesbroek, J. Birkmann, K. Bowen, M.A. Caretta, J. Carnicer, E. Castellanos, T.S. Cheong, W. Chow, G. Cissé G. Cissé, and Z. Zaiton Ibrahim. *Climate Change 2022: Impacts, Adaptation and Vulnerability.* Technical Summary. Cambridge University Press, Cambridge, UK and New York, USA, 2022.

[2] U.S. Energy Environmental Protection Agency. Climate change indicators: Heat waves. `https://www.epa.gov/climate-indicators/climate-change-indicators-heat-waves`, July 2022.

[3] U.S. Energy Environmental Protection Agency. Climate change indicators: Sea level. `https://www.epa.gov/climate-indicators/climate-change-indicators-sea-level`, July 2022.

[4] U.S. Energy Environmental Protection Agency. Climate change indicators: Bird wintering ranges. `https://www.epa.gov/climate-indicators/climate-change-indicators-bird-wintering-ranges`, July 2022.

[5] IPCC. *Climate Change 2022: Mitigation of Climate Change. Contribution of Working Group III to the Sixth Assessment Report of the Intergovernmental Panel on Climate Change.* Cambridge University Press, Cambridge, UK and New York, NY, USA, 2022.

[6] Louise Gren, Vilhelm B. Malmborg, John Falk, Lassi Markula, Maja Novakovic, Sam Shamun, Axel C. Eriksson, Thomas B. Kristensen, Birgitta Svenningsson, Martin Tunér, Panu Karjalainen, and Joakim Pagels. Effects of renewable fuel and exhaust aftertreatment on primary and secondary emissions from a modern heavy-duty diesel engine. *Journal of Aerosol Science*, 156:105781, 2021.

[7] UNEP. Emissions gap report 2022. `https://www.unep.org/resources/emissions-gap-report-2022`, October 2022.

[8] UNEP. Climate change: No 'credible pathway' to 1.5c limit, unep warns. `https://news.un.org/en/story/2022/10/1129912`, October 2022.

[9] Izzet Karakurt, Gokhan Aydin, and Kerim Aydiner. Sources and mitigation of methane emissions by sectors: A critical review. *Renewable Energy*, 39(1):40–48, 2012.

[10] DavidBonnici. How many cars are there in the world? `https://www.whichcar.com.au/news/how-many-cars-are-there-in-the-world`, October 2022.

[11] European Comission. Reducing co2 emissions from passenger cars. `https://climate.ec.europa.eu/eu-action/transport-emissions/road-transport-reducing-co2-emissions-vehicles/co2-emission-performance-standards-cars-and-vans_en`, October 2019.

[12] Öivind Andersson and Pål Börjesson. The greenhouse gas emissions of an electrified vehicle combined with renewable fuels: Life cycle assessment and policy implications. *Applied Energy*, 289:116621, 2021.

[13] Julie Blackley. How long do people keep their cars? `https://www.iseecars.com/how-long-people-keep-cars-study`, October 2022.

[14] NEF Bloomberg. Electric vehicle outlook 2020. *Executive Sum*, 2020.

[15] Falko Ueckerdt, Christian Bauer, Alois Dirnaichner, Jordan Everall, Romain Sacchi, and Gunnar Luderer. Potential and risks of hydrogen-based e-fuels in climate change mitigation. *Nature Climate Change*, 11(5):384–393, 2021.

[16] Rosanna Viscardi, Claudia Bassano, Giuseppe Nigliaccio, and Paolo Deiana. The potential of e-fuels as future fuels.

[17] Marta Yugo and Alba Soler. A look into the role of e-fuels in the transport system in europe (2030–2050). *Concawe Rev*, 28(1), 2019.

[18] Ralph EH Sims, Warren Mabee, Jack N Saddler, and Michael Taylor. An overview of second generation biofuel technologies. *Bioresource technology*, 101(6):1570–1580, 2010.

[19] Christian Thiel, Johannes Schmidt, Arnold Van Zyl, and Erwin Schmid. Cost and well-to-wheel implications of the vehicle fleet co2 emission regulation in the european union. *Transportation Research Part A: policy and practice*, 63:25–42, 2014.

[20] European Commission. Climate action. reducing co2 emissions from passenger cars. `https://climate.ec.europa.eu/eu-action/transport-emissions/road-transport-reducing-co2-emissions-vehicles/co2-emission-performance-standards-cars-and-vans_en`, July 2019.

[21] Qiang Dai, Jarod Kelly, Linda Gaines, and Michael Wang. Life cycle analysis of lithium-ion batteries for automotive applications. *Batteries*, 5:48, 06 2019.

[22] Hannah Ritchie, Max Roser, and Pablo Rosado. Energy. *Our World in Data*, 2022. https://ourworldindata.org/energy.

[23] Paul Baker, Oliver Chartier, Robert Haffner, Laura Heidecke, Karel van Hussen, Lars Meindert, Barbara Pia Oberč, Karolina Ryszka, Pantelis Capros, Alessia De Vita, et al. *Research and Innovation perspective of the mid-and long-term Potential for Advanced Biofuels in Europe*. European Commission, Directorate-General for Research and Innovation, 2017.

[24] IEA. Bioenergy – tracking report. `https://www.iea.org/reports/bioenergy`, September 2022. (Accessed on 01/22/2023).

[25] Anselm Eisentraut. Sustainable production of second-generation biofuels. 2010.

[26] Susan van Dyk Et al. Drop-in biofuels: The key role that co-processing will play in its production. *IEA Bioenergy*, 2019.

[27] Diesel Engine Registry. 2-stroke vs. 4-stroke engines. `https://dieselengineregistry.wordpress.com/2-stroke-vs-4-stroke-engines/`, October 2015.

[28] Rakesh Kumar Maurya, Rakesh Kumar Maurya, and Luby. *Characteristics and control of low temperature combustion engines*. Springer, 2018.

[29] John B Heywood. *Internal combustion engine fundamentals*. McGraw-Hill Education, 2018.

[30] Michael John Murphy, Joshua D Taylor, and Robert L McCormick. Compendium of experimental cetane number data. 2004.

[31] JN Bowden, AA Johnston, and JA Russell. Octane-cetane relationship. Technical report, SOUTHWEST RESEARCH INST SAN ANTONIO TX BELVOIR FUELS AND LUBRICANTS RESEARCH . . . , 1974.

[32] Thomas W Ryan III. Correlation of physical and chemical ignition delay to cetane number. *SAE transactions*, pages 687–699, 1985.

[33] Luc N Allard, Gary D Webster, Norman J Hole, Thomas W Ryan III, Dale Ott, and Craig W Fairbridge. Diesel fuel ignition quality as determined in the ignition quality tester (iqt). *SAE transactions*, pages 955–959, 1996.

[34] John E Dec. A conceptual model of dl diesel combustion based on laser-sheet imaging. *SAE transactions*, pages 1319–1348, 1997.

[35] İbrahim Aslan Reşitoğlu, Kemal Altinişik, and Ali Keskin. The pollutant emissions from diesel-engine vehicles and exhaust aftertreatment systems. *Clean Technologies and Environmental Policy*, 17(1):15–27, 2015.

[36] Sebastian Verhelst, James WG Turner, Louis Sileghem, and Jeroen Vancoillie. Methanol as a fuel for internal combustion engines. *Progress in Energy and Combustion Science*, 70:43–88, 2019.

[37] Pierre-Louis Ragon and Felipe Rodríguez. Estimated cost of diesel emissions control technology to meet future euro vii standards. *Working Paper*, 2021.

[38] Hua Zhao. *Advanced direct injection combustion engine technologies and development: diesel engines*, volume 2. Elsevier, 2009.

[39] NBN EN 590:2013+A1:2017. `https://www.nbn.be/data/r/platform/frontend/detail`, October 2017.

[40] M. M. El Wakil, P. S. Myers, and O. A. Uyehara. Fuel vaporization and ignition lag in diesel combustion. *SAE Transactions*, 64:712–729, 1956.

[41] Patrick A Caton, Leonard J Hamilton, and Jim S Cowart. Understanding ignition delay effects with pure component fuels in a single-cylinder diesel engine. *Journal of engineering for gas turbines and power*, 133(3), 2011.

[42] Mariana Hristova. Measurement and prediction of binary mixture flash point. *Central European Journal of Chemistry*, 11(1):57–62, 2013.

[43] RH Barbour, DJ Rickeard, and NG Elliott. Understanding diesel lubricity. *SAE transactions*, pages 1556–1566, 2000.

[44] Keith Dawe. Future biofuels for shipping. `https://www.globalmaritimeforum.org/news/future-biofuels-for-shipping`, March 2022. (Accessed on 28/02/2023).

[45] Neste. Op weg naar duurzaam transport. `https://www.neste.com/products/all-products/saf#1671a481`, July 2022. (Accessed on 2/03/2023).

[46] Neste. Wat is hvo of hvo100? `https://www.neste.be/neste-my-renewable-diesel-be-nl/hvo/wat-is-hvo`, July 2022. (Accessed on 2/03/2023).

[47] Neste. Renewable diesel (hvo). `https:https://www.neste.be/neste-my-renewable-diesel-be-nl/hvo/veel-gestelde-vragen`, July 2022. (Accessed on 2/03/2023).

[48] Claus Felby Chia-wen Carmen Hsieh. Biofuels for the marine shipping sector: An overview and analysis of sector infrastructure, fuel technologies and regulations. 2017.

[49] Dominik Rutz Ioannis Dimitriou. *Sustainable Short Rotation Coppice: A Handbook*. WIP Renewable Energies, 2015.

[50] Crops for Energy. Short rotation coppice (src). `https://www.crops4energy.co.uk/short-rotation-coppice-src/`, November 2008.

[51] Tom Robeyn, Sebastian Verhelst, Immanuel Vinke, Hannes Latine, and James Turner. Investigation of naphtha-type biofuel from a novel refinery process. Technical report, SAE Technical Paper, 2022.

[52] CIO Kamalu, OA Iwot, PC Okere, AO Ogah, and JC Obijiaku. Modeling and analysis of the relationship of octane, cetane and ignition delay usage.

[53] David P Lowe, Tian Ran Lin, Weiliang Wu, and Andy CC Tan. Diesel knock combustion and its detection using acoustic emission. *Journal of Acoustic Emission*, 29, 2011.

[54] Noel Bezaire, Kapila Wadumesthrige, KY Simon Ng, and Steven O Salley. Limitations of the use of cetane index for alternative compression ignition engine fuels. *Fuel*, 89(12):3807–3813, 2010.

[55] The Association for Emissions Control by Catalyst AECC (AISBL). Heavy-duty vehicles. `https://www.aecc.eu/legislation/heavy-duty-vehicles/`, November 2022.

[56] ASTM Committee D-2 on Petroleum Products and Lubricants. *Standard test method for cetane number of diesel fuel oil*. ASTM International, 2005.

[57] CFR Engines Inc. Cfr engines inc. cetane rating unit. `https://cfrengines.com/cetane-rating-unit/`, November 2022.

[58] CFR Engines Canada ULC. Iqt totally automated laboratory model. `https://iqt.cfrengines.com/iqt-talm-iqt-totally-automated-laboratory-model/`, November 2022.

[59] Hideyuki Ogawa, Akihiro Morita, Katsushi Futagami, and Gen Shibata. Ignition delays in diesel combustion and intake gas conditions. *International Journal of Engine Research*, 19(8):805–812, 2018.

[60] Ziliang Zheng, Tamer Badawy, Naeim Henein, and Eric Sattler. Investigation of physical and chemical delay periods of different fuels in the ignition quality tester. *Journal of engineering for gas turbines and power*, 135(6), 2013.

[61] Radivoje B Pešić, Aleksandar Lj Davinić, and Stevan P Veinović. New engine method for biodiesel cetane number testing. *Thermal Science*, 12(1):125–138, 2008.

[62] Prasenjeet Ghosh and Stephen B Jaffe. Detailed composition-based model for predicting the cetane number of diesel fuels. *Industrial & engineering chemistry research*, 45(1):346–351, 2006.

[63] Bernard Lewis and Guenther Von Elbe. *Combustion, flames and explosions of gases*. Elsevier, 2012.

[64] Manuel Dahmen and Wolfgang Marquardt. A novel group contribution method for the prediction of the derived cetane number of oxygenated hydrocarbons. *Energy & Fuels*, 29(9):5781–5801, 2015.

[65] D ASTM. 6890 standard test method for determination of ignition delay and derived cetane number (dcn) of diesel fuel oils by combustion in a constant vol. *American Society for Testing and Materials (ASTM)*, 2011.

[66] George Wilson III. Comparison of astm d613 and astm d6890. Technical report, US Army TARDEC Fuels and Lubricants Research Facility (SwRI) San Antonio . . . , 2016.

[67] Luc N Allard, Gary D Webster, Norman J Hole, Thomas W Ryan III, Dale Ott, and Craig W Fairbridge. Diesel fuel ignition quality as determined in the ignition quality tester (iqt)-part iv. *SAE transactions*, 2001.

[68] Nicos Ladommatos and John Goacher. Equations for predicting the cetane number of diesel fuels from their physical properties. *Fuel*, 74(7):1083–1093, 1995.

[69] Dianne Luning Prak, Jay Cooke, Terrence Dickerson, Andy McDaniel, and Jim Cowart. Cetane number, derived cetane number, and cetane index: When correlations fail to predict combustibility. *Fuel*, 289:119963, 2021.

[70] Ömer L Gülder, Gordon F Burton, and Robert B Whyte. Nrcc cetane index—1: An improved cetane number predictor. *SAE transactions*, pages 437–446, 1986.

[71] Seetar G. Pande and Dennis R. Hardy. A practical evaluation of published cetane indices. *Fuel*, 69(4):437–442, 1990.

[72] Manuel Dahmen and Wolfgang Marquardt. A novel group contribution method for the prediction of the derived cetane number of oxygenated hydrocarbons. *Energy & Fuels*, 29(9):5781–5801, 2015.

[73] Yisel Sánchez-Borroto, Ramon Piloto-Rodriguez, Michel Errasti, Roger Sierens, and Sebastian Verhelst. Prediction of cetane number and ignition delay of biodiesel using artificial neural networks. *Energy Procedia*, 57:877–885, 2014.

[74] AS Ramadhas, S Jayaraj, C Muraleedharan, and K Padmakumari. Artificial neural networks used for the prediction of the cetane number of biodiesel. *Renewable Energy*, 31(15):2524–2533, 2006.

[75] Ramón Piloto-Rodríguez, Yisel Sánchez-Borroto, Magin Lapuerta, Leonardo Goyos-Pérez, and Sebastian Verhelst. Prediction of the cetane number of biodiesel using artificial neural networks and multiple linear regression. *Energy Conversion and Management*, 65:255–261, 2013.

[76] Pepijn De Geyter and Sebastian promotor Verhelst. Oplevering van een turbodieselmotorproefstand voor brandstoffenonderzoek, 2021.

[77] Dong Han, Ke Li, Yaozong Duan, He Lin, and Zhen Huang. Numerical study on fuel physical effects on the split injection processes on a common rail injection system. *Energy conversion and management*, 134:47–58, 2017.

[78] XLJ Seykens, LMT Somers, and RSG Baert. Modelling of common rail fuel injection system and influence of fluid properties on injection process. *Proceedings of VAFSEP*, pages 6–9, 2004.

[79] Frédéric Boudy and Patrice Seers. Impact of physical properties of biodiesel on the injection process in a common-rail direct injection system. *Energy Conversion and Management*, 50(12):2905–2912, 2009.

[80] Roberto Finesso and Ezio Spessa. Ignition delay prediction of multiple injections in diesel engines. *Fuel*, 119:170–190, 2014.

[81] Richard Stone. *Introduction to internal combustion engines*, volume 3. Springer, 1999.

[82] Tomaž Katrašnik, Ferdinand Trenc, and Samuel Rodman Oprešnik. A New Criterion to Determine the Start of Combustion in Diesel Engines. *Journal of Engineering for Gas Turbines and Power*, 128(4):928–933, 09 2005.

[83] Dennis Assanis, Zoran Filipi, Scott Fiveland, and Michalis Syrimis. A predictive ignition delay correlation under steady-state and transient operation of a direct injection diesel engine. *Journal of Engineering for Gas Turbines and Power-transactions of The Asme - J ENG GAS TURB POWER-T ASME*, 125, 04 2003.

[84] Revaz Zurabovich Kavtaradze, K Zeilinger, and G Zitzler. Ignition delay in a diesel engine utilizing different fuels. *High temperature*, 43:951–960, 2005.

[85] Michalis Syrimis, Kei Shigahara, and Dennis N. Assanis. Correlation between knock intensity and heat transfer under light and heavy knocking conditions in a spark ignition engine. *SAE Transactions*, 105:592–605, 1996.

[86] Wei Jet Thoo, Arman Kevric, Hoon Kiat Ng, Suyin Gan, Paul Shayler, and Antonino La Rocca. Characterisation of ignition delay period for a compression ignition engine operating on blended mixtures of diesel and gasoline. *Applied thermal engineering*, 66(1-2):55–64, 2014.

[87] Revaz Zurabovich Kavtaradze, K Zeilinger, and G Zitzler. Ignition delay in a diesel engine utilizing different fuels. *High temperature*, 43:951–960, 2005.

[88] Melih Yıldız and Bilge Albayrak Çeper. Zero-dimensional single zone engine modeling of an si engine fuelled with methane and methane-hydrogen blend using single and double wiebe function: A comparative study. *International Journal of Hydrogen Energy*, 42(40):25756–25765, 2017.

[89] Michael F.J. Brunt, Harjit Rai, and Andrew L. Emtage. The calculation of heat release energy from engine cylinder pressure data. *SAE Transactions*, 107:1596–1609, 1998.

[90] Kenneth S Kim, Michael T Szedlmayer, Kurt M Kruger, and Chol-Bum M Kweon. Optimization of in-cylinder pressure filter for engine research. Technical report, US Army Research Laboratory, Vehicle Technology Directorate Aberdeen Proving . . . , 2017.

[91] Lurun Zhong, N.A. Henein, and W. Bryzik. Effect of smoothing the pressure trace on the interpretation of experimental data for combustion in diesel engines. *SAE Transactions*, 113:525–543, 2004.

[92] Jaesung Chung, Junhyeong Oh, and Myoungho Sunwoo. A real-time combustion control with reconstructed in-cylinder pressure by principal component analysis for a crdi diesel engine. *Journal of Engineering for Gas Turbines and Power*, 139(6), 2017.

[93] Timothy Alexis Bodisco. *In-Cylinder Pressure and Inter-Cycle Variability Analysis for a Compression Ignition Engine: Bayesian Approaches*. PhD thesis, Queensland University of Technology, 2013.

[94] Koustav Dey. Characterization and rejection of noise from in-cylinder pressure traces in a diesel engine. 2012.

[95] Ahmed Al-Durra, Marcello Canova, and Steve Yurkovich. Application of extended kalman filter to on-line diesel engine cylinder pressure estimation. In *Dynamic Systems and Control Conference*, volume 48920, pages 541–548, 2009.

[96] CL Wong and DE Steere. The effects of diesel fuel properties and engine operating conditions on ignition delay. *SAE transactions*, pages 3873–3892, 1982.

[97] Florian vom Lehn, Liming Cai, Rupali Tripathi, Rafal Broda, and Heinz Pitsch. A property database of fuel compounds with emphasis on spark-ignition engine applications. *Applications in Energy and Combustion Science*, 5:100018, 2021.

[98] Yoshimitsu Kobashi, Masaki Todokoro, Gen Shibata, Hideyuki Ogawa, Toshihiro Mori, and Daichi Imai. Egr gas composition effects on ignition delays in diesel combustion. *Fuel*, 281:118730, 2020.

[99] WT Lyn and E Valdmanis. The effects of physical factors on ignition delay. Technical report, SAE Technical Paper, 1968.

[100] HO Hardenberg and FW Hase. An empirical formula for computing the pressure rise delay of a fuel from its cetane number and from the relevant parameters of direct-injection diesel engines. *SAE Transactions*, pages 1823–1834, 1979.

[101] AVL. Microifem piezo 4th generation piezo amplifier. `https://www.avl.com/document s/10138/2699442/MicroIFEM+4P4+Piezo`, May 2013.

[102] National Instruments. Pxi-6123 multifunction i/o module. `https://www.ni.com/nl-b e/support/model.pxi-6123.html`, April 2023.

[103] Omega Engineering. What is a thermocouple and how does it work? `https://www.omeg a.com/en-us/resources/thermocouple-hub`, May 2023.

[104] Yannick Huyghebaert, Dierickx, Jeroen, .-, Roger Sierens, Jeroen Vancoillie, and Sebastian Verhelst. Alternatieve brandstoffen voor vonkontstekingsmotoren : optimalisatie van waterstofmotoren en opbouw van een methanolmotorproefstand, 2010.

[105] Crouzet Automation. *AC Temperature Converter - Thermocouple K*, 11 2016.

[106] Adam Reeve. nptdms's documentation. `https://nptdms.readthedocs.io/en/stable/`, April 2023.

[107] National Instruments. *NI 9759 Electronic Throttle Driver Module User Manual*. NI.